ACTA POLYTECHNICA SCANDINAVICA

ELECTRICAL ENGINEERING SERIES NO. 100

Transient Voltage Distribution in Stator Winding of Electrical Machine Fed from a Frequency Converter

BOLARIN S. OYEGOKE

Helsinki University of Technology
Department of Electrical and Communications Engineering
Laboratory of Electromechanics
P.O Box 3000, FIN-02015 HUT, Finland

Dissertation for the degree of Doctor of Technology to be presented with due permission for public examination and debate in Auditorium S4 at Helsinki University of Technology (Espoo, Finland) on 27 May 2000, at 12 o' clock noon.

ESPOO 2000

Oyegoke, B. S.: Transient Voltage Distribution in Stator Winding of Electrical Machine Fed from a Frequency Converter. Acta Polytechnica Scandinavica, Electrical Engineering Series, No. 100, Espoo, 1999, 74 p. Published by the Finnish Academies of Technology. ISBN 951-666-537-3. ISSN 0001-6845.

Keywords: electrical machine, stator winding, voltage distribution, frequency converter

ABSTRACT

Standard induction motors are exposed to steep-fronted, non-sinusoidal voltages when fed from frequency converters. These wave patterns can be destructive to the insulation. The aim of the present work is to develop methods of predicting the magnitude and distribution of fast voltage within the stator winding of an electric machine fed from a frequency converter.

Three methods of predicting the magnitude and distribution of fast voltages within form windings commonly used in medium and high voltage machines are described. These methods utilise some aspects of previously published works on the surge propagation studies to achieve simplification of the solution without loss of accuracy. Two of these methods are applied to the voltage calculation in random winding commonly used in low voltage machines.

Multi-conductor transmission line theory forms the basis of the methods described in this work. Computation of the voltage distribution using either of these methods requires the calculation of the parameters for the slot and the end (over-hang) part of the winding. The parallel plate capacitor method, the indirect boundary integral equation method and the finite element method are the three possible methods of calculating the capacitance also described in this work. Duality existing between the magnetic and the electric field has been used for the inductance calculation.

Application of these methods to the voltage calculation in the first coil from the line-end of a 6 kV induction motor is shown to be successful. From the computed and measured voltage results it is evident that the improved accuracy for the capacitance values is sufficient to give good agreement between the measured and calculated inter-turn voltages without the need to infer the presence of a surface impedance effect due to the laminated core.

Application of two of these methods for the transient voltage calculation on the first coil from the terminal-end of low voltage induction motors with random windings is also shown to be successful. Comparison between the computed and the measured results shows that the turn-to-ground capacitance matrix obtained in over-hang part of the coil can be assumed the for the slot part of the coil. With this assumption modelling the first five turns in the line-end coil produce turn and coil voltage that match well with the corresponding measuring result.

The methods of voltage computation described in this work should be of great help to engineers and researchers concerned with the turn strength and over-voltage protection in high and low voltage motors.

PREFACE

This work was carried out in the Laboratory of Electromechanics, Helsinki University of Technology during the year 1995-1999. The work is applied to the transient voltage distribution in the stator winding of electric machine subjected to a fast rising voltage such as those arising in inverter fed motors, vacuum switches and lightning.

To my supervisor, Professor Tapani Jokinen, I would like to express my gratitude for the opportunity given to me to continue my post-graduate studies under his professorship. Your efforts in guiding me through those hard times are unforgettable. Furthermore, I am very grateful to Associate Professor Ivan Stoyanov Yatchev and Professor Alexander Krumov Alexandrov of the Department of Electrical Apparatus, Technical University of Sofia, Bulgaria, for the knowledge inspired in me during my visit to their Laboratory in Sofia.

In addition, I wish to acknowledge the effort of Dr Paavo Paloniemi and Dr Eero Keskinen of ABB Industry Oy for the useful discussion about this work at a very early stage of its development. Special thanks and appreciation to Dr Arkkio Antero, Professor Asko Niemenmaa and other members of the Laboratory of Electromechanics for the time devoted to the editing of my papers technically and otherwise. Their efforts are quite meritorious. Many thanks to Mr Pertti Saransaari and Mr Osmo Koponen for their support in making the experimental study possible. Financial support by the Imatran Voima is gratefully acknowledged.

To my family, a word can not express how grateful I am for your patience and continuous support. Above all infinite gratitude to GOD (ALLAH) the Almighty, the owner of all that is in the heaven and the earth and all that exists between (seen and unseen) for making this work a reality. If not by His will, this work would have remained a dream.

Espoo, June 1999

Bolarin S. Oyegoke

CONTENTS

LIST OF SYMBOLS

$A(w)$	Frequency response of a line
$A^1(w)$	Response of the line to step input
c	Velocity of light
c	Capacitance per unit length
$(\boldsymbol{C})$	Capacitance matrix
C_{e}	Turn to ground capacitance matrix in the over-hang region
C_{g}	Turn to ground capacitance
$(\boldsymbol{C}_{\mathrm{mod}})$	Modified capacitance matrix
$(\boldsymbol{C}_{\boldsymbol{i}})$	Current connection matrix
$(\boldsymbol{C}_{\boldsymbol{v}})$	Voltage connection matrix
C_{intcap}	Capacitance between two adjacent turns
C_{gst1}	Capacitance of turn 1 to the ground in the slot part
$d(w)$	Propagation coefficient of a line
$F(t)$	Inverse Fourier transform
G	Conductance of a line
$(\boldsymbol{I})$	Junction current column matrix
$(\boldsymbol{I})^{\mathrm{in}}$	Incident junction current column matrix
$(\boldsymbol{I})^{\mathrm{re}}$	Reflected junction current column matrix
$K_{\mathrm{proximity}}$	Coefficient of the proximity effect
K_{cf}	Proximity effect correction factor
l	Length of a line
$(\boldsymbol{L})$	Inductance matrix
$M_{12}, M_{13}..$	Mutual inductance
$\boldsymbol{Q}$	Charge
$(\boldsymbol{R})$	Resistance matrix
R	Resistance of a line
R_{sm}	Final form of a resistance in a line with skin and proximity effects
$(\boldsymbol{S})$	Voltage scatter matrix of a junction
$s = jw$	Laplace operator
t	Time
u	Electric scalar potential
u_{g}	Velocity of propagation
$\boldsymbol{U}$	Voltage
$(\boldsymbol{V})$	Junction voltage column matrix
$(\boldsymbol{V})^{\mathrm{in}}$	Incident junction voltage column matrix
$(\boldsymbol{V})^{\mathrm{re}}$	Reflected junction voltage column matrix
$(\boldsymbol{Y})$	Admittance matrix
$Y(w)$	Admittance of a line
$(\boldsymbol{Z})$	Impedance matrix
$Z(w)$	Characteristic impedance of a line
Z_{sabt}	Impedance of the space between two adjacent turns
Z_{ent}	Impedance at coil entrance
Z_{ext}	Impedance seen at the coil exit

Z_{g1}	Impedance calculated from the first turn of the coil
Z_{glt}	Impedance calculated from the last turn of the coil in the same slot
Z_{gnt}	Impedance calculated from the first turn of the next coil.
e_0	Permittivity of a free space (vacuum)
e_r	Relative permittivity of the insulation or dielectric constant
μ_0	Permeability of a free space (vacuum)
μ_r	Relative permeability of the insulation
d	Skin depth
r_1	Reflection coefficient at coil entrance
r_2	Reflection coefficient at coil exit
w	Angular frequency

DEDICATION

This work is dedicated to the glory of God Almighty, beside whom there is none. The Incomprehensible, the Knowledgeable, the Disposer of affairs, The Guarantor, the Watchful, the Guardian.

INTRODUCTION

1.1 Background

Cage induction motors have been the most popular electric motors in the 20th century. The dynamic progress made in the field of power electronics and control technology has led to increased application of cage induction motors in electrical drives. Their rated output power ranges from 70W to 500 kW, with 75% of them designed with four pole stators.

The squirrel cage induction motor is characterised by its robust and maintenance-free behaviour. Induction motors operating from a direct on line application with sinusoidal supply voltage have the limitation of delivering a near constant, unadjustable speed that is defined by the line frequency and the number of poles. In addition, induction motors fed by direct on line voltage develop only a small starting torque, drawing a large starting current.

In many applications, adjustable speed drives provide important advantages over constant speed drives. Adjustable Speed Drives give the possibility for automation and high cost efficiencies in industrial production processes and for transportation applications. Some applications, for instance electrical vehicles, would not have been possible without fast and accurate speed control. Because of these needs, adjustable speed drives have increasingly appeared in use in the recent years. An increasing number of adjustable speed drives are based on alternating current technology because of the good efficiency of this type of drive and the robustness of alternate electrical machines.

Adjustable speed drives permit the possibility to overcome the shortcomings of induction motors operating directly on line voltage, and satisfy most requirements of modern drives. The frequency converter with pulse-width modulation (PWM) and constant direct current voltage has established itself as the standard variable speed device for low voltage induction motors. With the increased emphasis on energy conversion and lower cost, the use of higher performance PWM drives has grown at an exponential rate.

For switching on the intermediate circuit voltage in PWM inverter, Silicon Controlled Rectifiers (SCR) at a frequency of 300 Hz were used before 1980. The SCR gave way to the current Gate Turn-off Thyristors (GTO). The GTO was commonly used from early 1980 to 1990. From 1990 until the present time, the insulated Gate Bipolar Transistors (IGBT) have become the new industry standard. The IGBT operates in the frequency range of about 20 kHz.

Unfortunately, inverters with progressive electronic components, such as IGBT, cause extremely steep and frequent peaks in the output voltage. These peaks impose large stresses on the winding insulation in a similar way to transient voltages caused by the fast switching of motors at the mains.

1.2 Winding failure

The basic stresses acting on the stator winding can be categorised into the following four groups:

1. Thermal
2. Electrical
3. Ambient
4. Mechanical

All these stresses are impacted by adjustable speed drive voltage waveforms, since the longevity of the winding is predicted on the basis of the integrity of the whole insulation system.

During the early stages of applying adjustable speed drives to ac motors, the major focus was on the thermal stress generated by the unwanted drive harmonics passed through to the motor and the associated heating. An

example is inverters that may use regular thyristors, such as variable voltage six-step inverters and current source inverters, which generate a rise time longer than 5 microseconds. More attention is given to rotor construction (rotor bar shapes) than to the capability of the stator insulation to withstand voltage, since the bar shape significantly influences the speed torque characteristics of the motor.

With modern PWM drive technology, which utilises much higher switching rates (IGBT), the stator winding insulation system has become the point of interest. This does not, however, imply that the rotor designs can be neglected.

1.3 Failure modes

Among many factors leading to the failure of ac motors fed by a frequency converter (e.g. PWM inverter) are the bearing failure and the inter-turn insulation failure.

Bearing problems account for about 50% of all machine failures (Schoen et al. (1995); Thorsen and Dalva (1995)). Next to the bearing problems is the failure of the stator winding. In the petrochemical industry, about 22% of the problems in the stator winding are caused by the failure in the inter-turn insulation (Thorsen and Dalva (1995)).

The bearing failure is associated with an increase in magnitude of the motor shaft voltage, which in turn is due to steep-fronted voltage such as that arising from the inverters and vacuum switching devices. An increase in shaft voltage results in current flow through motor bearings and electric discharge current within the bearings. The electric discharge current within the bearings leads to erosion of the bearing material and an early mechanical failure.

The inter-turn insulation failure, a common problem in inverter fed motors, could be a result of a defect introduced during manufacturing. This could have led to a flaw in the thin insulation between the conductors of the coil (inter-turn insulation). Another source of inter-turn insulation failure is in exploitation when a voltage that is higher than the nominal turn voltage is applied across a turn.

The problem associated with inter-turn voltage failure has received increase attention in recent years. This is due to the availability and use of new and improved materials and devices. The desire to produce cost-effective competitive products has resulted in greater exposure of the motor to high amplitude, repetitively produced steep-fronted transients (Murano et al. (1974a); Murano et al. (1974b); Cornick and Tlesis (1989); Cornick and Tlesis (1990); Cornick et al. (1992); Gupta et al. (1990)). This can therefore lead to an increase in the severity of the conditions which inter-turn insulation has to withstand.

Because of the reliability, compact size, low maintenance needs and long life, the vacuum switching devices are universally used in conjunction with large motors. In variable speed drive systems, PWM inverters are widely used. Both the vacuum devices and the inverters, however, have a drawback in that they are capable of producing high amplitude steep-fronted surges during switching operations.

The use of low loss cables between the vacuum interrupter (inverter) and the motor does not lower the amplitude of the surge or its front. Therefore, this cable cannot be thought of as protection against fast fronted waves.

Generally speaking, among possible failure modes of a machine fed from a frequency converter lie the following:

1. Turn to turn failure
2. Coil to coil failure
3. Phase to phase failure
4. Coil to ground failure
5. Open circuit failure

Of these failure modes, the phase to phase and phase to ground insulation is relatively easy to address and as a matter of fact is not normally the highest, as it was when operating on sine-wave power where the steady state turn to turn stress was relatively low.
In the light of the facts mentioned above, it has become very important to understand the surge phenomena in motor windings. The cause of surge phenomena, the system parameters that affect their amplitude and rise time and the ways in which these surges distribute themselves in winding, all need to be considered. Knowledge of the surge phenomena will allow quality design of the turn insulation and probably an adequate design of protective measures against dangerous surge.

2 PREVIEW OF PAST WORK

In this chapter, the situation of the voltage distribution in the stator winding of an induction motor when confronted by fast rising voltage is reviewed. Steep fronted surges have long been known to subject the turn insulation of a high voltage motor to voltage much higher than the rated value. The most common source of fast rise time surge is from the circuit breaker operation. To be precise, when the circuit breaker is close to a motor, the electrical breakdown across the contacts of the breaker launches a voltage surge down the power cable, which strikes the motor.

2.1 Preview of the past works on transient voltage distribution in form winding

While most of the theoretical investigation of surge phenomena has been concentrated on overhead lines and transformers, owing to their greater vulnerability, the effects of fast transients, such as switching or lightning surges on rotating machine insulation have been studied since the 1930's. Boehne (1930) is one of the first investigators to study the effect of fast transients on rotating machine insulation.

When a steep fronted surge such as that arising from an inverter or a vacuum switch arrives at the machine terminal, it propagates through the windings. This surge imposes dielectric stresses on the turn insulation. On the basis on this fact, Calvert (1934) considers a machine winding to be an inductance having uniformly distributed capacitance to earth as well as capacitance between the turns. His analysis of impulse-voltage distribution is concerned only with prediction of the rate of rise of the incoming surge, in order to enable the inter-turn voltages of coils to be kept within reasonable limits. However, Calvert, when dealing with machines of conventional design, did not say anything about the close coupling existing between electrically remote portions of the winding which are physically close together. An example of such a portion is those parts of the winding occupying the same slot. The facts mentioned above regarding the work of Calvert have also been confirmed by Robinson (1953) who proposed the theory of propagation in winding in which two-coil sides are inside each slot.

Studies performed by Cornick et al. (1989), Wright et al. (1983) and Stone et al. (1984) on the distribution of steep fronted transients with sub-microsecond rise time, show that the steep fronted transient distributions are quite non-uniform across the coils of the winding and the turns of the coils. In addition, the electrical stress was found highest across turns in coils near the terminal end of the winding. Thus, fast transients subject the inter-turn insulation in coils near the terminal end to very high electrical stress, which can cause breakdown of the thin insulation between the conductors that make the turn of the winding. This high electrical stress results in failure of the motor.

Treating the machine winding as a transmission line presents the simplest approach to analysing voltages due to surges in the stator winding of an electric machine. In this approach, the transmission line equations are used to calculate the voltages at any point on the winding. The parameters of the transmission line are found by approximating the coils as the elemental sections of the line, each represented by a series inductance and a shunt capacitance. This method presents a quick way to evaluate the voltages and has been applied by Knable (1957).

Knable's method has the disadvantage of being incapable of predicting voltage inside the coil. The low pass filtering properties of the winding are not accounted for by this method and any flattening of the surge front must be due to losses. However, Mcleay (1982) and Oyegoke (1997b) have pointed it out that a coil acts as a low pass filter even when losses are not included in the analysis.

The result of an impulse strength test on the turn insulation has been reported by Gupta et al. (1986). Of fifty-three typical coils procured from different manufacturers and tested singly in air, most failures were located at or very near the bends or the nose (or knuckles) where the conductors (strands/turn) had the least consolidation and the most severe misalignment. For 100 nanoseconds rise time impulses, the strength of typical coils varies over a wide range, from about 2 pu to 16 pu. Where one pu is the crest of the rated line to ground voltage. In other words, one pu is given as

$$1\text{pu} = \frac{\sqrt{2}}{\sqrt{3}} * \text{rated line voltage}$$

Weed (1922) showed that the fundamental principle whereby the non-uniformity in voltage distribution and oscillation can be eliminated from the winding, could be stated as follows:
"If the capacitance that is associated with any inductance is so disposed that the initial distribution of a suddenly impressed voltage (which is affected by the capacitance) is uniform with respect to inductance, the growth of current within the inductance will be uniform and the voltage distribution will therefore remain uniform, each element of capacitance receiving charge at the same rate it loses it."

On the basis of the importance of the self-capacitance and the capacitance to the ground, Rudenberg (1940a) adopted a special method of deriving the differential equations for the transformer winding analysis. In his attempt to predict the electric stresses between sections of a transformer winding, he began by considering the behaviour of the network when excited by a single harmonic voltage of an angular frequency w. He then expressed the applied unit function voltage by a Fourier integral of such harmonics. In 1954, Lewis pointed out that while Rudebergs' derivation of the network response to the individual harmonic is correct, his expression for the response of the voltage is not correct, because of inadequate summation of the frequency components. In summation of the components, the relative magnitudes and phases were not considered. The same method was applied to the motor winding by the same author. In Rudebergs' analysis of a motor winding, the elemental unit or cell of the winding was a coil. Rudeberg presumed that the winding has a relatively large number of coils and therefore classified the winding as a system with distributed parameters. Though his method took into consideration the mutual inductance and the mutual capacitance between two adjacent coils, the result obtained for voltage distribution may be inaccurate because generally, phase winding of motors consists of few coils.

The maximum terminal inter-section voltage as predicted by Rudeberg (1940b), is incorrect because of the inadequate summation of various frequency components as mentioned above.

In order to predict the voltage distribution in the motor winding, Lewis (1954) applied a system with lumped parameters in the form of a ladder network. In his work, a coil is a section of the network. If turns were taken as a section of the network, there is a tendency to have some value for turn voltage. Whatever the case is, either a coil or a turn is used as a section of the network. Voltage distribution predicted by this method will not be accurate enough. This is because the method neglects the mutual coupling between the inductance. Another fact is that a unit function voltage has been employed throughout and the resistive effect has been neglected. Therefore, the method cannot be used to analyse the effects of surge rise time that could be of interest in inverter fed motors. In both Lewis' and Weed's work, there is no coil subdivision into slot (iron) and over-hang parts.

Lovass et al. (1963) suggested differential equations of the general alternating ladder network that could take into consideration mutual coupling between two adjacent sections of the network. In their work, apart from the fact that losses are neglected, nothing is mentioned about the non-adjacent sections of the network. This method can be useful if the effect of an arbitrary input voltage is required.

Adjaye and Cornick (1979) applied a method based on a cascade two-port network to analyse the voltage distribution of the winding. In their work, the elemental unit of the network is a coil. It was presumed that the turn voltage is distributed uniformly throughout the coil. This method includes losses, however, if the system is to be modified in order to represent a coil such that voltage across a turn could be accounted for inaccurate results will be yielded, since the method neglects the mutual inductance between sections (coil or turn).

While the above-mentioned previous investigators have developed techniques to predict coil voltage under surge conditions, few attempts have been made to compute voltages within the first coil from the terminal.

A classical technique for inter-turn voltage calculation was developed by Rhudy et al. (1986). In their approach, a lumped element equivalent circuit represents each turn or coil. Such a technique cannot fully take into account wave propagation within a coil and consequently some loss of accuracy might occur.

Techniques utilising the travelling wave theory were proposed by Wright et al. (1983a). They made great contributions in understanding and computing the transient voltage distribution in machine windings, subjected to steep fronted surges. In their work, the multi-conductor transmission line theory is combined with the scatter matrix theory. The model was used by Wright et al. (1983b) to study the influence of coil and surge parameters on the transient inter-turn voltage distribution in the stator winding.

In this research area, Oraee and Mclaren (1985) developed a computational method based on the multi-conductor transmission line theory and the discrete Fourier-Transform algorithm to construct a frequency dependent model for the analysis of the voltage distribution in the first line end coil of stator windings.

The results of the measured and computed voltage distributions on a line-end coil embedded in a solid slot core using Electromagnetic Transient Program (EMTP) were reported by Mclaren and Abdel-Rahman (1988).

In the papers of Wright et al. (1983a), Oraee and Mclaren (1985), Mclaren and Abdel-Rahman (1988), the slot wall was assumed to be a flux barrier at the frequency of interest (1-10 MHz). However, Tavner and Jackson (1988) showed that a laminated slot environment does not act as an impenetrable earth screen at frequencies below (at least a frequency of) 20 MHz.

A computer model for predicting the distribution of steep fronted surges was also developed by Guardado and Cornick (1989). They combined the multi-conductor transmission line model and modal analysis with the parameter assumption of Wright et al. (1983a). Upon application of the coil admittance concept, Guardado and Cornick successfully extended the solution of the voltage distribution in a terminal end coil to a full winding representation.

A report of measurement and analysis of a surge distribution in a motor stator winding was given by Narang et al. (1989). The authors utilised a simple model that provides insight into the relevant mechanisms and a detailed model solved by the Electromagnetic Transients Program (EMTP). The influence of various coil parameters on the inter-turn and line-end coil voltages is also discussed in that paper. To account for the influence of motor terminal leads, the coil is represented by its pi-equivalent circuit.

Following this, Keerthipala and Mclaren (1990) presented the results of experimental recordings. The authors showed that a solid slot model cannot accurately replace the actual laminated slot environment in the study of steep fronted surge propagation in machine windings. From their analysis, it became known that maximum inter-turn voltages observed for the solid slot model are smaller (by a factor of about 2/3) than those for the laminated slot environment. They introduced the concept of surface impedance, but it was not described in their work.

Subsequent authors Qiong et al. (1995) proposed a method for calculating the surface impedance and incorporated it in a model for a pulse propagation study in a turbine generator.

A multi-conductor transmission line approach for calculating the machine winding electrical parameters for switching transient studies over a long period of time has recently been proposed by Guardado and Cornick (1996). The solution technique is based on the solution of one-dimensional diffusion equation. The coil parameters are calculated considering both the magnetic fluxes in the iron and in the air. However, the maximum inter-turn voltage due to steep fronted surge in the winding occurs within the first few microseconds of the first line end coil and therefore does not require a long computation period.
In a publication, Gupta et al. (1987a) reported the results of an extensive programme of surge monitoring. Gupta et al. (1987b) reported the result of impulse strength on the insulation capability of a large ac motor. Findings on why some windings have low strength were also reported by Gupta et al. (1987c). So many papers have been published on surge propagation studies in machine winding that it is very difficult to acknowledge them all.

2.2 Preview of the past works on transient voltage distribution in random winding

With the advent of adjustable speed drives for electrical machines, the problem of non-uniform voltage distribution within the motor winding due to steep fronted surges has extended to low voltage motors.

Persson (1992) investigated the amplitudes and the rise times of the inverter output voltage with particular reference to the Pulse Width Modulated (PWM) inverter. Using the basic transmission theory, Persson carried out simulations regarding voltage reflections for various cable lengths and rise times. The results of simulations are presented graphically by the same author. Further, his analysis confirms potential problems associated with the combination of long cables and short rise times. In addition, application precautions are described.

While only one voltage surge occurs from the circuit breaker when a motor is switched on, the new type of PWM drives using IGBTs can, however, create thousands of surges per second with rise times as short as 100 nanoseconds. Such drives subject the motor stator winding turn insulation to more surges in a few hours of operation than the motor would normally be expected to experience in 20 years of conventional operation.

To date there are few scientific papers published that demonstrate that the surges typical of adjustable speed drives can gradually degrade the turn insulation. The experimental work of Stone et al. (1992) with pure epoxy has conclusively shown that epoxy insulation can gradually age under the action of repetitive voltage surges, even in the absence of partial discharge.

Kaufhold et al. (1996) described the failure mechanism of low voltage inter-turn insulation because of partial discharges (PDs). The authors showed why and how the insulation design, the temperature and the applied voltage affect the failure mechanism. These authors made it clear in their analysis that the partial discharge occurs in the air-filled enamel wires that are touching. The partial discharges erode the insulation and consequently lead to an inter-turn insulation breakdown. The authors characterised the pulse from the converter as oscillating pulses with oscillating frequency ω and damping time constant T. The authors have successfully shown that in the air-filled gaps between the enamel wires that are touching one another, repetitive pulses with very steep front, lead to an increased number of partial discharge per time unit for greater values of ωT.

Bell and Sung (1996) and Kaufhold et al. (1996) concluded that the dielectric failure mechanism due to repetitive transient does not lead to immediate failure of the insulation, but it happens to be a gradual process determined by a lower limit imposed by corona inception voltage (CIV) or partial discharge.

As adjustable speed drives become more popular in the higher voltage ranges, we will have to watch carefully to ensure that insulation problems do not increase. In addressing this problem Oliver and Stone (1995) present

a broad overview of the types of adjustable speed drive converters. Their paper also covers a brief description of the effect of steep fronted surges in form winding near the line end.

From the experimental work performed on form windings (used on high and medium voltage motors) to study the distribution of voltage under surge conditions, Oyegoke (1997b), confirmed the work of the previous authors in showing that the highest voltage stress occurs on the first terminal-end coil. Distribution of voltage among turns of the first terminal-end coil being practically non-uniform for very steep fronted surges is also reported.

Switching frequencies of 10 to 20 kHz with 0.1 microsecond rise times are common with the current IGBT technology. In many applications the PWM inverter and the motor must be at separate locations, thus requiring long motor leads. Von Jouanne et al. (1995) examined the effect of long motor leads on high frequency PWM inverter fed drives. In their paper, cable transmission theory and cable capacitance analyses are presented. The voltage reflections were investigated in a similar way to that of Persson (1992), by using the Bewley lattice diagram technique. The effect of the inverter output pulse rise time and the cable length on the voltage magnitude at the terminals of the motor is illustrated in their paper. Results of simulation were experimentally verified.

The area where much confusion still exists in pulse width modulated adjustable speed drives is with the voltage waveform impact on the motor performance. The reports of Bonnett (1994), (1996) considered the effects of the maximum voltage, rate of rise, switching frequencies, resonance and harmonics. It is stated in his work that over-voltage and ringing can occur at both the beginning and end of each pulse from the inverter. However, it is the repetitions, along with the rise time, that have the most potential for insulation damage. The fact that as much as 85 % of the peak over-voltage can be dropped across the first turn of the first coil is mentioned. This is illustrated with a figure showing the range of the voltage drop across the first turns of the coil as a function of the voltage rise time. Similar studies have been discussed by Melfi et al. (1997) but with particular attention to the machines powered by the 1990's preferred drive of choice, (PWM ASD using IGBT technology) with a rise time in the range 50-200 nanoseconds. Mainly through experimental work, Melfi et al. (1997) have shown that the ASD induced transient voltage pulse at the motor terminals penetrates into the winding via oscillatory and travelling wave modes. Pulse propagation into the winding via travelling mode is not linearly distributed. For a rise time of 50 nanoseconds, 80 % of the terminal voltage appears across the first coil group, for instance in a machine with 6 coil groups per phase. The highest voltage stress between any two turns of winding which may be in contact was found to exist from the first turns of the line end coil to the last turns of the coil group.

Factors affecting motor over-voltage are discussed by Saunders et al. (1996) and shown to be as follows:

* Motor and cable surge impedance
* Motor load
* Cable length
* Magnitude of drive pulse
* Rise time of drive pulse
* Spacing of PWM pulses

Kerkman et al. (1996) and Skibinski et al. (1997) have made reports about the importance of cable natural oscillation frequency. In addition to rise time related excitation frequency in determining the maximum motor terminal voltage and the cable damping time, the line-to-line voltage polarity reversal is described as a new contributor to motor over-voltage. The fact that the type of modulator establishes the operating regions where over-voltage is of concern is also discussed. In addition to these, Kerkman et al. (1997) discussed the over-voltage reduction through pulse control, and the over-voltage reduction modification in the modulating signal.

The power supplied to the motor by a PWM inverter has some adverse effects such as increased heating, high peak voltages and increased audible noise. Lowery et al. (1994), highlighted some of the known possible

adverse effects PWM inverters cause low voltage induction motors and the impact these effects have on the given application. Some areas highlighted by Lowery and Petro (1994) include motor noise caused by different transistor types and switching strategies; additional motor heating produced by PWM inverter power and the operating speed-torque range; the effect that PWM inverter produced harmonics have on the low voltage induction motor; PWM inverter designs and their effect on motor insulation systems; voltage transient generated by semiconductor switching technologies employed in PWM inverters with particular attention to calculation of critical cable lengths to enhance an accurate determination of voltage pulse values at the motor terminals.

Controlling industrial motors with variable frequency drives such as those featuring pulse width modulation technology is becoming increasingly common because of speed control and energy saving advantages. Care should be taken to understand the consequences of applying such drives for a motor. Mecker (1992) examines the impact of variable frequency drives on motor insulation and cooling system. His work also includes recommendations to ensure reliable system designs.

In the 1980's, current source inverter (CSI) drive technology was widely used. Investigation of how well an ASD-powered low voltage mush wound machine withstands repetitive surge voltage was done by Quirt (1988). One important characteristic of such drive is that they produce a 1200-Volt spike with a 400 microseconds rise time at a rate of six times per 60 Hz cycles. This slow rise time allows a linear distribution of voltage across the windings. Although there is an increase in the volts per turn stress, this voltage is found to be below destructive levels.

Mechorn and Tang (1995) developed an EMTP model to simulate the behaviour of the drive-motor operation. The simulated inverter output voltage and motor terminal voltage correspond well with the measured results. However, nothing is mentioned of the internal voltage distribution among the coils and turns of the coil. In addition, from the motor terminal voltage measurement, the authors derived the characteristic impedance of the 25-hp motor and expressed it in terms of surge impedance of the cable. It should, however, be mentioned that the knowledge of the motor surge impedance is no substitution for an accurate prediction of the voltage at the motor terminal. This is because this impedance itself is not responsible for the increase in voltage at the motor terminal. Using the impedance to determine the peak terminal voltage could be misleading because it depends on many other factors apart from the cable length.

Hyppio (1995) studied the effect of feeder cable and described a simulation procedure to compute machine terminal voltage transient.

In future, the tendency of combining the frequency converter and large motors (form winding motors) cannot be ruled out. A detailed method for simulating the voltage distribution due to steep fronted inverter output voltage was described by Tang (1997) who proposed an equivalent circuit model for a line-end coil and solved the voltage by using a finite difference method. A simple method for calculating the voltage distribution is also discussed by the same author. His simplified method is similar to the method described by Oyegoke (1997).

2.3 Methods for computing voltage transients

There is not much difference between the methods of computing the voltage transients in transmission line systems and in the stator windings of electric motors, at least as applied by different authors so far. The methods presented in the previous section will fall into one of the following:

1. Lumped-parameter method
2. Fourier-transform method
3. Travelling-wave method

Though each of these methods has its own weakness, still they provide information that could help in understanding the transient voltage distribution within the winding of an electric machine subjected to a steep-fronted surge.

2.4 Basics of each method

2.4.1 Lumped-parameter method

This is a traditional method of calculating the transients in a power system and it uses the equivalent circuit with lumped elements, inductance, capacitance and resistance. The cables are represented by an artificial line made up of lumped elements arranged in a series of pi-sections.

2.4.2 Fourier-transform method

The frequency dependence of machine winding parameters, i.e. resistance, inductance and capacitance, can be accounted for by the use of the method based on the Fourier transform.

The basis of this method is that the response of the machine winding is found over the range of frequencies and the inverse Fourier transform is used to transform the result from the frequency domain into the time domain.

Response of a transmission line using the Fourier Transform can be described by considering a single-phase line whose frequency response is

$$A(w) = e^{-d(w)*l} \tag{1}$$

where
l is the length of the line
d is the propagation coefficient of the line

$$\begin{aligned} d(w) &= \sqrt{Z(w)\cdot Y(w)} \\ Z(w) &= R + jwL \\ Y(w) &= G + jwC \end{aligned} \tag{2}$$

where $R, L, C,$ and G are the resistance, inductance, capacitance and conductance of the line, respectively. The response of the line to step input is given as

$$A^1(w) = \frac{e^{-d(w)l}}{jw} \tag{3}$$

Response in the time domain is computed by applying the inverse Fourier transform

$$F(t) = \frac{1}{2p}\int_{-\infty}^{\infty} \frac{e^{-d(w)l}}{jw} e^{jwt}\, dw \tag{4}$$

The step response for a multi-phase system is found in a similar way by first transforming the multi-phase of the system into another set of components that have no mutual coupling between them.

2.4.3 Travelling-wave method

The transmission line equations are given as

$$\frac{dV}{dx} = -ZI = -(R + sL)I$$

$$\frac{dI}{dx} = -YV = -(G + sC)V \qquad (5)$$

where x is the distance along the line and $s = jw$.
It is possible to solve the above equations in many ways and use the solution to calculate the transient phenomena. Among the methods of solution to the above equations, one can include the Laplace transform method, the graphical method of Schnyder and Bergeron developed in 1930, and the lattice diagram technique described by Bewley in 1933. Though these methods differ from one another, the same result will be yielded, if the same assumptions are made.

2.5 Conclusion

From the literature review presented in the preceding part it is noticed that a steep fronted surge that strikes a stator winding results in a large voltage being impressed across the inter-turn insulation in the motor coil connected to the high voltage terminal. Distribution of voltage across the high voltage motor coils is not uniform. In short, the high frequency contact (in the megahertz range) of the surge voltage results in the capacitive division of the surge across the turn insulation, rather than control by the inductance. The shorter the rise times of the surge, the higher the frequency content and the greater the voltage across the first few turns of the winding. For a rise time greater than about 1000 nanoseconds, the voltage distribution among turns of the terminal end coil becomes practically uniform. In other words, no significant surge voltage exists across the turn insulation.

If a motor winding is subjected to high fast-fronted surges, then the breakdown strength of the turn insulation may be exceeded, causing turn insulation breakdown. The consequence of the turn insulation breakdown is that a considerable large circulating current occurs through the coil, which melts the ground insulation.

While much has been done on the voltage calculation in the form winding commonly used on high and medium voltage motors, the special factors involving the system parameters to be used for voltage calculation are not well covered by the literature. In addition, few authors discussed the detail of their experimental work on the subject. Until now, few articles have been available discussing voltage distribution in the winding of low voltage machines, where random windings are commonly used.

2.6 Aim and Contents of the present work

Taking into account the existing publications on the voltage distribution in the stator winding of induction motor confronted by fast rising voltage, the primary objective of this research work is to develop a method or methods capable of predicting the distribution and magnitude of fast rising (steep fronted) voltage in the stator winding of electrical machines fed from frequency converters.

To achieve this objective the following works are done:
- Study of the general theory of the multi-conductor transmission line theory as applied to the machine winding
- Methods of calculating the winding parameters to be used in voltage calculation are examined
- Detailed experimental work of surge propagation studies on form winding (commonly used on medium and high voltage machines)
- Three methods for voltage calculation on a form winding and comparison of results are studied
- Two methods for voltage calculation on a random winding are presented
- Detailed experimental work of surge propagation studies on random winding (commonly used in low voltage machines)
- Comparison between measured and computed voltages on the random winding machines

The main part of the present work has been published in the following journals and conference proceedings:
1. Oyegoke, B. S. 1997. Multiconductor Transmission Line and Bewley Lattice Diagram Techniques for the Transient Inter-turn Voltages in Electrical Machine Fed from a Frequency Converter. The Tenth Symposium on Electrical Apparatus and Technologies, Siela'97, 30-31 May, Plovdiv, Bulgaria, Conference Proceedings Vol. 1, pp. 251-256.

2. Oyegoke, B. S. 1997. Indirect Boundary Integral Equation Method as Applied for wave Propagation in the Stator Winding of an Electric Machine. IEE Proc.-Sci. Meas. Technol., Vol. 144 No. 5, pp. 223-227.

3. Oyegoke, B. S. 2000. A Comparative Analysis of Methods for Calculating the Transient Voltage Distribution within the Stator Winding of an Electric Machine Subjected to Steep-Fronted Surge. Electrical Engineering (Archiv für Elektrotechnik), Vol. 82 No 3-4, pp. 173-182.

4. Oyegoke, B. S. 1999. Effect of the Overhang Capacitance on Fast-rising surge Distribution in Winding of a Large AC Motor. IEE Proc.-Sci. Meas. Technol., Vol. 146 No. 6, pp. 299-303.

5. Oyegoke, B. S. 1999. Simulating the Voltage Distribution due to the PWM Voltage Patter in the Stator Winding of a Low Voltage Induction Motor. IEEE International Symposium on Diagnostics for Electrical Machines, Power Electronics and Drives, IEEE SDEMPED'99, 1-3 September Gijön, Spain, Conference Proceedings, pp. 125-130.

6. Oyegoke, B., Lampola, P. 1999. Effect of the PWM Inverter Output Voltage on the Stator Windings of Induction Motors. 8th European Conference on Power Electronics and Applications EPE'99, 7-9 September Lausanne Switzerland.

7. Oyegoke, B. S. 2000. Voltage Distribution in the Stator Winding of an Induction Motor Following a Voltage Surge. Electrical Engineering (Archiv für Elektrotechnik), Vol. 82 No 3-4, pp. 199-205.

3 METHODS USED IN THE PRESENT WORK

This chapter focuses on how the multi-conductor transmission line theory can be applied to electrical machine winding. Machine winding is divided into parts. The basic transmission line equation is written for a part of winding consisting of three lines in parallel.

3.1 Coil and its subdivision into parts

For the purpose of voltage calculation within the first line-end coil of an electrical machine, the turn conductors have to be modelled as a transmission line. To model turn conductors as transmission lines, the first line-end coil has been divided into five parts, defined by the cable and the slot junctions (j1, j2, j3, j4, j5) as shown in Fig. 1, for the first line-end coil consisting of eleven turns. The five parts are modelled separately as untransposed lines and interconnected in an appropriate manner to form a coil. Mutual coupling among coil parts is neglected on the following basis.

The two over-hang parts on the opposite sides of the stator core are considered uncoupled because eddy-current in the core lamination provides effective shielding at high frequencies. Over-hang and slot parts are uncoupled because of the eddy-current in the lamination core. The two parts of the coil at the coil-entry are uncoupled since they are nearly perpendicular to each other over most of their length and are further shielded from each other by eddy-currents in adjacent coils.

Insulation between the lamination permits magnetic coupling to the coils inside adjacent slots, Tavner and Jackson (1988). However, the two slot parts of the coil under study are not coupled because of the eddy-current in the neighbouring coils. The resulting eddy-currents in neighbouring coils are considered more

effective in shielding the two parts of the coil under study. These subdivision techniques make the multi-conductor transmission line applicable to the stator coil.

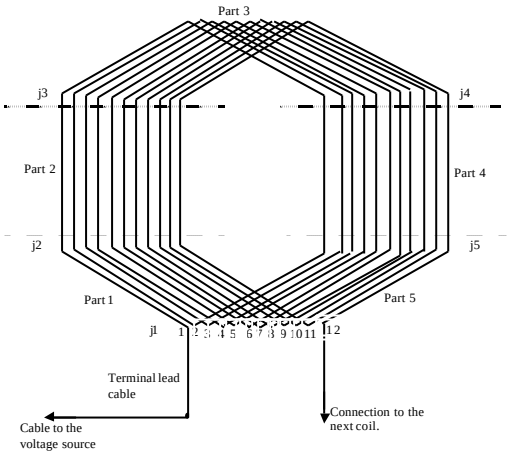

Fig. 1: Coil and its subdivisions into parts.

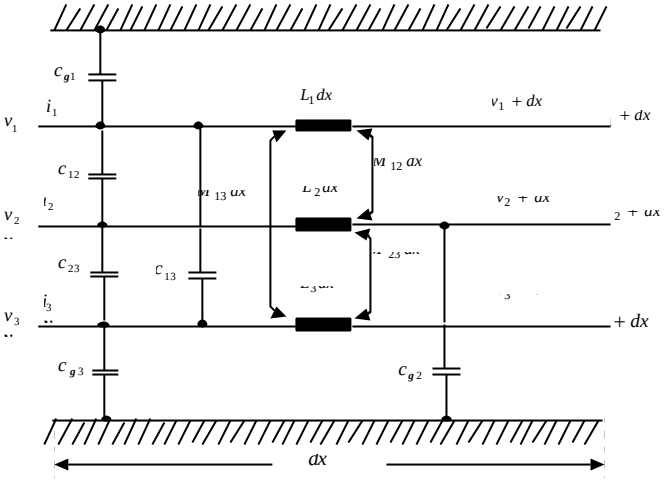

Fig. 2: Elemental part of a three-turn coil.

3.2 Multi-conductor transmission line theory

The basic theory of the multi-conductor transmission line is described in this section for an elemental part consisting of three conductors in parallel. The theory is explained here for the case of lossless three conductor lines. In an elemental part of three conductor lines in Fig. 2, there is capacitance to ground and mutual capacitance. In addition, there is inductance and the mutual inductance between the lines. Therefore, it is possible to write the following equations:
For the currents

$$di_1 = -C_{g1}dx\frac{dv_1}{dt} - C_{12}dx\frac{d}{dt}(v_1 - v_2) - C_{13}dx\frac{d}{dt}(v_1 - v_3)$$

$$di_2 = -C_{g2}dx\frac{dv_2}{dt} - C_{21}dx\frac{d}{dt}(v_2 - v_1) - C_{23}dx\frac{d}{dt}(v_2 - v_3)$$

$$di_3 = -C_{g3}dx\frac{dv_3}{dt} - C_{31}dx\frac{d}{dt}(v_3 - v_2) - C_{31}dx\frac{d}{dt}(v_3 - v_1)$$

or

$$\frac{di_1}{dx} = -(C_{g1} + C_{12} + C_{13})\frac{dv_1}{dt} + C_{12}\frac{dv_2}{dt} + C_{13}\frac{dv_3}{dt}$$

$$\frac{di_2}{dx} = -(C_{g2} + C_{21} + C_{23})\frac{dv_2}{dt} + C_{21}\frac{dv_1}{dt} + C_{23}\frac{dv_3}{dt}$$

$$\frac{di_3}{dx} = -(C_{g3} + C_{32} + C_{31})\frac{dv_3}{dt} + C_{32}\frac{dv_2}{dt} + C_{31}\frac{dv_1}{dt}$$

In matrix form

$$\frac{d}{dx}\begin{bmatrix} i_1 \\ i_2 \\ i_3 \end{bmatrix} = -\begin{bmatrix} C_{g1}+C_{12}+C_{13} & -C_{12} & -C_{13} \\ -C_{21} & C_{g2}+C_{21}+C_{23} & -C_{23} \\ -C_{31} & -C_{32} & C_{g3}+C_{31}+C_{32} \end{bmatrix}\frac{d}{dt}\begin{bmatrix} v_1 \\ v_2 \\ v_3 \end{bmatrix} \tag{6}$$

or

$$\frac{d}{dx}[\boldsymbol{I}] = -[\boldsymbol{C}]\frac{d}{dt}[\boldsymbol{V}] \tag{6´}$$

In addition, the following equation can be written for the voltages

$$dv_1 = -L_1 dx\,\frac{di_1}{dt} - M_{12}dx\,\frac{di_2}{dt} - M_{13}dx\,\frac{di_3}{dt}$$

$$dv_2 = -M_{21}dx\,\frac{di_1}{dt} - L_2 dx\,\frac{di_2}{dt} - M_{23}dx\,\frac{di_3}{dt}$$

$$dv_3 = -M_{31}dx\,\frac{di_1}{dt} - M_{32}dx\,\frac{di_2}{dt} - L_3 dx\,\frac{di_3}{dt}$$

or

$$\frac{dv_1}{dx} = -L_1\frac{di_1}{dt} - M_{12}\frac{di_2}{dt} - M_{13}\frac{di_3}{dt}$$

$$\frac{dv_2}{dx} = -M_{12}\frac{di_1}{dt} - L_2\frac{di_2}{dt} - M_{23}\frac{di_3}{dt}$$

$$\frac{dv_3}{dx} = -M_{31}\frac{di_1}{dt} - M_{32}\frac{di_2}{dt} - L_3\frac{di_3}{dt}$$

In matrix form

$$\frac{d}{dx}\begin{bmatrix} v_1 \\ v_2 \\ v_3 \end{bmatrix} = -\begin{bmatrix} L_1 & M_{12} & M_{13} \\ M_{21} & L_2 & M_{23} \\ M_{31} & M_{32} & L_3 \end{bmatrix}\frac{d}{dt}\begin{bmatrix} i_1 \\ i_2 \\ i_3 \end{bmatrix} \tag{7}$$

$$\frac{d}{dx}[\boldsymbol{V}] = -[\boldsymbol{L}]\frac{d}{dt}[\boldsymbol{I}] \tag{7'}$$

Differentiating Eq.7' with respect to x will give

$$\frac{d^2}{dx^2}[\boldsymbol{V}] = -[\boldsymbol{L}]\frac{d^2}{dxdt}[\boldsymbol{I}] \tag{8}$$

Differentiating Eq.6' with respect to t will give

$$\frac{d^2}{dxdt}[\boldsymbol{I}] = -[\boldsymbol{C}]\frac{d^2}{dt^2}[\boldsymbol{V}] \tag{9}$$

A combination of Eqs.8 and 9 gives Eq.10

$$\frac{d^2}{dx^2}[\boldsymbol{V}] = [\boldsymbol{L}][\boldsymbol{C}]\frac{d^2}{dt^2}[\boldsymbol{V}] \tag{10}$$

It has been proved by Weeks (1972) that for lossless lines in a uniform perfect dielectric

$$[\boldsymbol{L}][\boldsymbol{C}] = \frac{1}{u^2}[\mathbf{1}]$$

where

$[\mathbf{1}]$ is a unit matrix, u the propagation velocity, which on the other hand can be expressed with respect to the velocity of light as

$$u = \frac{1}{\sqrt{e_0 e_r \mu_0 \mu_r}} = \frac{c}{\sqrt{e_r \mu_r}} \tag{11}$$

where

$c = \frac{1}{\sqrt{e_0 \mu_0}} = 3 \cdot 10^8$ m/s is the velocity of light

$e_0 = 8.85 \cdot 10^{-12}$ F/m

$\mu_0 = 4p \cdot 10^{-7}$ H/m

Henceforth, for three lines in parallel, Eq.10 becomes

$$\frac{d^2}{dx^2}\begin{bmatrix} v_1 \\ v_2 \\ v_3 \end{bmatrix} = \frac{1}{u^2}\begin{bmatrix} 1 & 0 & 0 \\ 0 & 1 & 0 \\ 0 & 0 & 1 \end{bmatrix}\frac{d^2}{dt^2}\begin{bmatrix} v_1 \\ v_2 \\ v_3 \end{bmatrix} \tag{12}$$

where

$$\frac{d^2v_1}{dx^2} = \frac{1}{u^2}\frac{d^2v_1}{dt^2}$$

$$\frac{d^2v_2}{dx^2} = \frac{1}{u^2}\frac{d^2v_2}{dt^2} \qquad (12')$$

$$\frac{d^2v_3}{dx^2} = \frac{1}{u^2}\frac{d^2v_3}{dt^2}$$

with the solution in the form of

$$\begin{aligned} v_1 &= \overline{v_1}\P\left(x \pm ut\right) \\ v_2 &= \overline{v_2}\P\left(x \pm ut\right) \\ v_3 &= \overline{v_3}\P\left(x \pm ut\right) \end{aligned} \qquad (13)$$

where $\P(t)$ is the Dirac function 'delta function' (or impulse function) which is mathematically equivalent to the effect of a unit concentrated source at time t.

From Eq.7

$$\frac{d}{dx}\begin{bmatrix} v_1 \\ v_2 \\ v_3 \end{bmatrix} = \begin{bmatrix} v_1 \\ v_2 \\ v_3 \end{bmatrix} = -\begin{bmatrix} L_1 & M_{12} & M_{13} \\ M_{21} & L_2 & M_{23} \\ M_{31} & M_{32} & L_3 \end{bmatrix}\frac{d}{dt}\begin{bmatrix} i_1 \\ i_2 \\ i_3 \end{bmatrix} \qquad (14)$$

also

$$\frac{d}{dt}\begin{bmatrix} i_1 \\ i_2 \\ i_3 \end{bmatrix} = \pm u\begin{bmatrix} i_1 \\ i_2 \\ i_3 \end{bmatrix} \qquad (15)$$

From Eqs.14 and 15

$$\begin{bmatrix} v_1 \\ v_2 \\ v_3 \end{bmatrix} = \mp u\begin{bmatrix} L_1 & M_{12} & M_{13} \\ M_{21} & L_2 & M_{23} \\ M_{31} & M_{32} & L_3 \end{bmatrix}\begin{bmatrix} i_1 \\ i_2 \\ i_3 \end{bmatrix}$$

or

$$[\boldsymbol{V}] = \mp[\boldsymbol{Z}][\boldsymbol{I}] \qquad (16)$$

where

$$Z = u\begin{bmatrix} L_1 & M_{12} & M_{13} \\ M_{21} & L_2 & M_{23} \\ M_{31} & M_{32} & L_3 \end{bmatrix} = \mathrm{u}[\boldsymbol{L}]$$

and from above

$$[\boldsymbol{L}][\boldsymbol{C}] = \frac{1}{u^2}[1]$$

$$[\boldsymbol{L}] = \frac{1}{u^2}[\boldsymbol{C}]^{-1} \tag{17}$$

The characteristic impedance is

$$\boldsymbol{Z} = \frac{1}{u}[\boldsymbol{C}]^{-1} \tag{18}$$

The characteristic admittance is

$$\boldsymbol{Y} = \boldsymbol{Z}^{-1} = u[\boldsymbol{C}] \tag{19}$$

From the fundamental equation of the transmission line described above, it can be seen that the knowledge of the capacitance matrix and the propagation velocity inside the winding is sufficient for the calculation of the voltage distribution. Alternatively, the propagation velocity may be combined with the inductance matrix.

4 COMPUTATION OF WINDING PARAMETERS

Whichever method is to be applied for the voltage calculation, the principal problem is calculating the winding parameters to be used in calculations e.g. capacitance, inductance, and losses. Hence, the task in this chapter is to describe various ways of calculating the winding parameters that may be necessary for the transient voltage calculation.

In fact, capacitance is the most straightforward to calculate and it involves computations based on geometry and permittivity. In the following section, three techniques for the capacitance calculation are presented.
Inductance calculations are the most difficult, since they involve problems related to magnetic flux penetration in a laminated iron structure at high frequencies. Probably the easiest way to overcome this difficulty is to assume that the magnetic flux does not penetrate the iron laminations at all and the iron acts as a boundary within which the flux is constrained. A specialised computer program can be used to calculate the inductance. Alternatively, calculation of inductance can be based on the theory of flux penetrations in a slab at high frequency, estimating the effective permeability of the iron, and then performing an inductance calculation.

The duality existing between the electric and magnetic field for a homogeneous medium presents a third alternative means for inductance calculation. This method utilises the relationship between a constantly assumed wave velocity in the winding and the capacitance as shown in the previous section.

The assumption that the magnetic flux does not penetrate the iron lamination, or that the iron acts as a boundary within which the flux is constrained, simply treats the laminated slot environment as a solid conductor whereby the depth of penetration is very small at high frequency. This assumption has been used in the present studies. A satisfactory result of voltage distribution has been obtained in the present study despite the fact that Tavner and Jackson (1988) showed that a laminated slot environment does not act as an impenetrable earth screen at frequencies below a frequency of 20 MHz.

Magnetic flux distribution in the slot and over-hang part of the first line-end coil of an electrical machine for instance at 1 MHz and 10 MHz is shown in Fig. 3.

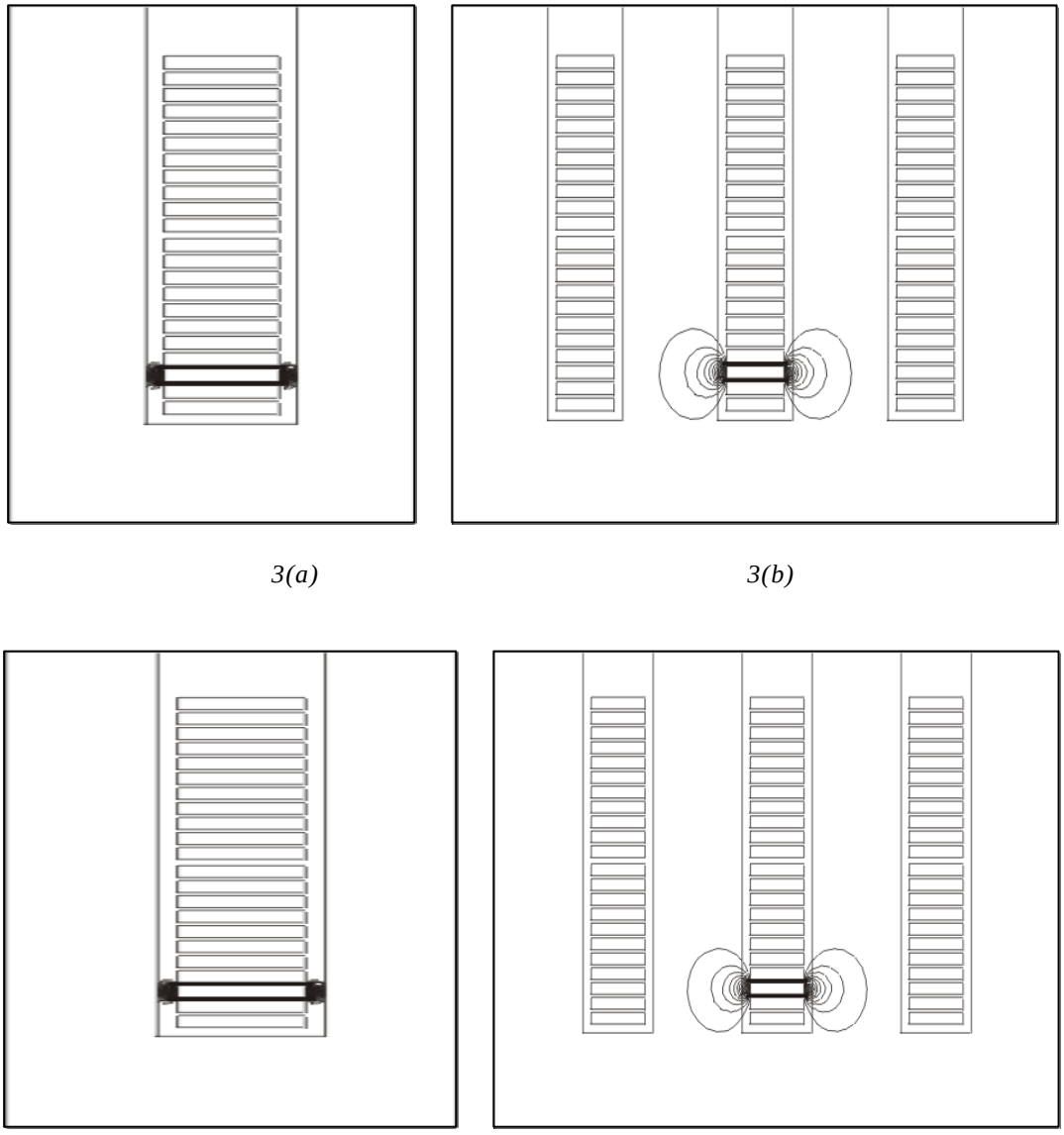

3(a) *3(b)*

3(c) *3(d)*

Fig. 3(a), (b), (c), (d) : Flux plot for the slot and over-hang part of the first line-end coil.
(a) Flux plot inside the slot at 1 MHz,(b) Flux plot in the over-hang part at 1 MHz,
(c) *Flux plot inside the slot at 10 MHz, (d) Flux plot in the over-hang part at 10 MHz.*

4.1 Parallel plate capacitor approximation

In the form winding, the system of turn conductors in the slot and in the over-hang region shows rectangular symmetry. Turn conductors are parallel to each other. In addition, slot walls are parallel to turn conductor surfaces. Treating the slot wall as an equipotential surface, capacitance between slot wall and turn and between turn conductors can be computed using the parallel-plate capacitor approximation.

$$c = \frac{e_0 e_r b_s}{d} \tag{16}$$

where c is the capacitance per unit length, b_s is the conductor width, and d is the separation between conductors or between conductor and slot wall. The same way the capacitance in the over-hang region can be modelled. However, the role of the slot wall is played by the sides of the adjacent coils in the over-hang region.

4.2 Indirect boundary integral equation method

To determine the partial capacitance between conductor i and all the other conductors, a two-dimensional Laplace equation for the electric scalar potential u

$$\frac{\partial^2 u}{\partial x^2} + \frac{\partial^2 u}{\partial y^2} = 0 \tag{17}$$

has to be solved under the following assumptions:
1. Inter-conductor capacitance exists between turn conductor sides in the same slot.
2. All conductor sides in the same slot, except for the conductor side under consideration, are at zero potential.
3. The stator core is at zero potential.

The second and third assumptions are referred to as Dirichlet boundary conditions and can be formulated mathematically as follows:

$$u(r_i) = 1\ ;\ \ u(r_{n+1}) = 0;\ \ u(r_j) = 0, \qquad \begin{matrix} j = 1,\ldots..,n \\ j \neq i \end{matrix}\ , \tag{18}$$

where r_i and r_j are the cross-section boundaries of the i-th and j-th conductors; $r_{n+1} = r_g$ is the slot boundary. Setting the unit potential to the conductor i does not lead to a loss of generality, due to the linearity of the problem.

The solution of the Laplace equation is presented as a single layer potential in the form

$$u(P) = -\frac{1}{4\mathrm{p}} \sum_{i=1}^{n+1} \oint_{r_i} s_{(\mathrm{M}_i)} \ln(r^2_{PMi}) dr_i + A, \tag{19}$$

where

s	is the unknown density of the single layer (having the physical sense of charge density);
P, M_i	are the points of observation and influence respectively;
$r_{\mathrm{PM}i}$	is the distance between the points P and M_i ;
A	is an arbitrary constant.

Applying Eq.19 to the boundary $r = \sum_{i=1}^{n+1} r_i$ and taking into account the boundary conditions in Eq.18, the following system of integral equations of the first kind is obtained

$$\begin{aligned} &-\frac{1}{4\pi} \sum_{j=1}^{n+1} \oint_{r_j} s_{(\mathrm{M}_j)} \ln(r^2_{Q_k M_j}) dr_j + A = 1, \quad Q_k \in r_k\ ;\ k = i \\ &-\frac{1}{4\pi} \sum_{j=1}^{n+1} \oint_{r_j} s_{(\mathrm{M}_j)} \ln(r^2_{Q_k M_j}) dr_j + A = 0, \quad Q_k \in r_k\ ;\ \begin{matrix} k = 1 \div n+1 \\ k \neq i \end{matrix} \end{aligned} \tag{20}$$

To determine the constant A and to avoid the logarithmic behaviour of the potential at infinity, the following equation has been added and solved together with Eq. 20

$$\sum_{j=1}^{n+1} \oint_{r_j} s_{(M_j)} dr_j = 0 . \tag{21}$$

The partial capacitance C_{ij} between conductor i and conductor j is defined by

$$C_{ij} = \varepsilon \left| \int_{r_j} s_{(M_j)} dr_j \right| . \tag{22}$$

4.3 Finite element method

There is not much difference between the finite method and the indirect boundary integral equation method discussed in the previous section. This is because both methods involve discretization of the boundary into segments. In addition, the matrix involved in calculation is dense.

In the finite element sense, the solution of the Laplace equation in terms of potential can be written as

$$U_0(r) = \sum_{i=1}^{n+1} \int_{?s_i} s_i(r') G\left(r \diagup r'\right) ds' \tag{23}$$

where the Green function is

$$G\left(r \diagup r' \right) = -\frac{1}{2\pi e} \ln \left| r - r' \right| \tag{24}$$

or

$$U_0(r) = -\frac{1}{4\pi e} \sum_{i=1}^{n+1} \int_{?s_i} s_i(r') \ln \left| r - r' \right|^2 ds'$$

(25)

It can be seen that in Eq. 25, the integration constant is missing and this makes it different from the indirect boundary integral equation method described earlier.

4.3.1 Finite element solution

The cross-section boundary of each conductor is divided into segments. Each function $s_i(r')$ is now approximated within its domain by a set of linearly independent basis function b_{ik}:

$$s_i(r') = \sum_{k=1}^{m} L_{ik} b_{ik}(r') \tag{26}$$

Application of the Galerkin method to the equation will help to determine the coefficients L and hence the charge distribution which is the solution of the problem.

In the Galerkin procedure, equations 25 and 26 are combined. The resulting equation is multiplied on both sides by one of the basis functions associated with the jth segment, b_{jl}, and integrated over this subdomain giving

$$\int_{?s_j} U_0(r)b_{jl}(r)ds = -\frac{1}{4pe}\sum_{i=1}^{n+1}\sum_{k=1}^{m} L_{ik}\int_{?s_j}\int_{?s_i} b_{ik}(r')b_{jl}(r)\ln|r-r'|^2 ds' ds \qquad (27)$$

$$j = 1,2,3.....n+1$$
$$l \neq j$$

In matrix form

$$\boldsymbol{U} = \boldsymbol{bL} \qquad (28)$$

Once $\boldsymbol{L}$ is known, the charge distribution computed from Eq. 28 and the capacitance is determined from the total charge on the conductor in similar way to that given by Eq. 22.

The solution of the Laplace equation using the Galerkin procedure corresponds to the boundary element method whereby many Gauss points are used within each domain (segment). However, in many applications such as the one under consideration, it is sufficient to take the surface charge to be constant within each subdomain. This is often referred to as piecewise constant approximation.

4.3.2 Piecewise constant approximation

As mentioned above, the surface charge is taken to be constant within each subdomain. Therefore, Eq. 27 becomes

$$\int_{?s_j} U_0(r)ds = -\frac{1}{4pe}\sum_{i=1}^{n+1}\int_{?s_j}\int_{?s_i} s_i(r')\ln|r-r'|ds'ds \qquad (29)$$

where s_i is constant within each subdomain. Let $q_i = s_i ?s_i$, obviously, q_i is the charge on a unit length strip Δs_i wide of one or other of the turn conductors. If U_j is the average potential on the jth strip, then from Eq. 29 we have

$$U_j = -\frac{1}{4pe}\sum_{i=1}^{n+1}\frac{q_i}{?s_i\,?s_j}\int_{?s_j}\int_{?s_i}\ln|r-r'|^2 ds'ds \qquad (30)$$

This in matrix form becomes

$$\boldsymbol{U} = \boldsymbol{bQ} \qquad (31)$$

where $\boldsymbol{U}$ and $\boldsymbol{Q}$ have significance as voltage and charge.

The matrix $\boldsymbol{b}$ is defined by

$$b_{ij} = -\frac{1}{4pe\,?s_i\,?s_j}\int_{?s_i}\int_{?s_j}\ln|r-r'|^2 ds'ds \qquad (32)$$

To compute b_{ii} it is necessary to consider a straight-line element aligned with one of the axes.

$$b_{ii} = -\frac{1}{4pe?s_i^2}\int_0^{?s_i}\int_0^{?s_j}\ln|x-x'|dx'dx \tag{33}$$

This method should be handled with care when calculating the capacitance involving say two conductors. Application of this method to a capacitance problem involving two objects will necessitate inclusion of the integration constant *A* and hence an additional equation in a similar way to that in indirect boundary integral equation method.

4.4 Method for resistance calculation

The spectral content of a fast fronted surge is of very high frequency. Consequently, the surge current in the coil conductors will be severely skin-effect limited and is assumed to have a negligible effect on the inductance matrix of the coil part.

The resistance matrix is calculated in a similar manner to that used for overhead transmission lines from the sum of the losses in the forward and return paths. The forward losses are due mainly to the displacement current or skin effect phenomena and are calculated from Z_{sk}.

$$Z_{\text{sk}} = \frac{l}{a\,d\,s} \tag{34}$$

The skin depth "δ" is given by

$$d = \sqrt{\frac{2}{?\,\mu s}}$$

where l is the length of the turn, w is the angular frequency, s is the copper conductivity and a is the perimeter of conductor.

The skin depth can be calculated for any frequency component by treating the current as flowing in the skin depth layer corresponding to the chosen frequency. In order to simplify the analysis in the time domain, a single frequency value has been selected for the loss evaluation. According to the other authors Wright et al. (1983a), this frequency is such that a quarter wave corresponds to the rise time of the applied voltage pulse. However, since there is no method available for calculating the resistance due to the return path in such a complex geometry as an electrical machine, it has been found a good choice to assume that these losses are of the same magnitude as those of the forward path, in accordance with the previous authors Guardado and Cornick (1989). Hence,

$$R_{\text{sk}} = 2Z_{\text{sk}} \tag{35}$$

Proximity effect due to an adjacent conductor has been considered in accordance with the other authors Wright et al. (1983a). Typical values of skin depth penetration with the relevant high frequencies are 0.066 mm and 0.021 mm respectively, for 1 MHz and 10 MHz.

4.4.1 Proximity effect

The resistance computed by Eq.35 takes into consideration only the skin effect. However, the effect of the other conductors in the same slot should be taken into account, hence the proximity effect.

Proximity effect calculation is a complex problem, but a simple way of accounting for it has been proposed by Lammenal and Stalf (1966). The resistance value for voltage calculation has its final form given by

$$R_{sm} = R_{sk} K_{proximity} \tag{36}$$

where $K_{proximity}$ is calculated in the following way by Lammenal and Stalf 1966

$$K_{proximity} = \left(1 + \frac{2}{3}\left(n^2 - 1\right)\right), \tag{37}$$

where n is the number of turns in the coil. Wright et al. (1983a) found it a good choice to consider the proximity effect due to adjacent conductors, i.e. n = 3 for a coil with more than three turns. Eq.37 thus gives the value of 6.3333 for the proximity factor.

4.4.2 Correction factor

Due to imperfect coupling between turns of the coil, a correction factor becomes necessary. The correction factor depends on the height of the turn conductor and the inter-turn insulation thickness. For instance, a coil with a turn height of 3 mm and a turn insulation thickness of 0.2 mm will have a correction factor of about 0.88 and a proximity factor of about 6. Henceforth, Eq.37 becomes

$$K_{proximity} = K_{cf}\left(1 + \frac{2}{3}\left(n^2 - 1\right)\right), \tag{44}$$

where K_{cf} is the proximity effect correction factor.

4.5 Limitation of the multi-conductor transmission line model of winding

Three theoretical approaches using the multi-conductor transmission line theory described in this work are limited to the first coil from the line end. The experimental work performed by the present author has shown that it is the first coil in which the highest inter-turn voltage occurs. Thus, it is unlikely, that there will be any need to predict voltages on any coil except the line-end coil.

Limiting the model to the first line-end coil will require a certain impedance to represent the remaining coils. A technique based on the voltage reflection mechanism at the junction of the first line-end coil and the second coil has been proposed by Oyegoke (1997b). The method for calculating the terminating impedance does not lead to loss of accuracy on the magnitude of the peak inter-turn voltage.

The methods of voltage calculation are valid for a short time after the transient has impinged on the coil. However, to some extent this limitation corresponds to the practical situation since Cornick and Thompson (1982) has previously demonstrated that it is only during the initial period of the transient disturbance that high inter-turn stresses occur.

4.6 Conclusions

Capacitance is the most straightforward parameter to evaluate. Three methods for doing this are described. Computation of the inductance is difficult because it involves problems related to magnetic flux penetration in a laminated iron structure at high frequencies. One way to overcome this problem is to assume that magnetic flux does not penetrate the iron laminations. With this assumption in mind, the three possible ways of evaluating the inductance are:

*to use a specialised computer program,
*to estimate the effective permeability of the iron using the theory based on flux penetrations in a slab at high frequency,
*to use the duality existing between the electric and magnetic field for a homogeneous medium.

5 METHODS FOR INTER-TURN VOLTAGE CALCULATION ON FORM WINDING

This chapter deals with the reasons why the conventional treatment of machine winding transient phenomena using ladder-network has failed in the analysis of predicting the voltage distribution in the form winding. Three alternative methods based on the multi-conductor transmission line approach are described.

5.1 Why not ladder-network for voltage calculation in form winding

The conventional treatment of machine winding transient phenomena that neglects the mutual coupling due to other turns or windings is equivalent to treating the winding as a single wire and ignores the presence of other conductors. However, there are many times in the study of travelling waves when the effect of other conductors cannot be neglected. Sometimes their influence is so vital as to change the characteristics of the phenomenon completely and entirely erroneous results are obtained if they are not considered.

The above-mentioned point explains why ladder-network has failed in the analysis of predicting voltage distribution in the form winding mostly used on medium and high voltage motors. This can further be explained in the following way. Although each coil can be treated as a low pass filter, i.e. each turn has series inductance and shunt capacitance, individual turns cannot be considered as independent low pass filters since this would be equivalent to treating the coil as a ladder-network. This is invalid because of the fact that each turn has mutual inductance and mutual capacitance with all other turns.

Furthermore, the transmission line model, which visualises the surge arriving on the first turn, travelling along each turn in succession and finally leaving the coil, also failed for the following reason. Upon the application of the surge, a voltage appears on each turn simultaneously but with differing amplitude, thus producing high inter-turn stresses. As a result of this, it may be concluded that magnetic and electric coupling between turns plays an important role in the propagation of surges through a coil, and their presence cannot be neglected at least in the analysis of the voltage distribution in form windings.

5.2 Multi-conductor transmission line theory for inter-turn voltage calculation in form windings

In this section, three approaches are presented for predicting the magnitude and distribution of the transient voltages in the stator winding of an electric machine subjected to a steep fronted surge. The primary aim of the present study is to find out which method (methods) is (are) suitable for predicting the surge distribution in the stator winding of an ac motor fed from a frequency converter. Three methods are compared in this section. Similar comparison has been done by Oyegoke (1997a), who investigated the performance of three methods on a seven-turn mock-up coil embedded in a laminated slot environment. The peak inter-turn voltage appearing in the middle of the mock-up coil is unusual and may be due to the absence of the terminal lead cable that is always there in a real machine. In addition, in the study made by Oyegoke (1997a), the absence of the copper resistance led to the introduction of a new inductance matrix, which helped to stabilise the ill conditioning effect of the equivalent circuit for the circuit simulator. The need to investigate the performance of these methods on an actual machine is justified. In the present work, the cable from the voltage source, the terminal lead cable and the machine winding are considered as a single system and not separately. Copper resistance is also included in the model for simulation. The numerical and experimental results on an actual machine (6.3 kV induction motor) are provided. The three methods presented in this section, like those described by Oyegoke (1997a), will not account for additional surface impedance due to flux penetrating the laminated stator core at the frequency of interest (1 to 10 MHz). One of the methods has been chosen in order to investigate the effect of copper resistance on the inter-turn voltage calculation.

5.2.1 Multi-conductor transmission line and scatter matrix concept (MTLSMC)

Over-voltage due to a steep-fronted surge has been studied in a system consisting of a cable connected to the first line-end coil made of eleven turns. In order to model turn conductors as transmission lines, the coil has been divided into five parts, defined by the cable and the slot junctions (j1, j2, j3, j4, j5) as shown in Fig. 1, for the first line-end coil consisting of eleven turns. The five parts are modelled separately as untransposed lines and interconnected in an appropriate manner to form a coil. Mutual coupling among coil parts is neglected on the following basis.
The two over-hang parts on the opposite sides of the stator core are considered uncoupled because eddy-current in the core lamination provides effective shielding at high frequencies. The over-hang and slot parts are uncoupled because of the eddy-current in the lamination core. The two parts of the coil at the coil-entry are uncoupled since they are nearly perpendicular to each other over most of their length and are further shielded from each other by eddy-currents in adjacent coils.

Tavner and Jackson (1988) shows that insulation between the lamination permits magnetic coupling to the coils inside adjacent slots. However, the two slot parts of the coil under study are not coupled because of the eddy-current in the neighbouring coils. The resulting eddy-currents in neighbouring coils are considered more effective in shielding the two parts of the coil under study.

5.2.2 Scatter matrix derivation for junction j1

The scatter matrix theory was first applied to voltage distribution problem in machine winding by Wright et al. (1983a). However, for the purposes of clarity, the derivation of the scatter matrix is presented here for junction j1 of a three-turn coil. The scatter matrix of other junctions can be derived in a similar way. Junction j1 of a three-turn coil will be the junction between three single conductor transmission lines and a pair of two-conductor lines as shown in Fig.4. The first of these two-conductor lines is the cable feeding the coil and the second is the conductor leading to the next coil of the phase winding.

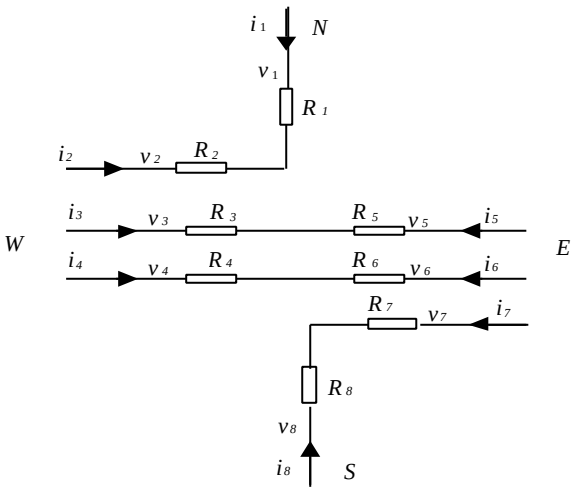

Fig. 4: Junction j1 of a three-turn coil with copper resistance.

Some authors, e.g. Wright et al. (1983a), included dielectric losses in their models. In this, paper dielectric losses are neglected. The copper resistance of each part is halved and each half is included in the junction at each end of the part. The problem now is to find the scatter matrix, which will represent the junction and the loss elements shown in Fig. 4.

Applying Kirchoff's voltage law to Fig. 4 gives

$$v_1 - i_1R_1 - v_2 + i_2R_2 = 0$$
$$v_3 - i_3R_3 - v_5 + i_5R_5 = 0$$
$$v_4 - i_4R_4 - v_6 + i_6R_6 = 0$$

$$v_7 - i_7 R_7 - v_8 + i_8 R_8 = 0$$

By constructing appropriate resistance matrices, the above equations can be condensed into

$$(\boldsymbol{C_v})(\boldsymbol{V}) - (\boldsymbol{C_v})(\boldsymbol{R})(\boldsymbol{I}) = 0 \tag{20}$$

where

$$(\boldsymbol{C_v}) = \begin{bmatrix} 1 & -1 & 0 & 0 & 0 & 0 & 0 & 0 \\ 0 & 0 & 1 & 0 & -1 & 0 & 0 & 0 \\ 0 & 0 & 0 & 1 & 0 & -1 & 0 & 0 \\ 0 & 0 & 0 & 0 & 0 & 0 & 1 & -1 \end{bmatrix}; \ (\boldsymbol{V}) = \begin{bmatrix} v_1 \\ v_2 \\ v_3 \\ v_4 \\ v_5 \\ v_6 \\ v_7 \\ v_8 \end{bmatrix} \text{ and } (\boldsymbol{I}) = \begin{bmatrix} i_1 \\ i_2 \\ i_3 \\ i_4 \\ i_5 \\ i_6 \\ i_7 \\ i_8 \end{bmatrix}$$

Where $(\boldsymbol{C_v})$ is the voltage connection matrix,

$$(\boldsymbol{R}) = \begin{bmatrix} R_1 & 0 & 0 & 0 & 0 & 0 & 0 & 0 \\ 0 & R_2 & 0 & 0 & 0 & 0 & 0 & 0 \\ 0 & 0 & R_3 & 0 & 0 & 0 & 0 & 0 \\ 0 & 0 & 0 & R_4 & 0 & 0 & 0 & 0 \\ 0 & 0 & 0 & 0 & R_5 & 0 & 0 & 0 \\ 0 & 0 & 0 & 0 & 0 & R_6 & 0 & 0 \\ 0 & 0 & 0 & 0 & 0 & 0 & R_7 & 0 \\ 0 & 0 & 0 & 0 & 0 & 0 & 0 & R_8 \end{bmatrix}$$

Bearing in mind that the voltage and current vectors can be decomposed into incident and reflected components, as given below, also helps to understand the final expression of the scatter matrix.

$$(\boldsymbol{V}) = (\boldsymbol{V})^{\text{in}} + (\boldsymbol{V})^{\text{re}} \tag{21}$$

$$(\boldsymbol{I}) = (\boldsymbol{I})^{\text{in}} + (\boldsymbol{I})^{\text{re}} \tag{22}$$

The characteristic impedance of the transmission lines meeting at the junction relates the voltage vector and the current vector (and their constituent parts). For example the system of Fig. 4.

$$[v_1]^{\text{in}} = [z_1][i_1]^{\text{in}} \qquad \text{line N}$$

$$\begin{bmatrix} v_1 \\ v_2 \\ v_3 \end{bmatrix}^{\text{in}} = \begin{bmatrix} z_2 & z_{23} & z_{24} \\ z_{32} & z_3 & z_{34} \\ z_{42} & z_{43} & z_4 \end{bmatrix} \begin{bmatrix} i_2 \\ i_3 \\ i_4 \end{bmatrix}^{\text{in}} \qquad \text{line W}$$

and

$$\begin{bmatrix} v_5 \\ v_6 \\ v_7 \end{bmatrix}^{\text{in}} = \begin{bmatrix} z_5 & z_{56} & z_{57} \\ z_{65} & z_6 & z_{67} \\ z_{75} & z_{76} & z_7 \end{bmatrix} \begin{bmatrix} i_2 \\ i_3 \\ i_4 \end{bmatrix}^{\text{in}} \qquad \text{line E}$$

$$[v_8]^{\text{in}} = [z_8][i_8]^{\text{in}} \qquad \text{line S}$$

i.e.

$$(\boldsymbol{V})^{\text{re}} = -(\boldsymbol{Z})(\boldsymbol{I})^{\text{re}} \tag{23}$$

and

$$(\boldsymbol{V})^{\text{in}} = (\boldsymbol{Z})(\boldsymbol{I})^{\text{in}} \tag{24}$$

where in this case

$$(\boldsymbol{Z}) = \begin{bmatrix} z_1 & 0 & 0 & 0 & 0 & 0 & 0 & 0 \\ 0 & z_2 & z_{23} & z_{24} & 0 & 0 & 0 & 0 \\ 0 & z_{32} & z_3 & z_{34} & 0 & 0 & 0 & 0 \\ 0 & z_{42} & z_{43} & z_4 & 0 & 0 & 0 & 0 \\ 0 & 0 & 0 & 0 & z_5 & z_{56} & z_{57} & 0 \\ 0 & 0 & 0 & 0 & z_{65} & z_6 & z_{67} & 0 \\ 0 & 0 & 0 & 0 & z_{75} & z_{76} & z_7 & 0 \\ 0 & 0 & 0 & 0 & 0 & 0 & 0 & z_8 \end{bmatrix}$$

Alternatively, the admittance matrix may be used:

$$(\boldsymbol{I})^{\text{re}} = -(\boldsymbol{Y})(\boldsymbol{V})^{\text{re}} \tag{25}$$

and

$$(\boldsymbol{I})^{\text{in}} = (\boldsymbol{Y})(\boldsymbol{V})^{\text{in}} \tag{26}$$

where

$$(\boldsymbol{Y}) = (\boldsymbol{Z})^{-1}$$

Combining Eqs.20-24 gives

$$[(\boldsymbol{C_v}) - (\boldsymbol{C_v})(\boldsymbol{R})(\boldsymbol{Y})](\boldsymbol{V})^{\text{in}} = [-(\boldsymbol{C_v}) - (\boldsymbol{C_v})(\boldsymbol{R})(\boldsymbol{Y})](\boldsymbol{V})^{\text{re}} \tag{27}$$

Applying Kirchoff's current law to Fig. 4 gives

$$\begin{aligned} i_1 + i_2 &= 0 \\ i_3 + i_5 &= 0 \\ i_4 + i_6 &= 0 \\ i_7 + i_8 &= 0 \end{aligned}$$

from which

$$(\boldsymbol{C_i})(\boldsymbol{I}) = \boldsymbol{0} \tag{28}$$

where

$$(\boldsymbol{C_i}) = \begin{bmatrix} 1 & 1 & 0 & 0 & 0 & 0 & 0 & 0 \\ 0 & 0 & 1 & 0 & 1 & 0 & 0 & 0 \\ 0 & 0 & 0 & 1 & 0 & 1 & 0 & 0 \\ 0 & 0 & 0 & 0 & 0 & 0 & 1 & 1 \end{bmatrix}$$, is the current connection matrix.

Eqs.21-24 and 28 combine to give

$$[(\boldsymbol{C_i})(\boldsymbol{Y})](\boldsymbol{V})^{\text{in}} = [(\boldsymbol{C_i})(\boldsymbol{Y})](\boldsymbol{V})^{\text{re}} \tag{29}$$

In order to express $(\boldsymbol{V})^{\text{re}}$ explicitly, Eqs.27 and 29 are combined to give

$$(\boldsymbol{V})^{\text{re}} = (\boldsymbol{S})(\boldsymbol{V})^{\text{in}} \tag{30}$$

where

$$(\boldsymbol{S}) = \begin{bmatrix} -(\boldsymbol{C}_v) - (\boldsymbol{C}_v)(\boldsymbol{R})(\boldsymbol{Y}) \\ (\boldsymbol{C}_i)(\boldsymbol{Y}) \end{bmatrix}^{-1} \begin{bmatrix} (\boldsymbol{C}_v) - (\boldsymbol{C}_v)(\boldsymbol{R})(\boldsymbol{Y}) \\ (\boldsymbol{C}_i)(\boldsymbol{Y}) \end{bmatrix} \tag{31}$$

Thus, the scatter matrix can predict the reflected voltages $(\boldsymbol{V})^{\text{re}}$ caused by any combination of incident voltages $(\boldsymbol{V})^{\text{in}}$ impinging on the junction. $(\boldsymbol{Y})$ is the admittance matrix and is calculated as a product of the wave velocity and the junction capacitance matrix, i.e.

$$(\boldsymbol{Y}) = u(\boldsymbol{C}) \tag{32}$$

The capacitance matrix for a three-turn coil part is given by

$$(\boldsymbol{C}) = \begin{bmatrix} C_{\text{int}} + C_g & -C_{\text{int}} & 0 \\ -C_{\text{int}} & 2C_{\text{int}} + C_{2g} & -C_{\text{int}} \\ 0 & -C_{\text{int}} & C_g \end{bmatrix} \tag{33}$$

where C_{int} signifies the capacitance between two adjacent conductors, C_g is the capacitance to the ground for the uppermost conductor inside the slot; the same is for the bottom conductor in a three-turn coil. Neglecting the effect of the high frequency magnetic flux penetration into the iron lamination leads to the assumption that the magnetic flux is limited to the paths in the insulation, for which the relative permeability is unity. Hence, the wave velocity is given as Eq. 4.

One slot/over-hang junction, for instance j2, of a three-line coil is shown in Fig. 5. This is a special case of junction j1, and the analysis follows a similar way leading to the same form of Eq.26. For junction j2 in Fig. 5,

$$(\boldsymbol{C}_v) = \begin{bmatrix} 1 & 0 & 0 & -1 & 0 & 0 \\ 0 & 1 & 0 & 0 & -1 & 0 \\ 0 & 0 & 1 & 0 & 0 & -1 \end{bmatrix}, \text{ and } (\boldsymbol{C_i}) = \begin{bmatrix} 1 & 0 & 0 & 1 & 0 & 0 \\ 0 & 1 & 0 & 0 & 1 & 0 \\ 0 & 0 & 1 & 0 & 0 & 1 \end{bmatrix}$$

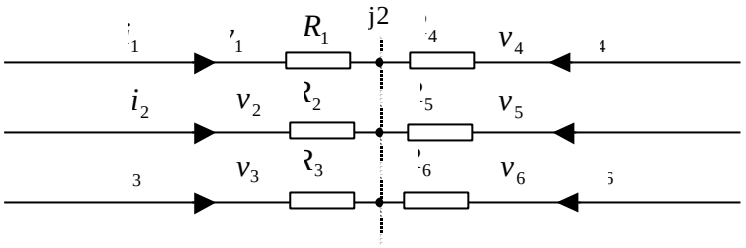

Fig. 5: Junction j2 of a three-turn coil with copper resistance.

In a similar way, one can derive the scatter matrix for any junction formed by N number of lines.

After evaluating the parameters, a unit impulse is sent from the switch, the multi-conductor and scatter matrix theories are applied to obtain the incident and the reflected waves at each junction and at each conductor that forms the junction. This calculation is performed for the whole period of interest. The real waveform of interest is then imposed. This method is similar to the one applied to an electrical machine winding by Wright et al. (1983a).

5.3 Multi-conductor transmission line and averaging techniques concept (MTLATC)

5.3.1 Wave propagation

The voltage across turns in the stator winding of an electric machine is believed to propagate in the space between adjacent turns. This space forms a transmission line with surge impedance

$$Z_{\text{sabt}} = \frac{1}{u \cdot C_{\text{intcap}}} \tag{34}$$

where
C_{intcap} is the inter-turn capacitance and u is the velocity of propagation calculated using Eq.11 with the relative dielectric permittivity of the insulation material between the turn conductors. The inter-turn voltage wave is scattered upon arrival at a coil exit to the next coil or the coil entrance due to impedance discontinuity.

5.3.2 Wave scattering

The surge impedance seen by the wave at the coil entrance is calculated from

$$Z_{\text{ent}} = \frac{1}{u_{\text{g}} \cdot C_{\text{gst1}}} \tag{35}$$

where C_{gst1} is the capacitance of turn 1 to the ground in the slot part, and u_{g} is the velocity of propagation calculated using Eq.11 with the relative dielectric permittivity of the material between the turn conductor and the slot wall.

The impedance seen at the coil exit is computed by

$$Z_{\text{ext}} = Z_{\text{g1}} + Z_{\text{g2}}\,;\; Z_{\text{g2}} = \frac{Z_{\text{glt}} \cdot Z_{\text{gnt}}}{Z_{\text{glt}} + Z_{\text{gnt}}} \tag{36}$$

where Z_{g1} is the surge impedance calculated from the first turn of the coil, Z_{glt} is the surge impedance calculated from the last turn of the coil in the same slot, and Z_{gnt} is the surge impedance calculated from the first turn of the next coil.

5.3.3 Wave reflection coefficients

At the coil entrance $\rho_1 = \frac{Z_{ent} - Z_{sbat}}{Z_{ent} + Z_{sbat}}$, at the coil exit $\rho_2 = \frac{Z_{ext} - Z_{sbat}}{Z_{ext} + Z_{sbat}}$ (37)

5.3.4 Voltage calculation

Computation of the inter-turn voltage by this method requires the solution with respect to voltage of the capacitance equivalent network in Fig. 6. Contrary to work of the previous authors, Narang et al. (1989), the cable from the voltage supply and the terminal-lead cable are included in the circuit. The voltages of interest are the voltages at nodes 1 to 12 for the eleven-turn coil of this analysis, in accordance with the numbering in Fig. 1. Inter-turn voltages are evaluated by subtracting one voltage from another, i.e. the voltage across turn number one is obtain by subtracting the voltage at node 2 from the voltage at node 1.

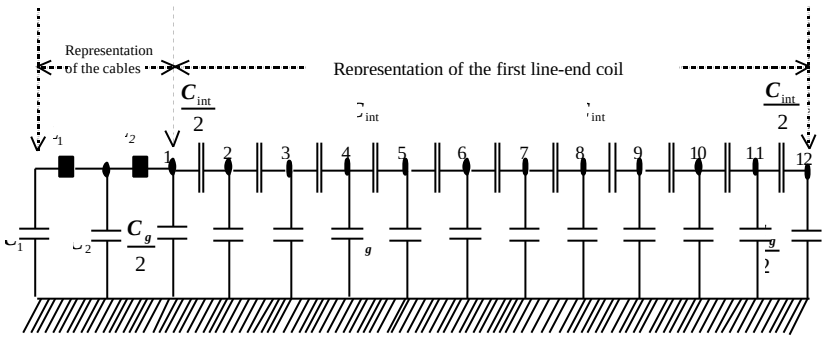

Fig. 6: Capacitance equivalent network of an eleven-turn coil connected to a terminal lead cable and a cable from the voltage supply.

The turn voltages calculated in this way form the starting point of the Bewley lattice diagram employed in averaging techniques. A similar method was used by Narang et al. 1989. The surge in this analysis has a rise time from zero to about 200 nanoseconds and is impressed at the beginning of the cable. The time required by this surge to travel one turn is 17.6 nanoseconds. The ratio of the rise time of the impinging surge at the motor terminal to the time required to travel one turn gives the time steps over which the lattice diagram is averaged. This gives 11 time steps over which the lattice diagram is averaged. The result of this calculation is MTLATC.

5.4 Multi conductor transmission line concept for circuit simulator (MTLCCS)

The equivalent circuit, for example of the two-turn coil in Fig. 7 requires the computation of four parameters, the self inductance of each conductor in a section, the mutual inductance between them, the capacitance of each conductor to ground and the mutual capacitance between them.

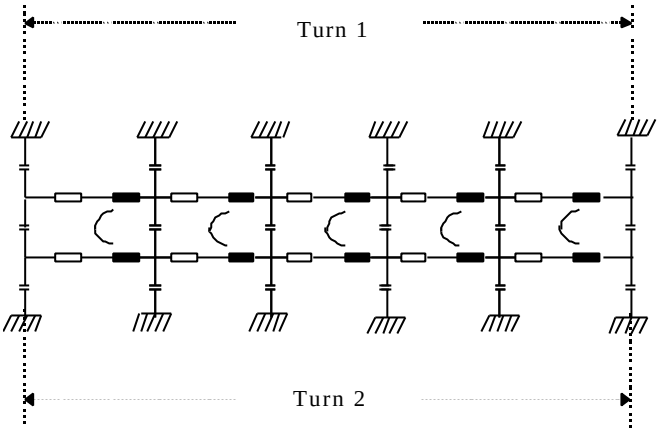

Fig. 7: Equivalent circuit of a two-turn coil model for circuit simulator.

The capacitance matrix $(\boldsymbol{C})$ for the slot and end region is calculated using the method described above. The inductance matrix $(\boldsymbol{L})$ is evaluated from a modified capacitance matrix $(\boldsymbol{C}_{\text{mod}})$ by the duality existing between electric and magnetic field equations in homogeneous systems:

$$(\boldsymbol{L}) = \frac{\mu_r e_r}{c^2} (\boldsymbol{C}_{\text{mod}})^{-1} \tag{38}$$

For the calculation of the modified capacitance matrix in Eq.38, the value of the relative dielectric permittivity used for both the mutual and capacitance to ground is 1. This is because inductance values are independent of the dielectric constants.

6 EXPERIMENTAL STUDIES OF VOLTAGE DISTRIBUTION IN FORM WINDING

This section presents results of the voltage transient test. The primary aim of these tests was to develop an experimental understanding of what happens after a voltage transient arrives at the stator winding of an electrical machine. The test was performed on the stator of an actual 6 kV induction motor. The present measurements were performed with a 42 V input voltage step function.

6.1 Measurement of the voltage distribution in the stator winding of a 6 kV induction motor under a fast rising step input voltage:-General arrangement

The voltage source delivered a unit step of about 42 Volts with a rise time, from zero to maximum, of about 200 nanoseconds. This voltage was injected into the cable feeding the motor via a short length of conductor since direct connection of the cable to the voltage source was difficult to achieve. In measuring waveforms at these frequencies (MHz range), it is important to make sure that the measuring devices do not interfere with the measured waveforms. The voltages were measured using high impedance probes (input impedance 1 $\text{M}\Omega$, input capacitance 6.5 pF) on a four-channel HP oscilloscope. The type of input cable between the voltage generator and the coil set-up was a Nokia type MCMK 3x16+16. During most of the measurements, the length of the input cable was about 4 m.

The rated line-to-line voltage of the motor under investigation was 6.3 kV. The stator phase windings of the machine were star connected, each phase had sixteen coils, and each coil had eleven turns. The voltage measurement was performed on the first two coils near the input line end. Two types of measurements were performed: /1/ measurement of the voltage across the first two line-end coils and /2/ measurement of the voltage across individual turns of the first line-end coil.

6.1.1 Measurement of the coil voltage

The voltage measurements were performed on the first two line-end coils of one phase of the stator winding of the 6.3 kV induction motor. The other two phases and the stator core were grounded for the experiment, and the rotor of the machine was removed. The voltage source was connected to the input end of the phase

winding via a short conductor and the 4m long input cable. Between the cable and the first line-end coil there was, additionally, a straight lead (silicon cable) about 1 metre long.

The coil voltage measurements were taken at the input terminal and at the end of each of the two coils. The difference in the measured voltage at the terminal and at the end of each coil constituted the voltage drop across the coil. Measured voltages across the first two coils are shown in Fig. 8. From the same figure, it can be seen that the first coil next to the input undergoes - by far - the highest voltage peak. In other words, the insulation of this coil is also subjected to the greatest voltage stress. Because of this, a more detailed study of the first coil was deemed necessary.

6.1.2 Measurement of the voltages over individual turns

Using the same experimental set up as described above, a detailed measurement of the voltage over each individual turn of the first line-end coil was then performed. Each turn conductor of this eleven-turn coil was exposed at appropriate positions to allow the measurement. Two experiments were performed: /1/ one measurement with the neutral end of the winding grounded and /2/ the other voltage measurement with the neutral end ungrounded, i.e. isolated. For both of these measurements, a 4m long input cable was used. Fig. 9 illustrates the mutual arrangement of the first four line-end coils and Fig. 10 shows the measurement locations within the first line-end coil.

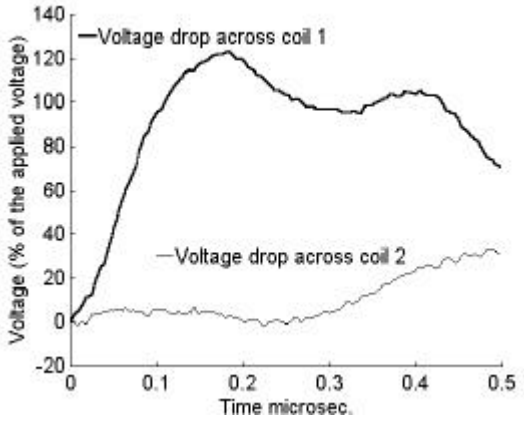

Fig. 8: Measured voltages across the first two line-end coils.

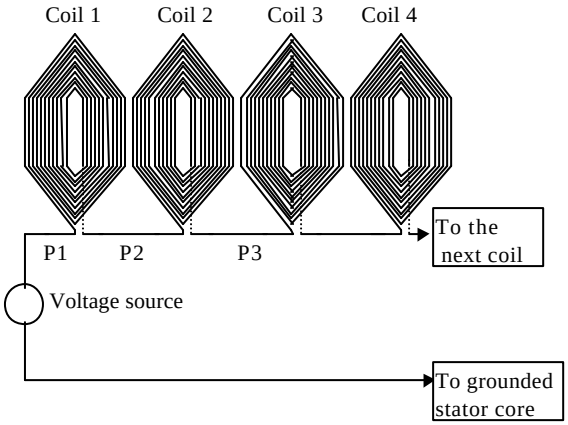

Fig. 9: Mutual arrangement of the first four line-end coils.

The measured turn-to-ground voltages of the first line-end coil are shown in Figs. 11 and 12 for the grounded and the ungrounded case, respectively. In Figs. 11 and 12, the uppermost curve is the measured voltage at point 1 and the lowest curve was measured at point 12, as shown in Fig. 10.

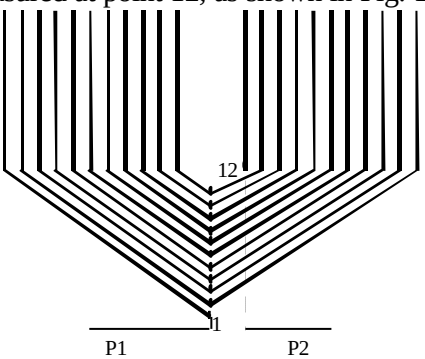

Fig. 10: Fraction of coil 1 showing the measurement locations marked with dots.

The voltages were measured with respect to the stator core that provides the return path for the current. The stator core was grounded throughout the measurements.

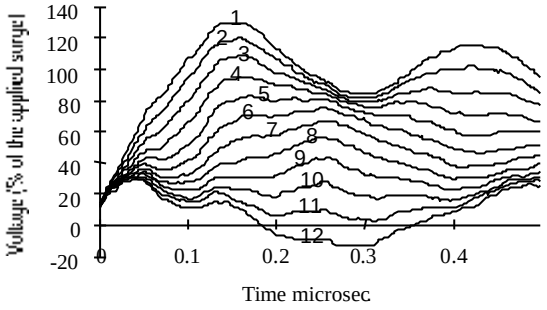

Fig. 11: Measured turn-to-ground voltages with the winding end grounded.

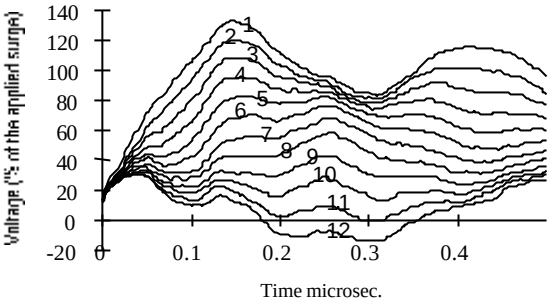

Fig. 12: Measured turn-to-ground voltages with the winding end ungrounded.

It is apparent from Figs. 11 and 12 that the turn-to-ground waveforms are practically identical in these two figures. Identical waveforms were recorded also for the inter-turn voltages, as shown in Fig 13 (1-11), regardless of whether the end of the stator winding set was grounded or ungrounded. The maximum voltages across individual turns, plotted as a function of the turn number *n* is given in Fig. 14. From the same figure, it can be seen that the highest voltage across a turn appears across turn no. 10 regardless of the condition at the end of the stator winding (grounded or ungrounded).

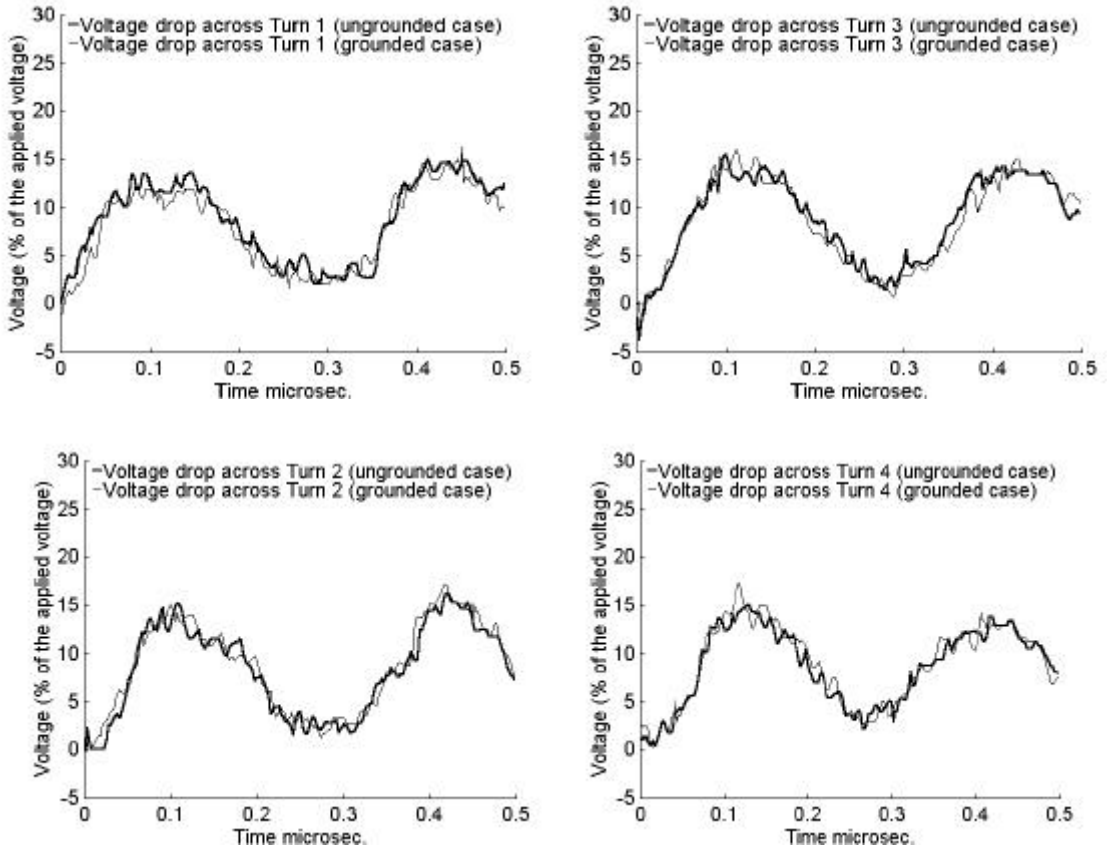

Fig. 13 (turns 1-4): Inter-turn voltage waveforms

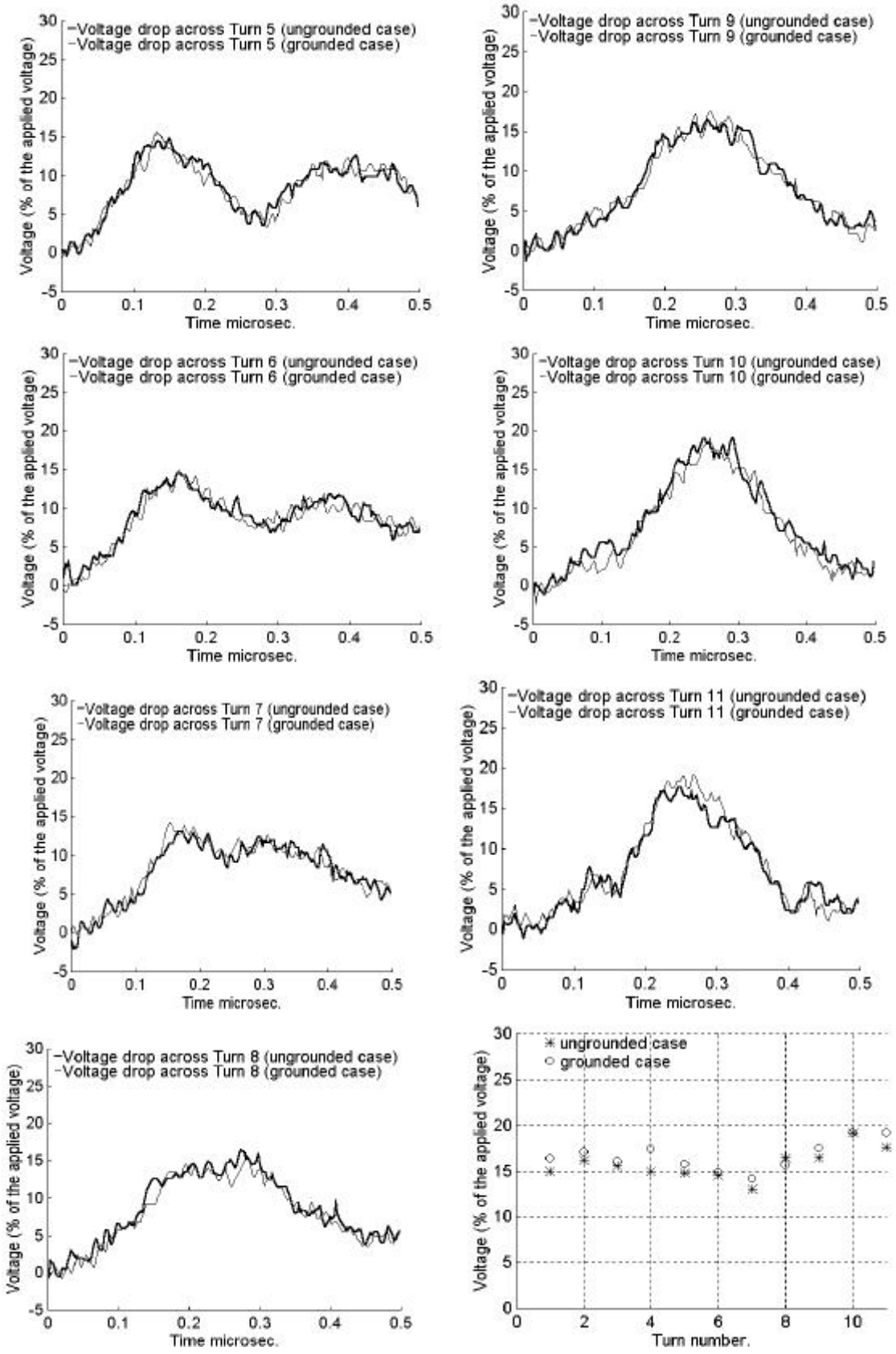

Fig. 13 (turns 5-11): Inter-turn voltage waveforms.
Fig. 13: Inter-turn voltage wave-forms for the Grounded and ungrounded stator winding end.

Fig. 14: Maximum voltages across individual turns.

6.2 Effect of different input cable lengths

The aim of the present work was to find out how a fast rising voltage, arriving from outside, behaves within the stator winding of an induction motor. It was found that it is useful to regard the stator winding as an electrical high frequency transmission line, with its characteristics determined by the distributed inductance and capacitance of the coil conductors. At the same time, it was clear that the individual stator coils constitute separate and localised circuits with reactance widely different in magnitude from those usually assumed for the nominal operating frequency of 50 Hz. From this, there is the corollary that the transient voltage distribution within the stator winding, as measured during a transient voltage applied to the input terminal, could considerably depend on the details of how the input voltage was applied. To conclude the present measurements, the maximum voltage across the turns of the first line-end coil was eventually measured for four different input cable lengths.

The results of this turn-to-turn voltage measurement are summarised in Table I. The peak value of the full voltage across the first line-end coil, as a function of the input cable length L is given in Table II.

Table I: Maximum voltage drop across turns of the first line-end coil (% of the applied voltage) as a function of the cable length L (m).

L	2.3	4.0	17.0	33.5	50.5
Turn no.	Voltage (% of the applied voltage)				
1	14.9	16.4	15.6	16.1	16.8
2	16.2	17.0	15.1	17.8	20.3
3	16.7	16.0	14.9	16.1	18.1
4	12.2	17.4	17.7	16.2	18.4
5	16.1	15.7	16.8	16.7	17.4
6	12.6	14.9	16.6	19.0	15.7
7	12.0	14.2	18.4	19.8	18.4
8	14.8	15.6	21.6	20.8	21.3
9	18.9	17.5	22.2	21.3	21.9
10	17.8	19.2	21.7	20.4	20.2
11	15.9	19.2	21.3	21.3	22.2

The highest turn-to-turn (inter-turn) voltages were found to occur towards the end of the coil, i.e. within the last three turns (n= 9, 10, 11) of the coil depending on the input cable length. With the cable length either L = 2.3m or L = 17m, the highest voltage was found to occur across turn no. 9. With L = 4m, the highest voltage occurred across turns no. 10 and 11, and with L = 33.5m, the highest voltage was found to occur across turns nos. 9 and 11. With L = 50.5m, the highest voltage was found to occur across the last turn of the coil (across turn no. 11).

Table II: Peak voltage drop across the first line-end coil (% of the applied voltage) as a function of the cable length L (m).

L	2.3	4.0	17.0	33.5	50.5
Voltage	114.0	123.1	173.5	183.0	177.3

It is also obvious from the results in Table I that, regardless of the input cable length, the voltage distribution due to this transient voltage is not identical for all the turns of the coil. The highest voltage drop due to the input surge appears to occur across turns nos. 9 and 11 for L = 17.0m and L = 50.5m, respectively. The maximum voltage peak value of the voltage across the first line-end coil, as a function of the cable length, is given in Table II. For all the cable lengths studied, the maximum inter-turn voltage occurred within the first 500 nanoseconds after the surge had arrived at the motor terminal. The peak voltage across the first line-end coil in Table II reaches 183 % of the applied voltage with a 33.5m cable. A peak of about 175 % of the applied voltage is recorded for the same coil with 50.5m long cable. This distribution of the maximum value as

a function of the cable length is not the case with the peak voltage across turns in the coil, as can be seen in Table III.

Table III: Highest voltage drop across turns of the first line-end coil (% of the applied voltage) as a function of the cable length, L (m).

L	2.3	4.0	17.0	33.5	50.5
Voltage	18.9	19.2	22.2	21.3	22.2

It should be borne in mind that the voltage value presented in Table III is not for one particular turn in the coil. The position of highest voltage changes as the cable length changes. As pointed out earlier, the position of the highest voltage varies between turns nos. 9-11, depending on the input cable length.

6.3 Conclusions

For the 200 nanoseconds rise time surge voltage used in this study, the following observations were made. The highest single coil voltage occurs across the first terminal end coil of the stator winding, with the voltage value reaching about 125 % of the applied surge. The peak voltage value, undergone by the second coil, was only 40 % of the applied surge. The further we move away from the input end of the stator winding, the lower the transient coil voltage tends to be. The surge distribution within the turns of the first terminal end coil is practically independent of the terminating condition at the neutral end of the winding, i.e. either grounded or ungrounded. This is seen from the measured turn-to-ground voltages in Figs. 7 and 8. The measured voltage peaks in Fig. 10 also confirm this conclusion. From the point of view of a voltage transient, a transmission line analogy appears to be useful.

It must be borne in mind that for a conventional AC electrical system, operating at 50 Hz frequency, a voltage pulse rise time of 200 nanoseconds corresponds to an extremely high frequency. The major Fourier components of this particular voltage transient lie around a few MHz, i.e. up to 10^5 times the line frequency. Because of this, the absolute magnitudes of all the circuit reactance are far from what one is accustomed to - with the consequent possibility of unexpected circuit behaviour.

By replacing the 4 m long input cable with a 33.5m long cable in the feeding circuit of the induction machine, the magnitude of the voltage transient across the first coil (see Table II) rose from 120 % to 180 % of the step voltage actually fed into the input cable. This is a very clear indication of the fact that the combination of steep-fronted voltage pulses and a long cable can, in actual practice, strongly accentuate transient peak voltages, maybe up to the point of a transient voltage being dangerous to the conductor insulation system. This result regarding the effect of the cable on the voltage results shows the need to use a distributed parameter model for the cable when dealing with fast transients. In general, a short cable will look like a capacitance but if the length is great compared to the wavelength, then a transmission line model with distributed parameters is necessary for the cable. To simulate the voltage at the motor terminal using travelling wave theory, the important parameter (for amplitude) is the ratio of the motor entry surge impedance to the cable surge impedance.

There is a clear indication that the main experimental features found in this investigation can be, at least approximately, understood by treating the stator winding of the induction machine as a transmission line. Within this picture, the transient and oscillatory features observed find a reasonable explanation in terms of a wave front propagating from one lumped oscillatory circuit - i.e. one coil section of the stator winding - to another one, and so on. It also appears that some of the features observed result from resonance conditions and from wave front reflection at circuit junctions at which the adjacent sections are not perfectly matched to each other. As a conclusion from the results of this experimental measurement it is important that the designer of a stator winding for an induction machine intended to be used with a pulse-operated variable speed drive takes into account electrical and magnetic phenomena up to several MHz frequencies, i.e. up to frequencies

widely surpassing those that have been conservatively considered. If this is not done, unexpected voltage behaviour can result - up to the point of presenting a danger to the machine insulation. From a practical point of view, it is worth noticing that, even for a high-power, high-voltage machine, the experimental characterisation of these and related effects can be performed using low voltage levels and standard workshop electronic instruments. The present test results could be of help to engineers and researchers concerned with conductor insulation strength and voltage surge protection of large AC motors.

7 RESULTS OF VOLTAGE CALCULATION ON FORM WINDINGS

The computed maximum voltage drop across turns due the three methods described in Chapter 5 of this work and the corresponding measured result can be seen from Fig. 15, where the agreement between the computed and the measured results is very close. Fig. 16 presents the measured and the calculated voltage wave forms across turn numbers 1 and 11, where the variation pattern of the voltage computed by the method based on the scatter matrix (MTLSMC), and the method based on the equivalent circuit (MTLCCS) can be seen to match the measured wave forms well.

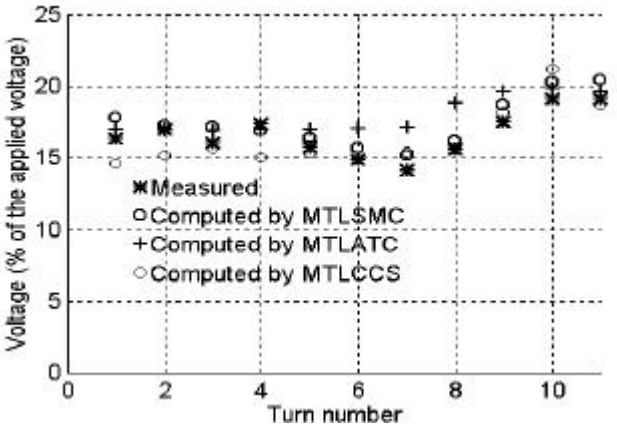

Fig. 15: Maximum voltage drop across turns as a function of turn number.

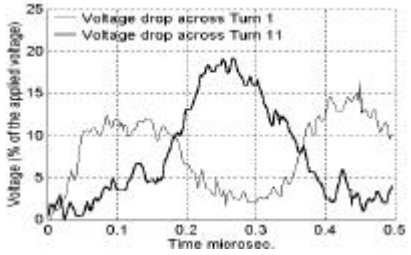

16(a)

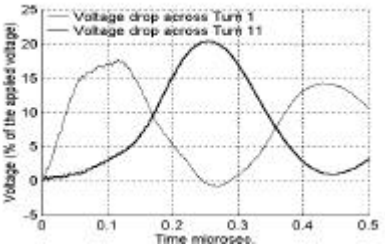

16(b)

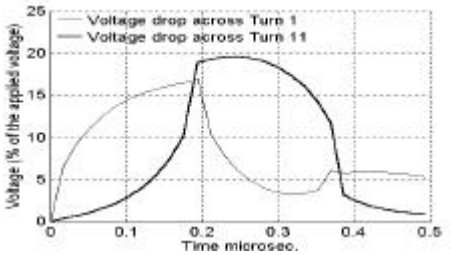

16(c)

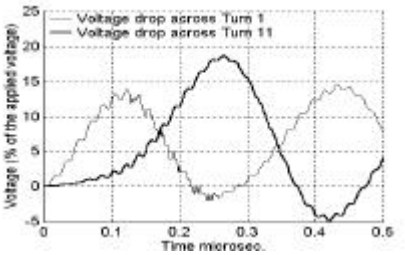

16(d)

Fig. 16 (a), (b), (c), (d): Waveform of voltage across turns numbers 1 and 11.
(a) measured voltage wave, (b) computed voltage wave using the MTLSMC, (c) computed voltage wave using the MTLAC, (d) computed voltage wave using the MTLCCS.

The discrepancy between the computed wave forms using the MTLATC and the measured wave forms is due, on the one hand, to the assumption that not more than two voltage waves get to a turn of the winding at a particular time step. This assumption is the same as saying that the tail of the pulse under consideration is as long as one turn travelling time (17.6 nanoseconds for this analysis). On the other hand, the discrepancy comes from the fact that the same reflection coefficient r_1 has been assumed for the coil entry and the coil exit. If different reflection coefficients are to be used in calculation as given by Eq.33, then the voltage wave across turn number 1 improves. However, the peak value of the voltage drop across turns increases much considerably more than the measured values. This is obvious especially for the turns towards the end of the coil where the highest turn voltage occurs. In order to reduce the uncertainty of the MTLATC, it is good to stop computation after the first peak of the voltage across the last turn of the coil since it has previously been found out that the highest inter-turn voltage occurs at this point.

It should be mentioned that the methods MTLSMC and MTLCCS give the possibility of evaluating the turn to ground voltages. The results of computation using these methods and the corresponding measured results are presented in Fig. 17.

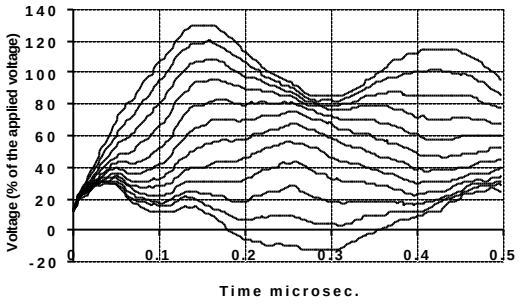

17(a)

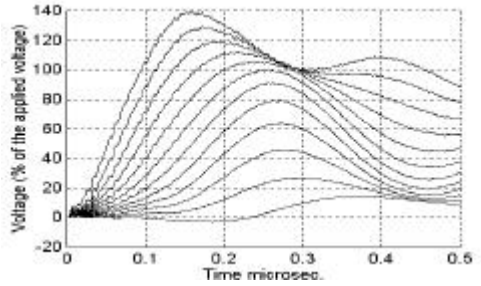

17(b)

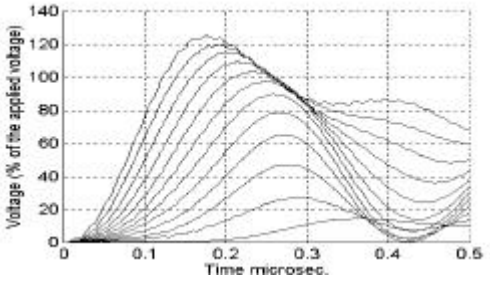

17(c)

Fig. 17 (a), (b), (c): Turn to ground voltage wave forms.
(a) measured voltage wave, (b) computed voltage wave using the MTLSMC, (c) computed voltage wave using the MTLCCS.

The behaviour of the three methods described in this paper using an actual machine winding is far better than those observed using a mock-up coil in the laminated slot environment described by Oyegoke (1997b). Both the measured and computed results show that it is the wave propagation along the individual turns of the coil that has a dominating effect, giving rise to high inter-turn voltages. Reflection takes place at the end of the first line-end coil and the second coil, due to an impedance mismatch at this point, thus causing a high inter-turn voltage on the turns towards the end of the first line-end coil.

The spreading of the reflected voltage wave on the turns towards the end of the first line-end coil depends on the wave front of the surge (pulse). The effect of the reflection due to the pulse rise time used in the present paper being spread over turns 9, 10 and 11 is confirmed by the measured and computed results.

The waveform of the pulse used in this paper for measurement and calculation has a rise time, from zero to maximum, of about 200 nanoseconds. A pulse with a very steep front may produce a reflection that will be spread only on the last turn in the first line-end coil, therefore causing the highest inter-turn voltage on that turn. The parameters for the motor and the winding construction used in this work are given in Tables IV and V. The cable between the voltage source and the motor has a surge impedance of about 50 Ohms and travelling time of about 25 nanoseconds. The velocity of wave propagation inside the cable is about half the speed of light namely $156 * 10^8 \, m/s$.

Table IV. The main parameters of the machine.

Rated voltage [V]	6300
Rated power [kW]	630
Rated speed [rpm]	2985
Rated frequency [Hz]	50
Winding Connection	Star
Number of phases	3
Number of poles	2
Air-gap diameter [mm]	420
Length [mm]	625

Table V. The winding constructions.

Number of stator slots	48
Number of slots per pole and phase	8
Number of turns per phase	176
Number of coils per phase	16
Number of turns in a coil	11
Conductor dimensions [mm]	11.5*2.36

8 EFFECT OF SOME PARAMETERS ON INTER-TURN VOLTAGE

8.1 Effect of copper resistance on the inter-turn voltage calculation

With the computer models described in the present work reasonably accurate, the effect of copper resistance on the accuracy of the turn voltage calculation is then investigated using the method MTLSMC. To accomplish this objective, the voltage distribution due to 25, 100, 150, 200, 250, 300 and 500 nanoseconds rise times pulse has been studied. For each of the pulses, calculations were made with and without copper resistance. The result of the calculation with copper resistance included in the computer model is called lossy, while the corresponding result of the calculation without copper resistance is called lossless. The results of calculation with and without copper resistance in the model for all these pulses are presented in Fig. 18.

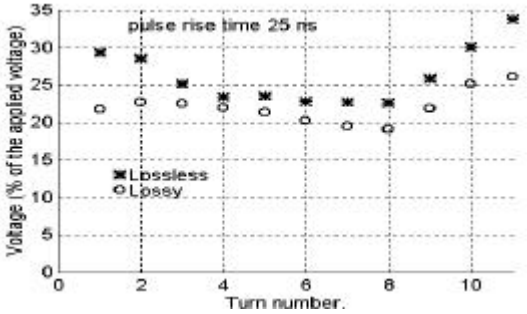

18(a)

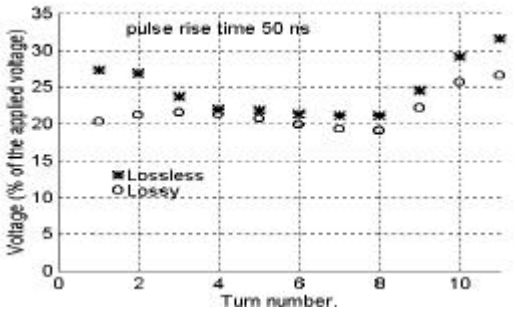

18(b)

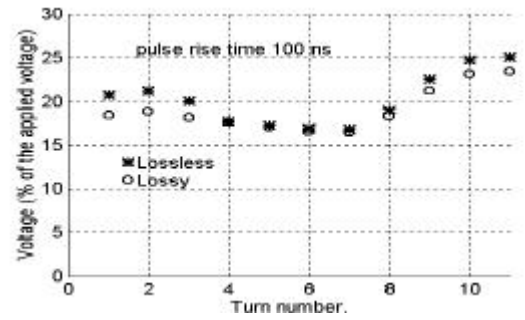

18(c)

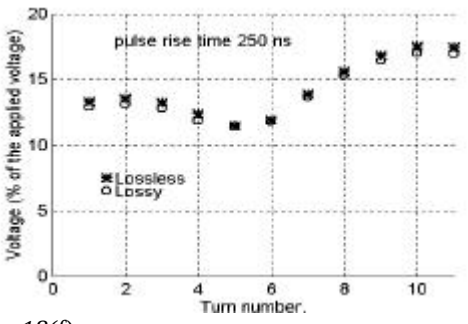

18(f)

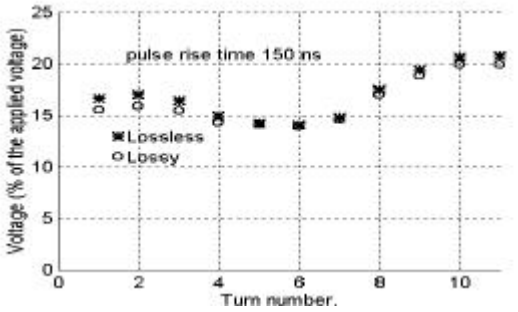

18(d)

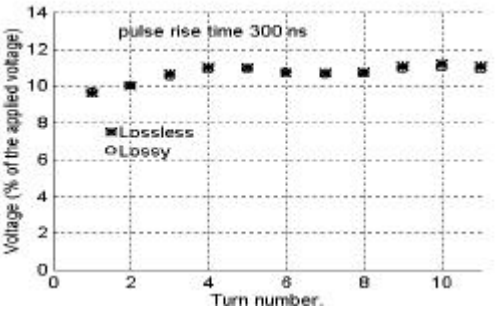

18(g)

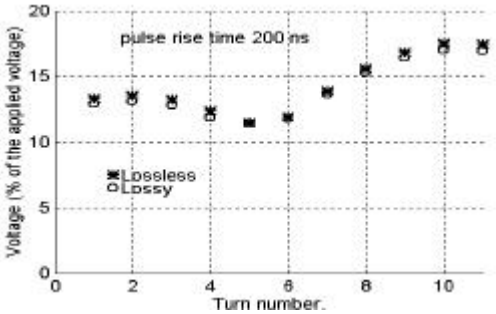

18(e)

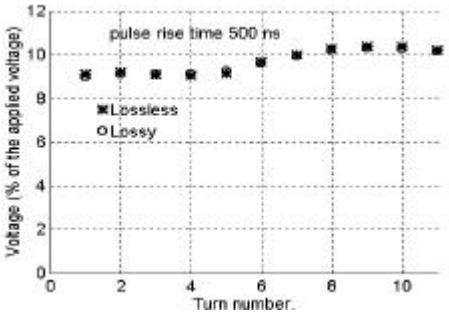

18(h)

Fig. 18 (a), (b), (c), (d), (e), (f), (g), (h): Variation of maximum voltages across turn with and without copper resistance

(a) computed using pulse with rise time 25 nanoseconds, (b) computed using pulse with rise time 50 nanoseconds,(c) computed using pulse with rise time 100 nanoseconds, (d) computed using pulse with rise time 150 nanoseconds, (e) computed using pulse with rise time 200 nanoseconds, (f) computed using pulse with rise time 250 nanoseconds, (g) computed using pulse with rise time 300 nanoseconds, (h) computed using pulse with rise time 500 nanoseconds.

From Fig 18, it can be seen that when one increases the pulse rise time, whether copper resistance is included in the model or not, the result of inter-turn voltage calculated using the lossy and lossless model remains practically the same. In this case, copper resistance may be neglected in the computational method. However, for pulses with a short rise time, there is a clear difference between the inter-turn voltage results obtained by the lossless and lossy models. In this case, copper resistance cannot be neglected in the computational method. With long rise time pulses, the magnitude of the inter-turn voltage becomes smaller and the distribution tends to be uniform. In contrast, short rise time pulses produce a high magnitude inter-turn voltage and the distribution is non-uniform.

8.2 Effect of the over-hang capacitance on the inter-turn voltage calculation

This section deals with a special aspect of the voltage distribution in the coils of electrical machines when confronted by fast-rising surge. The special aspect is the influence of the winding parameters especially the capacitance matrix for the slot and over-hang part of the winding. To model the capacitance, three methods

for capacitance computation described in the preceding section have been applied. For voltage calculation, the MTLSMC has been used.

8.2.1 Computation of the parameters

For the calculation of the scatter matrix $(\boldsymbol{S})$, it became obvious that two parameters need to be calculated - $(\boldsymbol{R})$ and $(\boldsymbol{Y})$. However, computation of the admittance $(\boldsymbol{Y})$ involves calculating the capacitance between the turns of the coil and the capacitance to the ground (slot wall in the slot part and adjacent coil sides in over-hang part).

8.2.2 Capacitance matrices

An accurate calculation of the capacitance matrices requires the solution of the electric field equations for both the slot and over-hang part of the coil. This will require the use of specialised computer programs. Two computer programs have been developed for this purpose. The first program uses the indirect boundary integral equation method (IBIEM) described in Chapter 2. The second program adopted the finite element method (FEM) also described in Chapter 2. Alternatively, since the system of turn conductors inside the core slot is rectangular, the capacitance matrices can be evaluated by approximating the sides of the turns to parallel plate capacitors (PPA) Mclaren and Abdel-Rahman 1988. It should be mentioned that the values of the capacitance to the current return path depend upon the coil part under consideration (slot or over-hang part). For the slot part, this capacitance results from the series combination of the inter-turn and main insulation. However, for the over-hang part, the air-gap between coils must be accounted for since the turns of the coils on either side of the coil under study are being taken to form the return earth path for the high frequency current. The air-gap between coil sides in the over-hang part is about one tooth width. This is large compared to the thickness of a thin insulation surrounding the coil. Therefore, for most machines in the over-hang part the dielectric is largely air. Hence, the relative dielectric permittivity of about one can be used when calculating the capacitance to the ground in this region. Fig. 19 shows the equipotential lines of electric scalar potential where a unit potential has been assigned to turn number 3 in the coil under consideration. The remaining turns of the coil under consideration and the turns of the adjacent coils are all at zero potential. In the same figure, immediate adjacent coil sides are modelled as well to show the inter-coil space. For the machine under investigation, this space is about 19 mm.

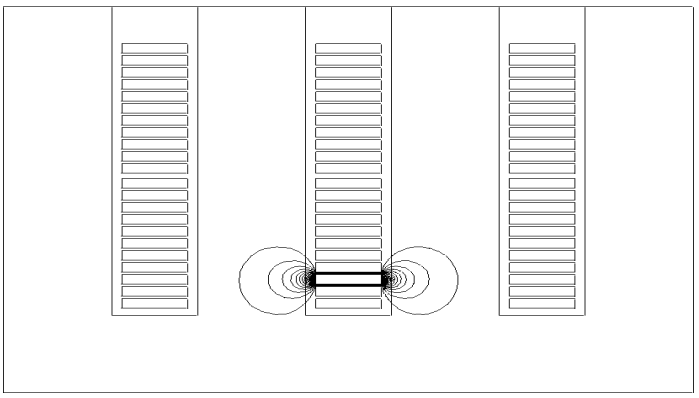

Fig. 19: Equipotential lines of electric scalar potential when turn number 3 is given a unit potential, and the remaining turns in the coil under consideration and turns in the surrounding coils zero potential.

This is large compared to the 1.75mm space occupied by the insulation surrounding the coil. The full capacitance matrix can be obtained from Eq.39.

$$(\mathbf{C}) = \begin{bmatrix} a+b & b & 0 & \cdots & \cdots & 0 \\ b & c+2b & b & \cdots & \cdots & 0 \\ 0 & b & c+2b & \cdots & \cdots & \cdots \\ \cdots & \cdots & b & \cdots & \cdots & \cdots \\ \cdots & \cdots & \cdots & \cdots & \cdots & \cdots \\ \cdots & \cdots & \cdots & \cdots & b & \cdots \\ \cdots & \cdots & \cdots & b & c+2b & b \\ \cdots & \cdots & \cdots & 0 & b & c+2b \\ 0 & 0 & 0 & 0 & b & d+b \end{bmatrix} \qquad (39)$$

where
a is the capacitance between the conductor of turn number one and the ground, b the capacitance between conductors of two adjacent turns, c the capacitance between the middle-turn conductor, the ground, and d the capacitance between the last turn conductor and the ground.

The capacitance matrix for the slot and over-hang region is of the form nxn where n is the number of turns in the coil. To calculate the capacitance to the ground in the over-hang part, all conductors in the coil are combined to form a single conductor of equivalent dimensions. The capacitance so obtained by any of the three methods for capacitance calculation is then divided among all the conductors that make the coil, with the upper and lower conductors having larger capacitance value because they present a larger part to the ground. The equipotential lines of electric scalar potential for such an approach are shown in Fig. 20 where potential of a unit value has been assigned to all the conductors of the coil under consideration and zero potential to conductors of the surrounding coils.

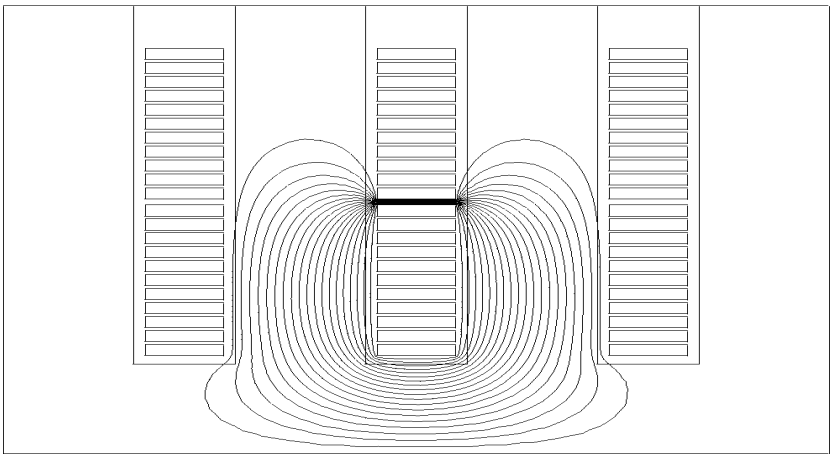

Fig. 20: Equipotential lines of electric scalar potential when all turns of the coil under consideration are given a unit potential and turns of the surrounding coils zero potential.

8.2.3 Computation of the admittance matrix

The admittance matrix of each part of a coil involved in a junction is calculated from Eq.32. The capacitance necessary for the evaluation of voltage distribution is given in Tables VI and VII. In these tables, results of three methods for capacitance computation are presented. A dielectric permittivity of 4 has been used for all capacitance except the capacitance to the ground in the over-hang region where the dielectric is largely air. Capacitance values due to PPA in Tables VI and VII are computed without considering the fringing effect.

Table V1. Capacitance value in pF/m, accounting for the air-gap between coil sides when calculating the capacitance to the ground in the over-hang part of the coil.

PPA		FEM		IBIEM		
Slot	**Over-hang**	**Slot**	**Over-hang**	**Slot**	**Over-hang**	
328.4	11.8	390.8	22.7	384.0	21.3	C_{1g}
96.4	4.4	123.6	8.5	120.8	7.9	C_{2g}
678.8	678.8	759.2	759.2	729.2	729.2	C_{12}
95.6	11.8	273.2	22.7	268.8	21.3	C_{ng}

Table VII. Capacitance value in pF/m, using the dielectric permittivity of the insulation surrounding the coil in the over-hang part when calculating the capacitance to the ground for this part of the coil.

PPA		FEM		IBIEM		
Slot	**Over-hang**	**Slot**	**Over-hang**	**Slot**	**Over-hang**	
328.4	41.9	390.8	80.4	384.0	75.2	C_{1g}
96.4	15.6	123.6	30.0	120.8	28.1	C_{2g}
678.8	678.8	759.2	759.2	729.2	729.2	C_{12}
95.6	41.9	273.2	80.4	268.8	75.2	C_{ng}

By making use of Table VI and matrix Eq.39, it is possible to construct the slot and over-hang capacitance matrix due to any of the three methods. In Table VI, using the capacitance due to FEM for the slot region : $a = C_{1g} = 390.8\,\text{pF/m}$; $b = C_{12} = 759.2\,\text{pF/m}$; $c = C_{2g} = 123.6\,\text{pF/m}$; $d = C_{ng} = 273.2\,\text{pF/m}$, and for the over-hang region we have: $a = C_{1g} = 22.7\,\text{pF/m}$; $b = C_{12} = 759.2\,\text{pF/m}$; $c = C_{2g} = 8.5\,\text{pF/m}$; $d = C_{ng} = a$. By a similar procedure, the capacitance matrix due to the other methods in the tables can be constructed. From Tables VI and VII, it can be seen that the accuracy of the IBIEM and the FEM method for capacitance is practically the same depending on the part of the coil under consideration (slot/over-hang). On the other hand the PPA method produces low capacitance values in comparison with the capacitance values obtained by the FEM and the IBIEM method for the slot and over-hang part of the coil. The result of the voltage distribution using the capacitance values obtained by these three methods for capacitance calculation is presented next.

8.2.4 Results

Fig. 21 presents the peak inter-turn voltages using the capacitance value in Table VI. Fig. 22 shows a similar result of calculation from the capacitance value in Table VII. Fig. 23 shows the computed waveform of the voltage across the last turn in the line-end coil. The result presented is calculated using the capacitance due to FEM in Tables VI and VII. In the same figure, the measured voltage waveform is also presented.

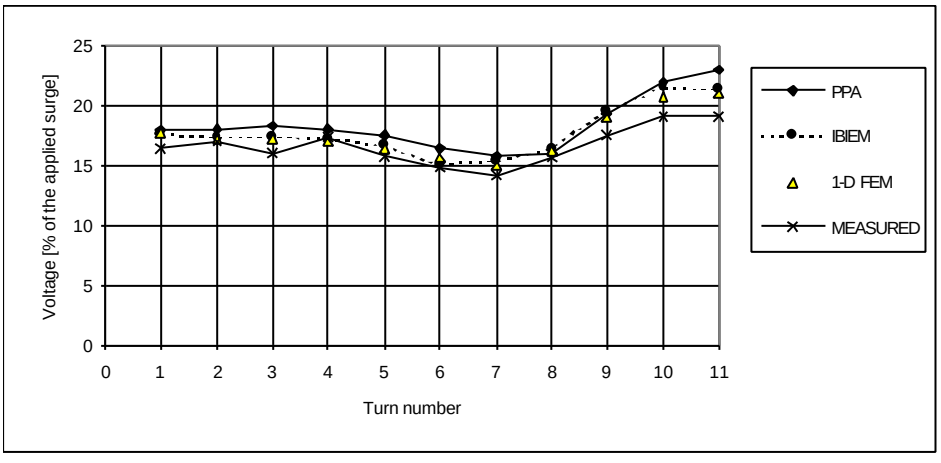

Fig. 21: Comparison of the measured and computed peak voltages across turns in the first terminal-end coil of a 6.3 kV induction motor. (Computation due to the capacitance values in Table VI).

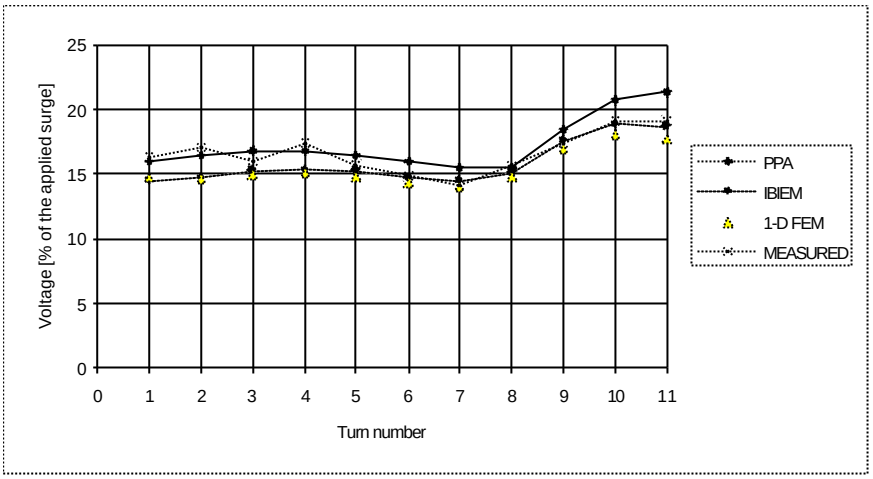

Fig. 22: Comparison of the measured and computed peak voltages across turns in the first terminal-end coil of a 6.3 kV induction motor. (Computation due to the capacitance values in Table VII).

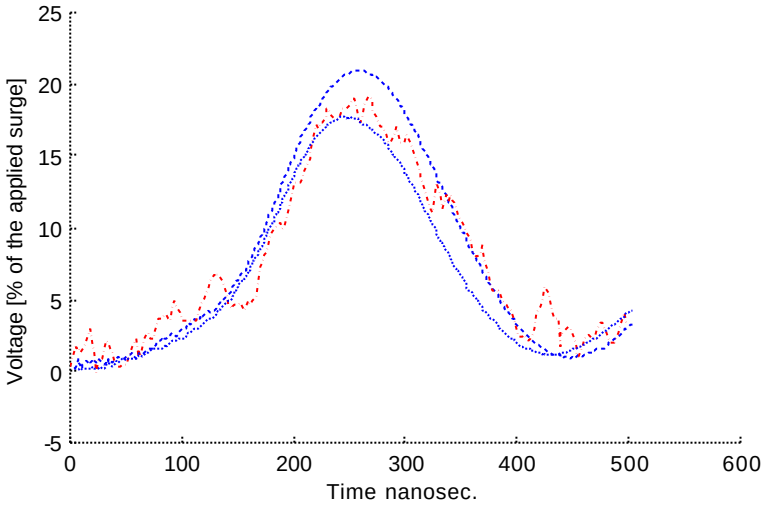

Fig. 23: Waveform of the voltage across turn number 11 in the first terminal end coil of a 6.3 kV motor.
–.–.– Measured waveform; ---- Computed waveform using the capacitance due to FEM in TabV1;
—— Computed waveform using the capacitance due to FEM in Tab VII.

8.2.5 Discussion of the results

The results of the capacitance due to the IBIEM and FEM as given in Table VI predict the magnitude of the turn voltages to a good accuracy as shown in Fig. 21. From the same figure, it can be seen that the capacitance due to the PPA in Table VII produces a slightly higher voltage across most of the turns than the IBIEM and the FEM. The highest discrepancy between computed voltage and measurement occurred towards the end of the coil where the highest turn voltage occurred irrespective of the method used for the capacitance calculation. If fringing is considered in the PPA calculation, a voltage distribution result similar to that of IBIEM and FEM is achieved. The waveform of the voltage across the last turn of the coil is given in Fig. 23 for the capacitance due to FEM. This compares well with the measurements.

The result of the capacitance due to the IBIEM and FEM as given in Table VII underestimates the magnitude of the turn voltages as shown in Fig. 22. The waveform of the voltage across the last turn of the coil is given in Fig. 23, for instance, for the capacitance due to FEM. However, the underestimation of the peak voltages is smaller in this particular case. However, there are cases when the error can be significantly large. Such cases

are considered next. From Fig. 22, it can be seen that the capacitance due to the PPA in Table VII produces an improved result over those in Table VI.

8.2.6 Analysis of other windings

To verify whether there is always a good agreement between the computed and measured peak inter-turn voltages when the air-gap between coil sides in the over-hang part is neglected when calculating the ground capacitance for the over-hang part, two other cases have been studied: the coil model used by Keerthipala and Mclaren (1990) and the stator coil studied by Narang et al. (1989). Fig. 24 presents the computed voltage between the last two turns of a coil studied by Keerthipala and Mclaren (1990). In the same figure, the measured voltage across this turn taken from the publication of Keerthipala and Mclaren (1990) is presented. The result of voltage between the last two turns of the line-end coil of the stator winding already studied by Narang et al. (1989) is presented in Fig. 25. The measured voltage between these turns is taken from the publication of Narang et al. 1989. It can be seen from the results in Figs. 24 and 25 that neglecting the air-gap when modelling the capacitance to the ground in the over-hang part can lead to a serious underestimation of the peak inter-turn voltage.

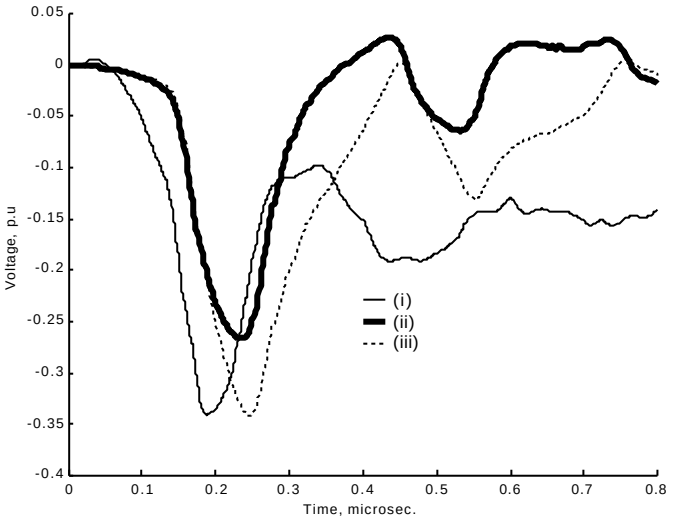

Fig. 24: Measured and computed voltage waveform between turns 9-10.
(i) Measured waveform taken from publication of Keerthipala and Mclaren 1990; (ii) Computed waveform when the air-gap between coil sides is neglected when calculating the capacitance to the ground in over-hang part; (iii) *Computed waveform when the air-gap between coil sides is considered when calculating the capacitance to the ground in over-hang part.*

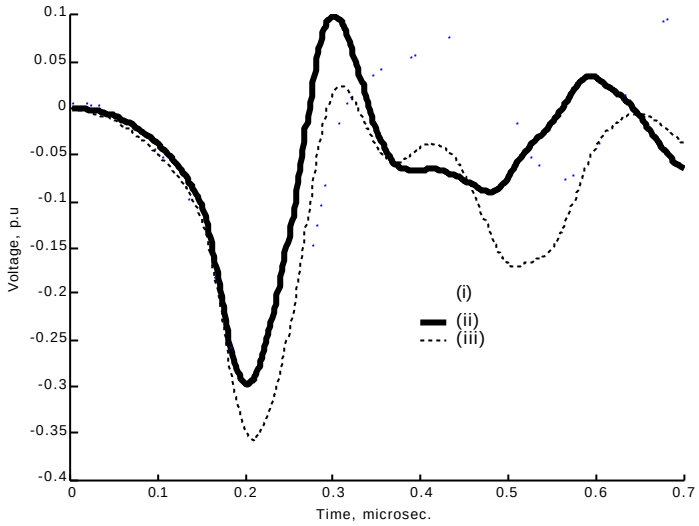

Fig. 25: Measured and computed voltage waveform between turns 5-6.

(i) *Measured waveform taken from publication of Narang et al. 1989;* (ii) *Computed waveform when the air-gap between coil sides is neglected when calculating the capacitance to the ground in over-hang part*; (iii) *Computed waveform when the air-gap between coil sides is considered when calculating the capacitance to the ground in over-hang part.*

8.2.7 Summary

The capacitance to the current return path depends upon the coil part under consideration (slot or over-hang part). For the slot region, this capacitance results from the series combination of the inter-turn and main insulation. However, for the over-hang part, the air-gap between coils must be accounted for since the turns of the coils on either side of the coil under study are being taken to form the return earth path for the high frequency current.

IBIEM and FEM calculate the capacitance accurately enough for permittivity of about a unit value to be used when calculating the capacitance to the ground in the over-hang part of the coil, see Fig. 21.

PPA for capacitance calculation without accounting for the fringing effect will overestimate the peak voltages across turns if a relative dielectric permittivity of one is used when evaluating the capacitance to the ground in the over-hang part. This is evident from Fig. 21.

PPA for capacitance calculation without accounting for the fringing effect will produce peak voltages close to the measured ones if the relative dielectric permittivity of the insulation surrounding the coil in the over-hang region is used when evaluating the capacitance to the ground in the over-hang part. This is evident from Fig.22

8.2.8 Conclusions

Three methods for simulation of the voltage distribution due to steep fronted surges in stator winding of medium or high voltage electric machines are presented. A detailed method for capacitance computation is also presented.

Whichever method is to be used for the computation of the capacitance to the ground in the over-hang part of the coil, the air gap between coils must be taken into consideration in order to have a precise peak voltage across turns. For all the cases studied in this paper, the dielectric permittivity of about a unit value is found adequate to give satisfactory peak voltages across turns of the first line-end coil. Capacitance due to parallel plate approximation gives a higher voltage across all turns than the indirect boundary element method and the finite element method when fringing effect is not considered.

From the comparisons between the results of voltage calculation using the three methods and the measured results presented in this paper the following points are evident.

All three methods can be used for the calculation of the inter-turn voltage distribution at least within the short period of time when the highest inter-turn voltages occur.

Although the methods described in this paper neglect the effect of high frequency magnetic flux penetration into the laminated core, the magnitude of the turn voltage and its wave pattern agree well with the measurement results. This is a very important result since the magnitude of the inter-turn (turn) voltage is of immediate importance to a machine insulation designer.

In a motor with multi-turn coil winding, the effect of the high frequency magnetic flux penetrating into the laminated core may not be the key factor that determines the amplitude of the inter-turn voltage in the multi-turn winding when confronted by fast-rising surge. The amplitude of the inter-turn voltage to a certain extent depends on the dielectric permittivity used when computing the capacitance to the ground in the over-hang part and the relative dielectric permittivity used when calculating the velocity of surge propagation in the winding.

These methods also find applications in the analysis of voltage distribution in the winding of electric machine fed from frequency converters that use pulse width modulated (PWM) technique.

For the inverter-fed motors, it will become necessary to model every connection in order to obtain more precise voltage calculations. The rise time of the inverter output pulse plays a significant role in motor insulation efficiency. However, the tail of the pulse to be used in calculations must be made longer than one turn travelling time for more precise knowledge of motor insulation. A very good performance in terms of the voltage magnitude and waveforms is shown by methods MTLSMC and MTLCCS, see Figs. 16(b) and 16(d).

In the analysis of the voltage distribution due to a pulse rise time greater than 100 nanoseconds, copper resistance may be neglected in the computational method.

9 METHODS FOR TRANSIENT VOLTAGE CALCULATION ON RANDOM WINDING

In this section, two methods of simulating the voltage distribution due to the PWM voltage pattern on the stator windings of an induction motor are presented. For the transient voltage calculation on the form windings, the turn capacitance to the ground and the inter-turn capacitance have to be calculated for both the slot and over-hang parts of the coil. Capacitance between non-adjacent conductors inside the slot and in the over-hang part of the coil may be neglected without loss of accuracy. However, on the random winding the per unit length capacitance that is necessary for the voltage computation has been determined on the part of the coil in over-hang region and same per unit capacitance value has been assumed for the part of the coil inside the slot. To validate the method adopted, the simulated results are compared with experimental results.

9.1 Problem definition

In order to predict the voltage distribution among the turns or coils of the stator winding fed by a frequency converter using the PWM techniques, it is necessary to use a distributed parameter model for the winding. This is because the machine behaviour at high frequencies such as those present in a PWM wave front is totally different from that at power frequency (50 Hz or 60 Hz). Calculation of the distributed parameter is very difficult. The parameters of the individual turns depend on their relative position within the slot and in the over-hang part. For example, a turn located near the slot wall will have a higher turn-to-ground capacitance compared to a turn located in the middle of the slot. In other words, a turn that is located in the middle of the slot will have a low turn-to-ground capacitance in the slot part of the coil because of the large separation of the turn conductor and the ground. Apart from this, other conductors surrounding it shield the conductor in the middle of the slot. In a similar way it can be said that the parameters of the individual turns depend also on their relative position in the over-hang part of the coil. For example, a turn located near the adjacent coil side will have a higher turn-to-ground capacitance in the over-hang region compared to a turn located in the middle

of the coil. In other words, a turn that is located in the middle of the coil will have a low turn-to-ground capacitance in the over-hang part of the coil because of the large separation of the turn conductor and the ground. Apart from this, other conductors surrounding it shield the conductor in the middle of the coil.

Furthermore, the relative positioning of the turn conductor in different slots and in the over-hang part may not be the same. It is possible that a turn located in the middle of the slot can be located very close to the adjacent coil in the over-hang part of the coil or vice versa. This means that the capacitance to ground varies from slot to slot and from slot to over-hang.

It should be mentioned that low voltage induction motors powered by PWM inverters have mostly of mush wound coils. The turns are randomly wound and the coils are either machine or manually inserted into the stator slots. Some manufacturers have developed methods for coiling so that the turns are not randomly wound and hence we can have some knowledge of the positioning of the turns inside the slot. This method appears more realistic when a turn is made of a single strand of conductor. In random wound machines a turn may consist of many (parallel) strands and it is more difficult to keep the turns in order. Therefore, the problem of determining the position of the conductors remained unsolved and subsequently the evaluation of the parameters involved in the transient voltage calculation remained unsolved. In the over-hang part, the turns (wires) will cross over conductors of adjacent coils.

Additionally, in a random wound machine, the placement of the individual turns within a slot will be quite random in nature and it is possible that the first and the last turn of the same coil are placed side by side as pointed out by Mechorn and Tang (1995). In this case, the two turns are separated only by a thin insulation layer of the two turns. Therefore, a voltage equal to a coil voltage is applied across these two adjacent turns. Hence, the maximum voltage that could appear between two adjacent turns in a random winding is equal to the coil voltage across the first line-end coil. Two methods for predicting this voltage are described in this section. The two methods used for the voltage calculation on random winding are the Multi-conductor transmission line and scatter matrix concept (MTLSMC) and the Multi-conductor transmission line concept for circuit simulator (MTLCCS) described in the preceding section.

9.2 Assumptions on estimation of motor parameters

In order to evaluate the necessary parameters for the voltage calculation some assumptions are made. Because of the high frequency involved, the magnetic material could be regarded as a flux barrier in a similar manner as previously assumed on voltage distribution within the form winding Wright et al. (1983), Mclaren and Abdel-Rahman (1988) and Narang et al. (1989). In this way, the mutual coupling between the part of the coil inside the slot and those in the adjacent slot can be disregarded.

9.3 Computation of the Capacitance Matrix for voltage calculation in random winding

In publications by Kerkman et al. (1996), Gubbala et al. (1995) and Skibinski (1996), the parameters used in the equivalent circuit are based on terminal measurements. Suresh et al. (1997) presented a method based on finite element analysis to estimate the distributed circuit parameters. Prediction of the voltage magnitude and distribution in the stator winding of an electric machine by means of the multi-conductor transmission line and the scatter matrix theories necessitates the calculation of capacitance only. For computation of the capacitance matrix, a method based on the indirect boundary integral equation method has been developed for this purpose. In fact, the computation of capacitance does not need to be carried out at high frequency since capacitance values are not influenced by frequency. Hence, a static capacitance is used in the present work.

In order to justify the effect of the turn position in the slot and outside the slot three examples (Chapter 9.6) are carried out and compared with the measurements. In the first example, a full capacitance matrix has been constructed for the part of the coil inside and outside the slot. A full capacitance matrix has been constructed for the part of the coil inside the slot and the capacitance to the ground has been used for the over-hang parts of the coil in the second example. In the third example the per unit length capacitance that is necessary for the

voltage computation has been determined from the part of the coil in over-hang region and the same per unit capacitance value has been assumed for the part of the coil inside the slot. In this way, the method described here differs from that of previous authors, showing that the majority of capacitance lies in the slot part of the coil. The off-diagonal elements in the capacitance matrix, which correspond to the mutual capacitance between turns, have been neglected.

To calculate the turn-to-ground capacitance component in the diagonal terms of the capacitance matrix, the adjacent coils are assumed to represent a ground plane where the return current flows in over-hang part of a coil. A similar assumption has been applied to voltage calculation in the form winding and has been used by several authors: Narang et al. (1989), Mclaren and Abdel-Rahman (1988). In fact, the adjacent coil sides in the over-hang part of the coil are separated by insulation thickness equal to twice the thickness of the turn insulation. This insulation thickness is smaller than the insulation that is separating the slot part of the coil and the slot wall, so it is found that majority of the capacitance lies in the over-hang part of the coil.

A further simplification adopted in calculating the capacitance matrix of a random winding is that all turns contained in a coil are treated as a single solid conductor whose perimeter coincides with that of the complete coil. Capacitance between adjacent coils is then calculated by the indirect boundary integral equation method and this capacitance is distributed equally among all turns of the coil under consideration. Thus, the capacitance matrix used for this analysis has only the diagonal terms.

9.4 Voltage calculation on random winding

After evaluating the necessary parameters, a unit impulse is sent from the switch that represents the inverter. The scatter matrix theory has been combined with the multi-conductor transmission line theory to obtain the incident and the reflected waves at each junction in a similar way to that described for the voltage calculation on the form winding. This calculation is performed for the whole period of interest. Finally, the waveform of the inverter output voltage (pulse) is imposed.

An alternative method for voltage calculation on machine winding is the use of high frequency equivalent circuit of the coil whereby a turn is used as an elemental part of the circuit as shown in Fig 26. The equivalent circuit of a two-turn coil in Fig. 26 requires the computation of the self-inductance L of each turn, the mutual inductance M between turns and the capacitance to the ground C_g of each turn, and the mutual capacitance C_{12} between them. All these parameters are necessary for the transient voltage simulation on the form winding.

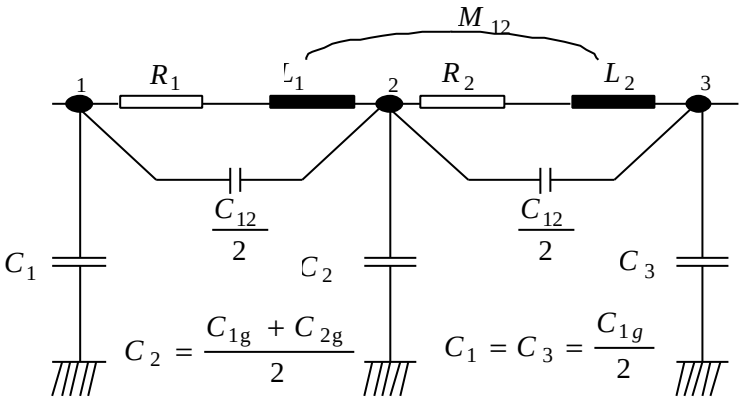

Fig. 26: Equivalent circuit of a two-turn coil.

The mutual inductance and the mutual capacitance have been omitted in the voltage simulation on the random winding. The capacitance obtained in the previous section has been used on the circuit. However, the calculation of the inductance matrix is evaluated from a modified capacitance matrix by the duality existing between electric and magnetic field equations in homogeneous systems, as previously discussed.

9.5 Measurement arrangements on a random winding machine

In the measurement, it was used an induction motor having the rated power of 15 kW, the rotational speed of 2860 rpm and the rated voltage of 380 V. The machine has a three-phase random, diamond winding. The number of the poles is 2, the stator slots 36 and the stator slots per pole and phase 6. The main parameters of the machine and the winding construction are given in Tables X and XI.

The machine has 19 measurement conductors in different parts of the coils in the same phase. The measurement points are in every turn in the first coil and, furthermore, at the terminals of the other coils. The measurement conductor types are the same as the main conductor in the stator winding. The lengths of the measurement conductors are 700 mm.

The type of inverter used is Yaskawa Varispeed-616 G3. It is a sinusoidal-wave PWM-inverter, in which IGBT transistors are used. The rated power is 27.4 kVA, the frequency 0 - 400 Hz and the switching frequency 0.4 - 15 kHz.

The voltage distribution was measured with a Tektronix 2430A 150 MHz digital oscilloscope. The measuring instruments are 20 MHz probes. The measurements are made using a 3 meters long cable of the type Nokia VSB-ATON 5x6S. Lampola 1992 presents a more detailed analysis of the induction machine.

Table X. The main parameters of the machines.

Main parameters	Random
Rated voltage [V]	380
Rated power [kW]	15
Rated speed [rpm]	2860
Rated frequency [Hz]	50
Connection	star
Number of phases	3
Number of poles	2
Air-gap diameter [mm]	135
Length [mm]	160

Table XI. The winding constructions.

Winding	Random
Number of stator slots	36
Number of slots per pole and phase	6
Number of turns in phase	78
Number of coil groups	6
Number of turns in coil section	13
Conductor [mm]	3*0.85

9.6 Sensitivity of turn position

In order to justify the fact mentioned in Section 9.3 about the effect of the turn position in the slot and outside the slot the following calculated examples are carried out and compared with the measurement results. For the voltage calculation the MTLSMC has been used in this section.

9.6.1 Full capacitance matrix of the slot and over-hang part of the coil

The full capacitance matrix has been constructed for the slot part of the coil in accordance with the position assumed for individual turns inside the slot as shown in Fig. 27a. The same full capacitance matrix (in pF/m) has been assumed for the part of the coil in over-hang region. The full capacitance matrix in pF/m, evaluated in the slot part of the coil is

$$C = \begin{bmatrix}
464 & -90 & -85 & -43 & -8 & -1 & -2 & -61 & 0 & -62 & -62 & -6 & -6 \\
-90 & 507 & -2 & -42 & 0 & 0 & -14 & -68 & 0 & 0 & -20 & -123 & -111 \\
-85 & -2 & 439 & -51 & -53 & -16 & -26 & 0 & -12 & -98 & -10 & 0 & -60 \\
-43 & -42 & -51 & 511 & -62 & -95 & -114 & -55 & -2 & -45 & 0 & 0 & -2 \\
-8 & 0 & -53 & -62 & 398 & -88 & -85 & -42 & -44 & -2 & -11 & -2 & -2 \\
-1 & 0 & -16 & -95 & -88 & 476 & -2 & -8 & -46 & -5 & -44 & -76 & -93 \\
-2 & -14 & -26 & -114 & -85 & -2 & 545 & -94 & -41 & -51 & -74 & 0 & -42 \\
-61 & -68 & 0 & -55 & -42 & -8 & -94 & 527 & -103 & -5 & -3 & -69 & 0 \\
0 & 0 & -12 & -2 & -43 & -46 & -41 & -103 & 540 & -217 & -10 & -44 & 0 \\
-62 & -0 & -98 & -45 & -2 & -5 & -51 & -5 & -217 & 540 & 0 & -8 & -28 \\
-62 & -20 & -10 & 0 & -11 & -44 & -74 & -3 & -10 & 0 & 422 & -122 & -36 \\
-6 & -123 & 0 & 0 & -2 & -76 & 0 & -69 & -44 & -8 & -122 & 487 & -16 \\
-6 & -111 & -60 & -2 & -2 & -93 & -42 & 0 & 0 & -28 & -36 & -16 & 428
\end{bmatrix}$$

This matrix should be multiplied by the relative dielectric constant of the medium. In this case a relative dielectric constant of 4 has been used. By changing the position of the turn no. 1 with the turn nos. 7 and 13 as shown in Figs. 27a-c, we construct different capacitance matrix for the slot part of the coil. Each of these capacitance matrixes is used in calculation of the transient voltage distribution.

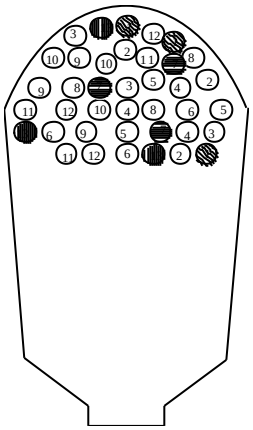

27a Initially assumed position of turns.

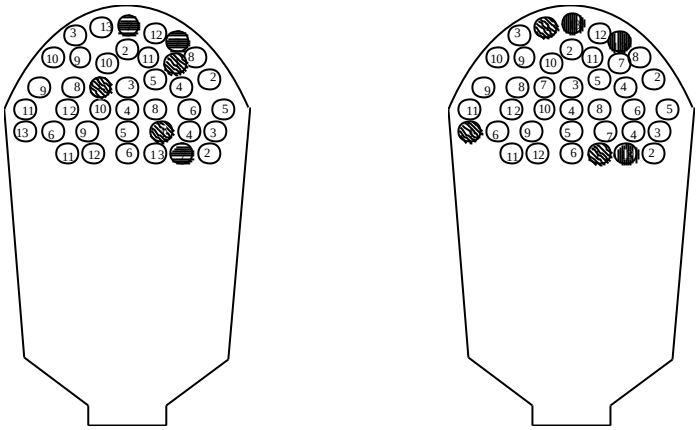

27b Position of the turns 1 and 7 are changed. *27c Position of the turns 1 and 13 are changed.*

Fig. 27: Initially assumed position of the turns and two other cases.

9.6.2 Full capacitance matrix for the slot and turn to ground capacitance for the over-hang part of the coil

A full capacitance matrix has been constructed for the slot part of the coil in accordance with the position assumed for individual turns inside the slot as shown in Fig. 27a. However, for the over-hang part only the turn to ground capacitance contained in the diagonal elements of the capacitance matrix has been used. In other words mutual capacitance has been neglected. The computation procedure of this capacitance to the ground is explained in the section 9.3. The capacitance matrix for the over-hang part of the coil is

$$C_e = \begin{bmatrix} 58 & 0 & 0 & 0 & 0 & 0 & 0 & 0 & 0 & 0 & 0 & 0 & 0 \\ 0 & 58 & 0 & 0 & 0 & 0 & 0 & 0 & 0 & 0 & 0 & 0 & 0 \\ 0 & 0 & 58 & 0 & 0 & 0 & 0 & 0 & 0 & 0 & 0 & 0 & 0 \\ 0 & 0 & 0 & 58 & 0 & 0 & 0 & 0 & 0 & 0 & 0 & 0 & 0 \\ 0 & 0 & 0 & 0 & 58 & 0 & 0 & 0 & 0 & 0 & 0 & 0 & 0 \\ 0 & 0 & 0 & 0 & 0 & 58 & 0 & 0 & 0 & 0 & 0 & 0 & 0 \\ 0 & 0 & 0 & 0 & 0 & 0 & 58 & 0 & 0 & 0 & 0 & 0 & 0 \\ 0 & 0 & 0 & 0 & 0 & 0 & 0 & 58 & 0 & 0 & 0 & 0 & 0 \\ 0 & 0 & 0 & 0 & 0 & 0 & 0 & 0 & 58 & 0 & 0 & 0 & 0 \\ 0 & 0 & 0 & 0 & 0 & 0 & 0 & 0 & 0 & 58 & 0 & 0 & 0 \\ 0 & 0 & 0 & 0 & 0 & 0 & 0 & 0 & 0 & 0 & 58 & 0 & 0 \\ 0 & 0 & 0 & 0 & 0 & 0 & 0 & 0 & 0 & 0 & 0 & 58 & 0 \\ 0 & 0 & 0 & 0 & 0 & 0 & 0 & 0 & 0 & 0 & 0 & 0 & 58 \end{bmatrix}$$

By changing the position of the turn number one we construct different capacitance matrix for the slot part while the capacitance matrix of the over-hang part is kept constant. This capacitance is used in calculation of the transient voltage distribution.

9.6.3 Results

The result of calculation and its corresponding measurement result are given in Figs. 28-34 for the case of Chapter 9.6.1, in which the full capacitance matrix has been used for the slot and over-hang part of the coil.. Figs. 28-31 present the computed and corresponding measured turn to ground voltage at the terminal and end of the first line end coil. Figs. 32-34 presents the computed and measured voltage across the line-end coil.

Table X presents a summary of computed and measured results for the three different positions assumed for the turn no. 1.

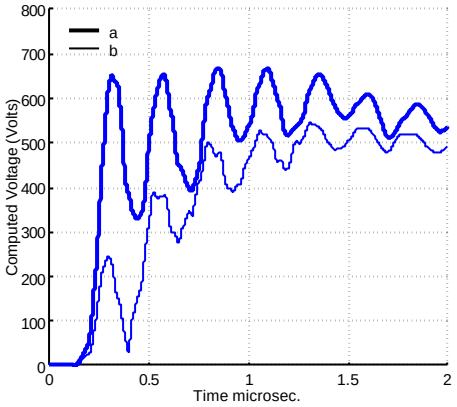

Fig. 28: Motor terminal voltage (a) and voltage at the end of the first line-end coil (b) in the case of the initially assumed position of the turns in Fig. 27a.

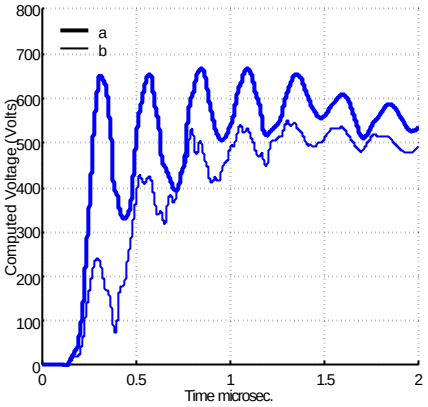

Fig. 29: Motor terminal voltage (a) and voltage at the end of the first line-end coil (b) in the case Fig. 27b.

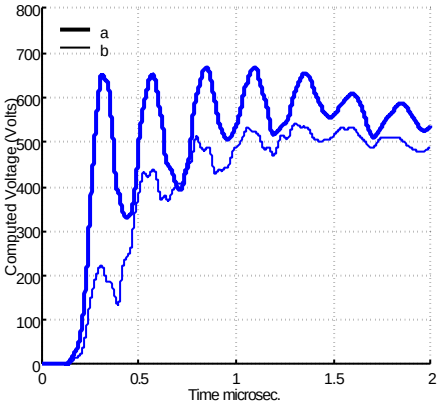

Fig. 30: Motor terminal voltage (a) and voltage at the end of the first line-end coil (b) in the case Fig. 27c.

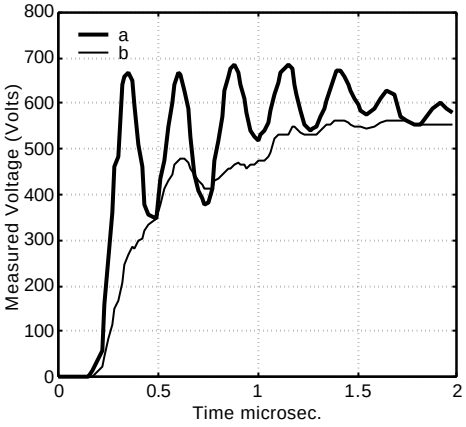

Fig. 31: Measured voltage at the motor terminal (a) and at the end of the first line-end coil (b).

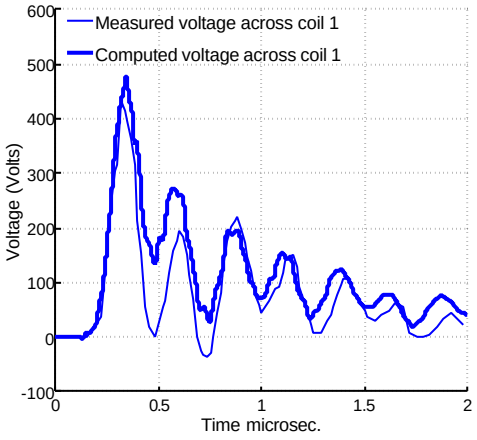

Fig. 32: Voltage drop across the first coil in a random winding in the case of the initially assumed position of the turns in Fig. 27a (Measured and Computed result).

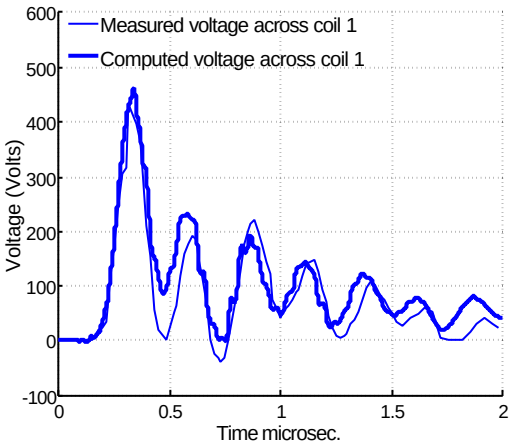

Fig. 33: Voltage drop across the first coil in a random winding in the case Fig. 27b (Measured and Computed result).

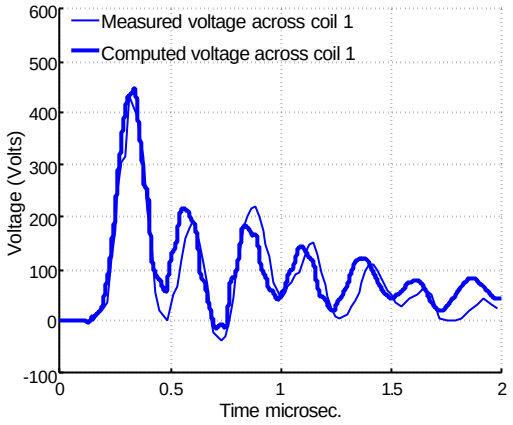

Fig. 34: Voltage drop across the first coil in a random winding in the case Fig. 27c (Measured and Computed result).

Table X: Summary of the computation result using a full capacitance matrix for the slot and over-hang part of the coil and three different position for turn no. 1. A: *Initial position of the turns as in the case Fig. 27a; B: The turn no. 1 assumes the position of the turn no. 7 as in the case Fig. 27b; C: The turn no. 1 assumes the position of the turn no. 13 as in the case Fig. 27c; D: Measured results.*

	A	B	C	D
	Coil Voltage, V			
Coil no. 1	476	462	448	433
Turn Voltage, V				
Turn no. 1	35	33	34	85
Turn no. 2	36	35	40	82
Turn no. 3	39	39	35	82
Turn no. 4	40	37	39	78
Turn no. 5	41	39	41	74

From Figs. 28-34 and Table X, it can be seen that the position of the turns inside and outside the slot does not influence very much on the coil voltage in the studied cases. However, the position of the turns influences on the turn voltage. It should be mentioned that the calculated voltage across coil 1 presented in Table X is not very far from the corresponding measured coil voltage. However, the computed turn voltages are not well in balance with the measurement. The result of calculations and corresponding measurements are given in Figs. 35-41 in case of Chapter 9.6.2, in which the full capacitance matrix has been used for the slot part and the capacitance to the ground for the over-hang part of the coil. Figs. 35-38 present the computed and corresponding measured turn to ground voltage at the terminal and end of the first line end coil. Figs. 39-41 presents the computed and measured voltage across the line-end coil.

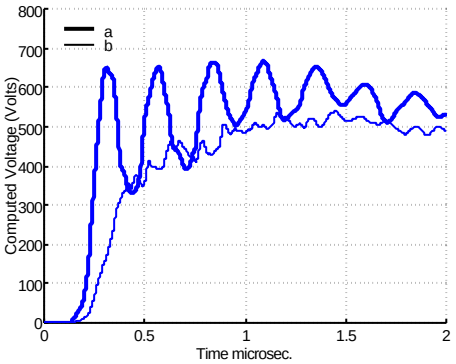

Fig. 35: Motor terminal voltage (a) and voltage at the end of the first line-end coil (b) in the case of the initially assumed position of the turns in Fig. 27a.

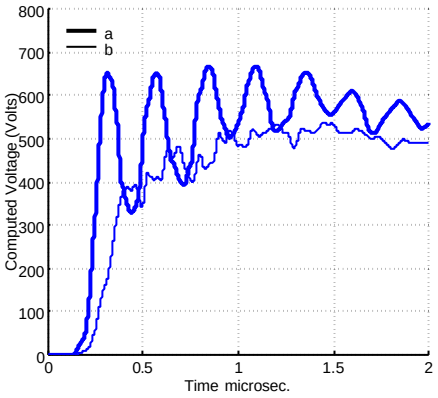

Fig. 36: Motor terminal voltage (a) and voltage at the end of the first line-end coil (b) in the case Fig. 27b.

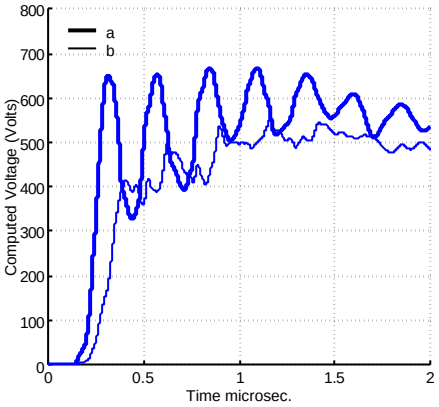

Fig. 37: Motor terminal voltage (a) and voltage at the end of the first line-end coil (b) in the case Fig. 27c.

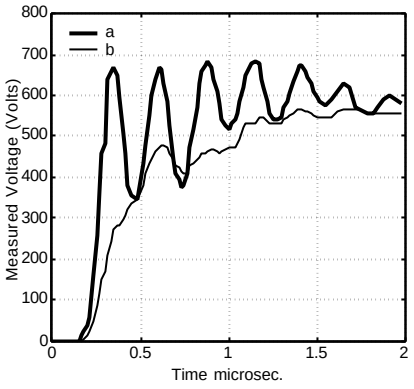

Fig. 38: Measured voltage at the motor terminal (a) and at the end of the first line-end coil (b).

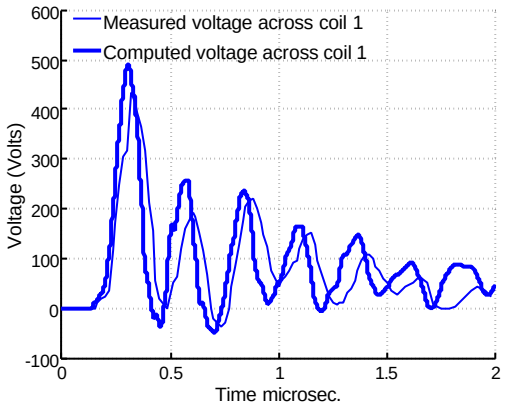

Fig. 39: Voltage drop across the first coil in a random winding in the case of the initially assumed position of the turns in Fig. 26a (Measured and Computed result).

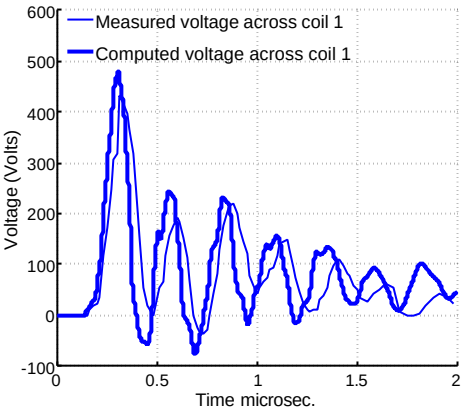

Fig. 40: Voltage drop across the first coil in a random winding in the case Fig. 26b (Measured and Computed result).

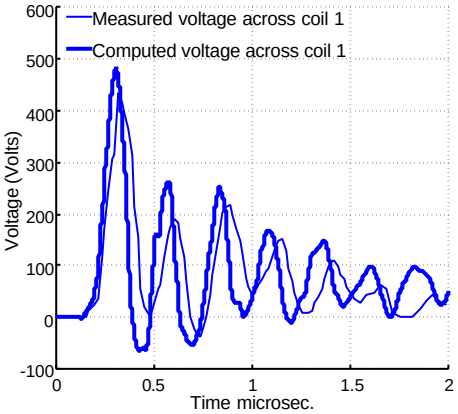

Fig. 41: Voltage drop across the first coil in a random winding in the case Fig. 27b (Measured and Computed result).

Table XI presents a summary of the computed and measured results for the three different positions assumed for the turn no. 1.

Table XI: Summary of the computation result using a full capacitance matrix for the slot and over-hang part of the coil and three different position for turn no. 1. A: *Initial position of the turns as in the case Fig. 27a; B: The turn no. 1 assumes the position of the turn no. 7 as in the case Fig. 27b; C: The turn no. 1 assumes the position of the turn no. 13 as in the case Fig. 27c; D: Measured results.*

	A	B	C	D
	Coil Voltage, V			
Coil no. 1	491	481	483	433
Turn Voltage, V				
Turn no. 1	48	48	39	85
Turn no. 2	49	40	38	82
Turn no. 3	38	42	35	82
Turn no. 4	43	45	39	78
Turn no. 5	46	43	43	74

From Figs. 35-41 and Table IX, it can be seen that the voltage across the coil no. 1 and the voltage across the turns are higher than the value obtained in the previous example. Again we see that the position of the turns does not influence very much on the coil voltage but it influences on the turn voltages. The coil voltage is not as good as in the previous example. Although, the turn voltage shows some improvement, however, the accuracy still remains insufficient.

The result of examples presented here shows a need for another method of transient voltage calculation in a random winding which will be independent of the turn position in and outside the slot. Such a method is described next.

9.6.4 Turn to ground capacitance of the over-hang part is assumed for the slot part

As the third approach tested in this work the same capacitance matrix obtained in the over-hang region C_e given above is also assumed for the slot part of the coil. By so doing the mutual capacitance is completely eliminated from the analysis and there will be no need to know which turn is in the middle of the slot or close to the slot wall. Mutual inductance is neglected as well. This does not means that these parameters are not existing. They are existing but as a first approximation, it is assumed that they are of secondary importance. This approximation can be traced back to the transformer point of view where it is well known that it is the capacitance to the ground that is actually giving rise to a non-uniform voltage distribution inside the winding. To have uniform voltage distribution inside the transformer winding, the winding constructions are made such that the series capacitance is much higher than the capacitance to the ground. It is therefore, assumed in the present work that the turn capacitance to the ground in the slot exist. Additionally, the turn capacitance to the ground exists in over-hang region. Furthermore, there is the resistance and inductance for the part of the coil inside the slot and over-hang region.

The result of computation and measurement using this approach is presented in Figs. 42–44. Figs. 42 and 43 present the computed and measured voltage at the motor terminal and at the end of the first line-end coil. Fig. 44 presents the computed and measured voltage across the line-end coil.

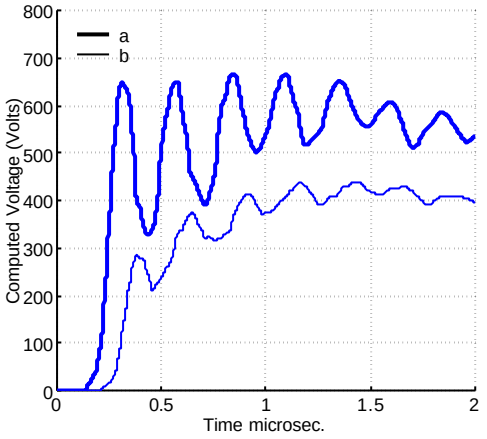

Fig. 42: Motor terminal voltage (a) and voltage at the end of the first line-end coil(b) (Computed result).

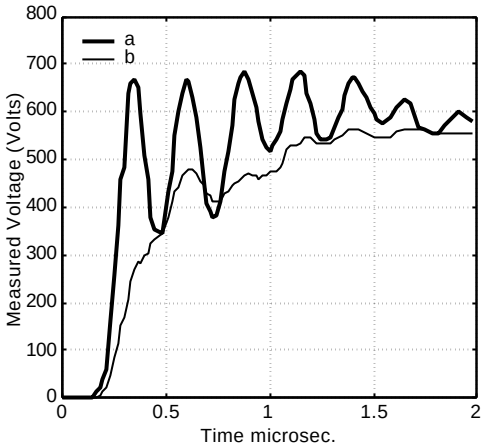

Fig. 43: Motor terminal voltage (a) and voltage at the end of the first line-end coil(b) (Measured result).

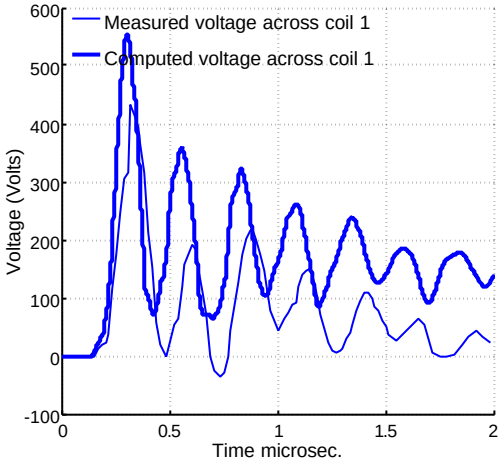

Fig. 44: Measured and Computed voltage drop across the first coil.

From Figs. 42, it can be seen that neglecting the capacitance between turns leads to an under-estimation of the voltage to the ground at the end of the first coil. The consequence of this is that the voltage across the coil no. 1 shown in Fig. 44 is higher than the value obtained in the previous examples. Again it was found out that the position of the turns does not influence very much on the coil voltage but it influences on the turn voltages. The coil voltage is not as good as in the previous example. Although, the turn voltage shows some improvement, however, the accuracy still remains insufficient.

The initial distribution of voltage is an instantaneous distribution that could be seen within the first few nanoseconds of the turn voltage to ground in Figs. 28 to 31. This voltage could be thought of as been determined simply by the capacitance between the turns of the coil.

Immediately after the initial distribution the distribution due to the propagation of surge along individual turns of the coil follows. This results in steep wave front for the first few turns of the coil and low steep front for other turn to ground voltage wave towards the last turn of the coil.

Neglecting the capacitance between the turns means simply that one assumes surge propagation along individual turns of the coil. The consequence of this is that the computed voltage across the line-end coil is higher than the corresponding measured voltage as shown in Fig. 44. It was found out that if the first five turns from the line-end coil are modelled, the accuracy of this method can be improved without any need to consider the mutual capacitance or to know the position of the turns in the slot and in the over-hang region. In addition, reasonable estimation of voltage across the first five turns in the line-end coil can be made. This technique for modelling the voltage distribution in random winding is presented in the section 9.6.5, where the

MTLSMC and the MTLCCS has been applied for the voltage calculation. Satisfactory results have been obtained in all the cases studied.

9.6.5 Computed results using the MTLSMC and MTLCCS

Measured and simulated voltage results on a random winding (380 V induction motor) using the MTLSMC and MTLCCS are presented in this section. To verify the accuracy of the two methods presented in the preceding part, calculation and measurement have been performed on a random winding machine where the conductor positions are not fixed and are unknown inside and outside the slot. Results of such a verification test are presented in Figs. 45 to 50.

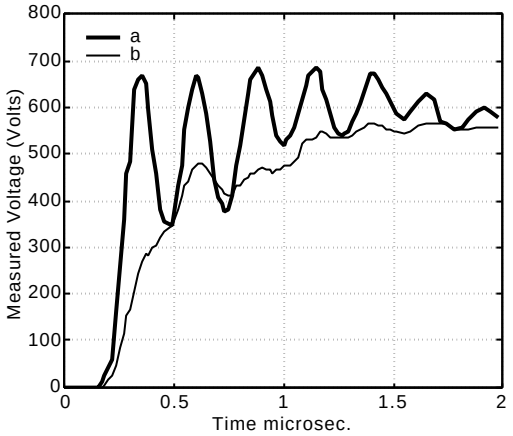

Fig. 45: Motor terminal voltage (a) and voltage at the end of the first coil (b) in a random winding. (Measured result) .

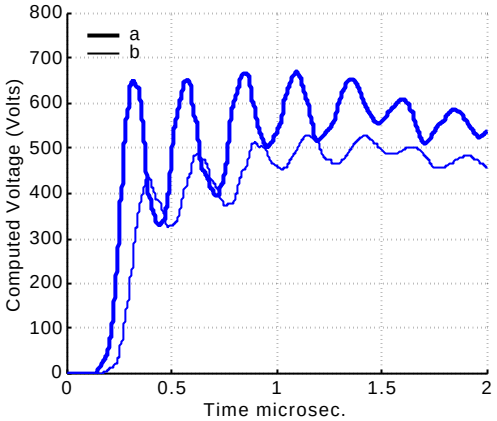

Figure 46: Motor terminal voltage (a) and voltage at the end of the first coil(b) in a random winding result (Computed result using the MTLSMC).

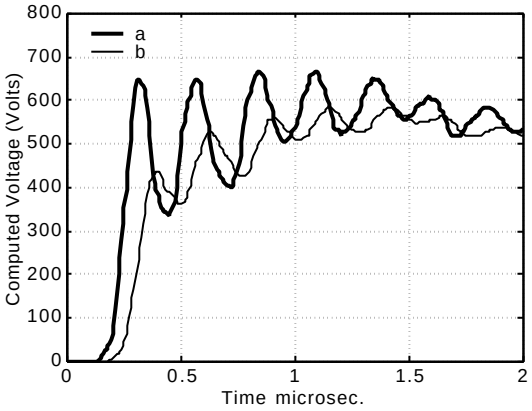

Fig 47: Motor terminal voltage (a) and voltage at the end of the first coil (b) in a random winding. (Computed result using the MTLCCS).

Fig. 45 presents the measured turn-to-ground voltages. Fig. 46 presents the computed voltage-to-ground at the motor terminal using the MTLSMC. In the same figure the measured voltage-to-ground at the end of the first coil is also presented. Fig. 47 presents the computed voltage-to-ground at the motor terminal using the MTLCCS. In the same figure, the measured voltage-to-ground at the end of the first coil is also presented.

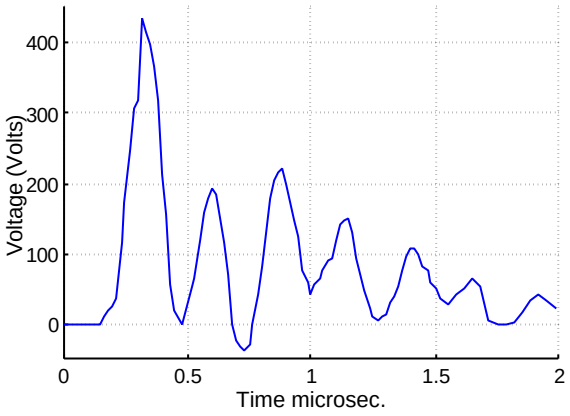

Fig 48: Voltage drop across the first coil in a random winding. (Measured result)

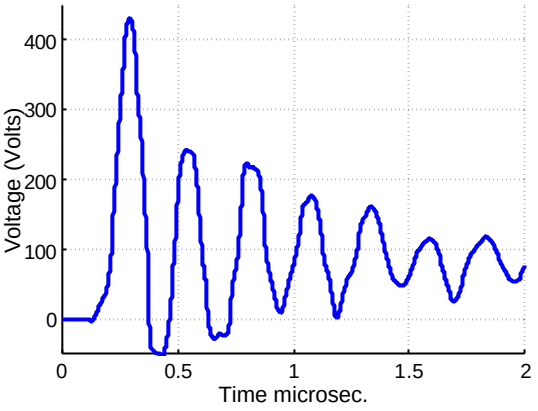

Fig 49: Voltage drop across the first coil in a random winding. (Computed result using the MTLSMC)

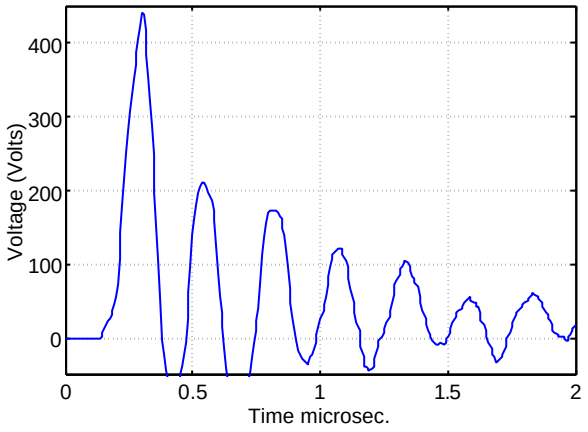

Fig 50: Voltage drop across the first coil in a random winding.(Computed result using the MTLCCS)

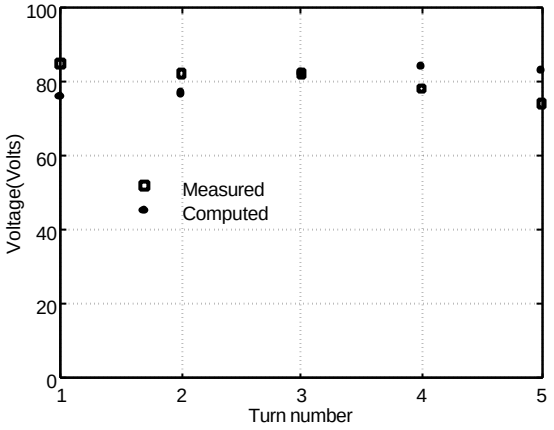

Fig 51: Maximum voltage drop across turns vs. Turn number measured and computed result using the MTLSMC on the random winding

Measured voltage drop across the first terminal-end coil is given in Fig. 48. The calculated voltage drop across the first coil from the terminal using the MTLSMC is given in Fig. 49. The calculated voltage drop across the first coil from the terminal using the MTLCCS is given in Fig. 50.

Computation of the voltage distribution in the random winding motor using the two methods described in this section has proved successful. The variation pattern of the simulated voltage matches the measured results well. The peak value of the voltage drop across the line-end coil is well predicted by the two methods proposed in this section. For completeness of the work on the random winding, the measured and the computed peak voltage drop across the first five turns in the line-end coil are plotted as a function of the turn number in Fig. 51.

9.7 Further studies on random winding

More investigation of the accuracy of both methods in simulating the voltage distribution in random winding is done with two other motors designated by Mk and Ml. The main parameters of the machines and their windings are given in Tables XII and XIII.

Table XII. The main parameters of the machines.

Main parameters	Random Mk	Random Ml
Rated voltage [V]	400	380
Rated power [kW]	3	7.5
Rated speed [rpm]	2800	1450
Rated frequency [Hz]	50	50
Connection	Star/Delta	Star/Delta
Number of phases	3	3
Number of poles	2	4
Air-gap diameter [mm]	90	125
Length [mm]	65	145

Table XIII. The winding constructions.

Winding	Random Mk	Random Ml
Number of stator slots	36	36
Number of slots per pole and phase	6	3
Number of turns in phase	54*12	34*6
Number of coil groups	12	6
Number of turns in coil section	54	34
Conductor [mm]	0.71	3*0.75

Computation results using the MTLSMC are presented in Figs. 52 and 53. Figs. 54 and 55 present the computation results using the MTLCCS.

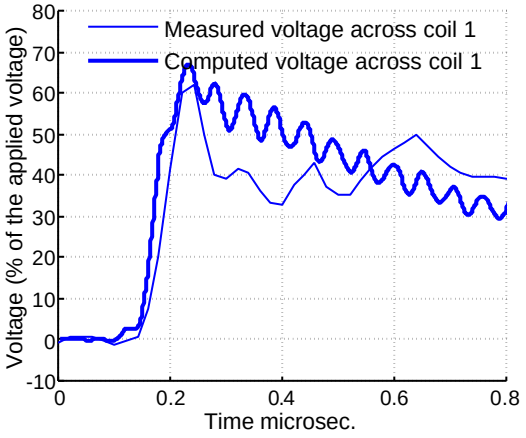

Fig. 52: Voltage drop across the first coil in Mk. (Computed with MTLSMC)

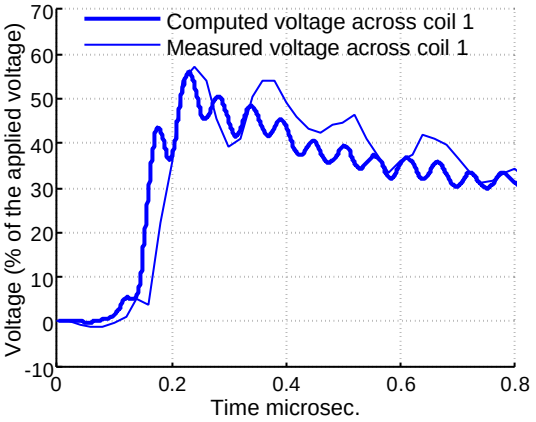

Fig. 53: Voltage drop across the first coil in Ml. (Computed with MTLSMC)

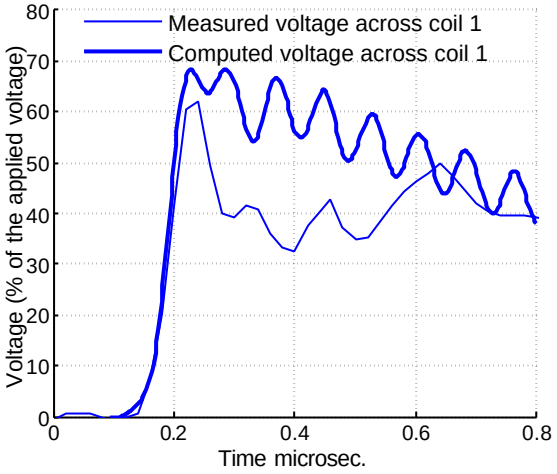

Fig. 54: Voltage drop across the first coil in Mk. (Computed with MTLCCS)

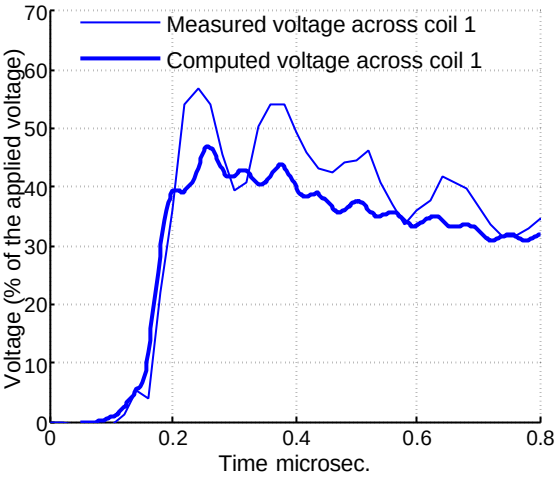

Fig. 55: Voltage drop across the first coil in Ml. (Computed with MTLCCS)

From the result of further studies, it can be seen that the performance of the proposed methods is good in calculating the voltage across the first line-end coil. These methods have some advantages over the existing models. This is because, while some models depends on a terminal measurement method to estimate the parameters to be used in their model, the present model does not require any measurements and can be used at the design stage. In addition, some models require detailed computation of the capacitance inside the slot portion of the coil where turn position is not known. The methods described here depend simply on the computation of the capacitance in the over-hang part of the coil. Therefore, the problem that involves calculation of capacitance of a coil, for instance consisting of 100 turns is reduced to a problem of solving the capacitance between only three conductors, i.e. the coil under investigation and two adjacent coils. We therefore do not need to know the position of turn conductors to evaluate the line-end coil voltage.

10 CONCLUSIONS

Transient voltage distribution in stator windings of electrical machines is investigated using three methods that are based on the multi-conductor transmission line theory.

The multi-conductor transmission line and averaging technique concept represents a quick means of evaluating the inter-turn (turn) voltage. The peak inter-turn voltage predicted by this method compared well with the measured results especially in the beginning of the coil and towards the end of the coil where the highest turn voltage occurs. The weakness of this method lies in the voltage waveforms, which are less satisfactory. However, since it is the voltage peak (magnitude) that is of importance to machine insulation designer, this method can be used for designing purposes.

The equivalent circuit model of the line-end coil for simulating the transient response in the winding of an electrical machine provides some information about the transient voltage distribution among turns of the coil. However, some discrepancy exists between the computed maximum inter-turn and measured voltages. A similar finding is applicable to the computed and measured voltage waveforms. This is because not all the travelling wave phenomena occurring in the winding can not be fully represented by the equivalent circuit. This shortcoming does not, however, render the method inapplicable to the voltage calculations in electrical machines at least within the short period when the highest voltage stress occurs. The proposed equivalent circuit can be used on a large motor. For the transient analysis on a small motor, another equivalent circuit in which a turn of the coil is used as an elemental part of the circuit can replace the proposed circuit.

The multi-conductor transmission line and scatter matrix concept is a detailed method of evaluating the inter-turn voltage. The computed peak inter-turn voltage and the voltage waveform agree well with the measured results. The travelling wave phenomena occurring in the winding are taken into consideration in this method to a much higher degree than in the equivalent circuit model and in the multi-conductor transmission line and

averaging technique concept. This method has shown a remarkable performance in predicting both the magnitude and the waveforms of the turn voltages to a level sufficient to be used in everyday design.

Applying any of these methods to the transient voltage calculation will require the computation of the winding parameters. Three methods are presented for capacitance computation. Inductance has been calculated from the relationship between a constantly assumed wave velocity and the capacitance. Resistance is calculated by a classical method that accounts for the skin and the proximity effects. Whichever method is to be used for the capacitance calculation, care must be taken in evaluating the capacitance to the ground in over-hang part of the coil. In addition, when calculating the transient voltage due to a voltage waveform with rise time less than 100 nanoseconds, inclusion of the resistance becomes compulsory if good accuracy of inter-turn voltage is required.

From the computed and measured voltage results presented in this work, it is evident that the improved accuracy for the capacitance value is sufficient to give good agreement between the measured and calculated inter-turn voltages without the need to take into account the presence of a surface impedance due to the laminated core.

The turn to turn or inter-turn voltage prediction is of significant importance in machines with form windings. The three methods described in this paper have shown competency in predicting these voltages to a level sufficient in the everyday design of machine insulation.

Two of these methods are applied for simulation of the voltage distribution due to the PWM voltage pattern on a low voltage machine where random windings are commonly used. Comparison of the numerical and measured results shows that for the transient voltage calculation on the random windings using either of the methods, knowledge of the capacitance to the ground in the over-hang part of the coil is sufficient for the voltage calculation. Such a method has been seen to give good agreement between the measured and computed coil voltage. The multi-conductor transmission line and scatter matrix concept produces results that vary between $\pm 5\%$ of the applied voltage. The coil voltage calculated on the random winding by means of the equivalent circuit produces results that vary between $\pm 10\%$ of the applied voltage.

The approach presented here does not require terminal measurement to predict the voltage distribution. In addition, it is not necessary to know the position of conductors inside the slot. The result also shows that we do not need any frequency dependent parameters to simulate the voltage distribution. The capability of the methods described in this work for voltage calculation in random winding should not be overestimated or underestimated. They appear promising and should be tested on several other motors.

References

Adjaye, R. E., Cornick, K. J. 1979. Distribution of switching surges in the line end coils of cable-connected motors, Proc. IEE Electric Power Applications, Vol. 2, Number 1, pp. 11-21.

Agrawal, A. K., Fowles, H.M., Scott, L. D., and Gurbaxani, S. M. 1979. Application of modal analysis to the transient response of multi-conductor transmission lines with branch. IEEE Trans. on EMC-21, pp. 256-262.

Bell, S., Sung, J.1996. Will your motor insulation survive a new adjustible frequency drive? IEEE Petroleum and Chemical Industry Conference, September 1996. pp. 125-130.

Boehne, E. W. 1930. Voltage Oscillations in Armature Windings Under Lightning Impulses-I, Transactions of the American I.E., pp. 1587-1615.

Bonnett, H., A. 1994. Analysis of the impact of pulse-width modulated inverter voltage waveforms on ac induction motors. IEEE Annual Pulp and Paper Industry Technical Conference. pp. 68-75.

Bonnett, H. A. 1996. A comparison between insulation systems available for PWM inverter fed motors. IEEE Petroleum & Chemical Industry Conference. September 1996. pp. 49-60.

Calvert, J. E. 1934. Protecting machines from lines surges. Transactions of the American I.E.E., Vol. 53, p. 139.

Cornick, K. J., Tleis, A. N. D 1989. Computer Simulation of First Pole-to-Close Multiple Prestriking Transients in Motor Systems. IEE Proc. Vol. 136 pt. B, No. 5. pp. 213-227.

Cornick, K. J., Tleis, A. N. D 1990. Factors Governing the Severity of Prestriking Transients in Motor Systems, IEE Proc. Vol. 137 pt. B, No. 1, pp. 14-24.

Cornick, K. J., Guardado, J. L., Bekaert, P.1992. Interturn voltages in machine windings evaluated from on-site test results and computer simulation. IEE Proc.-B, Vol. 139, No. 3, pp. 238-244.

Cornick, K. J., Thompson, T. R. 1982. Steep-fronted switching voltage transients and their distribution in motor windings. Part 1: System measurements of steep-fronted switching voltage transients. Proc. IEE, Vol. 129, Part B, pp. 45-55.

Gubbala, L.; Von Jouanne, A..; Enjeti, P. N.; Singh, C.; Toliyat, H. A. 1995 Voltage Distribution in the Winding of an AC Motor Subjected to High dv/dt PWM Voltages. IEEE PESC Conference Proceedings, pp. 579-585.

Guardado, J. L., Cornick, K. J. 1989. A computer model for calculating steep-fronted surge distribution in machine windings. IEEE Trans. on Energy Conversions, Vol. 4, No. 1, pp. 95-101.

Guardado, J. L., Cornick, K. J. 1996. Calculation of Machine Electrical Parameters At High Frequencies for Switching Transient Studies. IEEE Trans. on Energy Conversions, Vol. 11, No. 1, pp. 33-40.

Gupta, B. K., Kurtz, M., Stone, G. C., Sharma, D. K. 1986a. Impulse Strength of High Voltage Motor Coil Turn Insulation. IEEE Trans. on Energy Conversions, Vol. EC-l, No. 4, pp. 130-134.

Gupta, B. K., Sharma, D. K., Bacvarov, D. C. 1986b. Measured Propagation of surges in the winding of a large ac motor. IEEE Trans. on Energy Conversions, Vol. EC-l, No. 1, (with discussions) pp. 122 – 129.

Gupta, B. K., Lloyd, B. A., Sharma, D. K. 1990 Degradation of turn insulation in motor coils under repetitive surges. IEEE Trans. on Energy Conversions, Vol. 5, No. 2, pp. 320-325.

Gupta, B. K., Lloyd, B. A., Stone, G. C., Campell, S. R., Sharma, D. K., Nilsson, N. E. 1987a. Turn Insulation Capability of Large AC Motors Part 1- Surge Monitoring. IEEE Trans. on Energy Conversions, Vol. EC-2, No. 4, pp. 658-665 with discussion.

Gupta, B. K., Lloyd, B. A., Stone, G. C., Sharma, D. K., Fitzgerald, J. F. 1987b. Turn Insulation Capability of Large AC Motors Part 2- Impulse Strength. IEEE Trans. on Energy Conversions, Vol. EC-2, No. 4, pp. 666-673.

Gupta, B. K., Lloyd, B. A., Stone, G. C., Sharma, D. K., Nilsson, N. E., Fitzgerald, J. F. 1987c. Turn Insulation Capability of Large AC Motors Part 3- Insulation Co-ordination. IEEE Trans. on Energy Conversions, Vol. EC-2, No. 4, pp. 674-679 with discussion.

Hyypio, D. B. 1995. Simulation of Cable and Winding Response to Steep-fronted Voltage Waves. IEEE Conference records, pp. 800-806.

Kaufhold, M., Börner, G., Eberhardt, M., Speck, J. 1996. Failure Mechanism of the Inter-turn Insulation of Low Voltage Electric Machine fed by Pulse-Controlled. IEEE Electrical Insulation Magazine, Vol. 12, No. 5, pp. 9-16.

Keerthipala, W. W. L., Mclaren, P. G. 1990. The effect of laminations on steep-fronted surge propagation in large a.c. motor coil. IEEE Trans. on Energy Conversion, Vol. 11, No. 1, pp. 84-90.

Kerkman, R., Leggate, D., Skibinski, G. 1996. Interaction of Drive Modulation and Cable Parameters on AC Motor Transients. IEEE Industry Applications Meeting. Vol. 1, pp. 143-152.

Kerkman, R., Leggate, D., Schlegel, D., Skibinski, G. 1997. PWM Inverters and their Influence on Motor Over-voltage. IEEE Applied Electronics Conference, pp. 103-113.

Knable, H A. 1957. Short Cuts in Surge Analysis. Allis-Chalmers Electrical Review, First Quarter, pp. 30-33.

Lammenal, J., and Stalf, M. 1966. The Eddy Currents. ILIFFE, London.

Lampola, P. 1992 The influence of inverters on low-voltage cage induction motors insulation. Helsinki University of Technology, Electrical Engineering, Master's Thesis, 78p., In Finnish.

Lewis, T. J. 1954. The transient behaviour of ladder networks of the type representing transformer and machine windings. Proc. IEE Vol. 101, Pt. II, p. 541.

Lowery, T. F., Petro D. W. 1994. Application Consideration for PWM Inverter-Fed Low Voltage Induction Motors. IEEE Trans. On Industry applications, Vol. 30, No. 2, pp. 286-293.

Mclaren, P. G., Abdel-Rahman, M. H. 1988. Modelling of large ac motor coil for steep-fronted surge. IEEE Trans. on Industry Applications, Vol. 24, No. 3, pp. 422 – 426.

Mcleay, K. 1982. Voltage Distribution in Electrical Machine Stator Coils Due to Fast-fronted Switching Surges. PhD Thesis, HERIOT-WATT University, Department of Electrical and Electronic Engineering, p. 182.

Mechorn C. J., Tang, L. 1995. Transient Effect of PWM Drives on Induction Motors. IEEE Industrial and Commercial Power Systems Technical Conference, pp. 59-65.

Mecker, S. L. 1992 Consideration in Derating Induction Motors for Application on Variable Frequency Drives. IEEE Conference, pp. 191-197.

Melfi, M., Sung, J., Bell, S., Skibinski, G. 1997. Effect of Surge Voltage Rise Time on Insulation of Low Voltage Machine Fed by PWM Converters. IEEE Industry Application Meeting Vol. 1, pp. 239-246.

Murano, M., Fujii, T., Nishikawa, H., Nishiwaki, S., Okawa, M. 1974a. Voltage Escalation in Interrupting Inductive Current by Vacuum Switches. IEEE Trans. on Power Apparatus and Systems, Vol. PAS-93, pp. 264-271.

Murano, M., Fujii, T., Nishikawa, H., Nishiwaki, S., Okawa, M. 1974b. Three-phase simultaneous interruption in interrupting inductive current using vacuum switches. IEEE Trans. on Power Apparatus and Systems, Vol. PAS-93, pp. 272-280.

Nagy V. L., Rozsa, P. 1963. Matrix analysis of transient voltage distributions in alternating ladder networks. Proc. IEE Vol. 110, Number 9, pp. 1663-1670.

Narang, A., Gupta, B. K., Dick, E. P., Sharma, D. K. 1989. Measurement and analysis of surge distribution in motor stator windings. IEEE Transactions on Energy Conversion, Vol. 4, No. 1, pp. 126-134.

Oliver, J. A., Stone, G. C. 1995. Implication for the Application of Adjustable Speed Drive Electronics Motor Stator Winding Insulation. IEEE Electrical Insulation Magazine, pp. 32-36.

Oraee, H., Mclaren, P. G. 1985. Surge Voltage Distribution in Line-end coils of Induction Motors. IEEE Trans. on Power Apparatus and Systems, Vol. PAS-104, No. 7, pp. 1843 –1848.

Oyegoke, B. S. 1997. Multiconductor Transmission Line and Bewley Lattice Diagram Techniques for the Transient Inter-turn Voltages in Electrical Machine Fed from a Frequency Converter. The Tenth Symposium on Electrical Apparatus and Technologies, Siela'97, 30-31 May, Plovdiv, Bulgaria, Conference Proceedings Vol. 1, pp. 251-256.

Oyegoke, B. S. 1997a. A Comparative Analysis of Methods for Calculating the Transient Voltage Distribution within the Stator Winding of an Electric Machine Subjected to Steep-Fronted Surge. Proceeding of the Eighth International Conference on Electrical Machines and Drives, 1-3 September, Cambridge, U K, IEE Publication No. 444, 1997. pp. 294-298.

Oyegoke, B. S. 1997b. Transient Voltage Distribution in Stator Winding of Electric Machine Fed from Frequency Converter. Licentiate Thesis, Helsinki University of Technology, Department of Electrical and Communications Engineering, Laboratory of Electromechanics, p.61.

Persson, E. 1992. Transient Effect in Application of PWM Inverter to Induction Motors. IEEE Trans. On Industry Applications, Vol. 28, No. 5, pp. 1095-1101.

Qionq, L., Jianguo, J., Fengshi, Z. 1995. Modelling of Turbine Generator Stator Windings for Pulse Propagation Studies. Proceedings of the Second Chinese International Conference on Electrical Machines, CICEM'95. Hangzhou, China, pp. 741-746.

Quirt, R. C. 1988. Voltage to Ground in Load-Commutated Inverters. IEEE Trans. on Industry Applications, Vol. 24, No. 3, pp. 526-530.

Rhudy, R. G., Owen, E. L., Sharma, D. K. 1986. Voltage distribution among the coils and turns of a form wound ac rotating machine exposed to impulse voltage. IEEE Trans. on Energy Conversion, Vol. EC-l, No. 2, pp. 50-58.

Robinson, B. C. 1953. The Propagation of Surge Voltages through High Speed Turbo- alternators with Single-Conductor Windings. Proceedings of the Institution of Electrical Engineers, Vol. 100, Part II, pp. 453-467.

Rudenberg, R. 1940a. Performance of travelling waves in coils and windings, AIEE Transactions, Vol. 59, pp. 1031-1045.

Rudenberg, R. 1940b. Electric Oscillations and Surges in Subdivided Windings. Journal of applied Physics, Vol. 11, pp. 665-680.

Saunders, L. A., Skibinski G. L., Evon, T. S., Kempkes, L. D. 1996. Riding the Reflected Wave- IGBT Drive Technology Demands New Motor and Cable Considerations. IEEE Industry Application Meeting Vol. 1, pp. 75-84.

Schoen, R. R., G. Habetler, T. G., Kamran, F., Bartheld, R. G. 1995. Motor Bearing Damage Detection Using Stator Current Monitoring. IEEE Trans. on Industry Applications, Vol. 31, No. 6, pp. 1274-1279.

Skibinski, G. 1996. Design Methodology of a Cable Terminator to Reduce Reflected Voltage on Motors. IEEE IAS Conference Proceeding, pp. 153-161.

Skibinski, G., Leggate, D., Kerkman, R. 1997. Cable Characteristics and their Influence on Motor Over-voltage. IEEE Applied Power Electronics Conference, pp. 114-121.

Stone, G. C., Gupta, B. K., Kurtz, M., Sharma, D. K. 1984. Investigation of turn insulation failure Mechanisms in large ac motors. IEEE Trans. on Power Apparatus and Systems. Vol. PAS-103, No. 9, pp. 2588-2593.

Stone, G. C., Van Heeswijk R. G., Bartnikas, R. 1992. Investigation of the effect of repetitive voltage surges on epoxy insulation. IEEE Transactions on Energy Conversion, Vol. 7, No. 4, pp. 754-760 with discussion.

Suresh, G., Toliyat, H. A., Rendussara, D. A., Enjeti, P. N. 1997. Predicting the Transient Effects of PWM Voltage Waveforms on the Stator Windings of Random Wound Induction Motors. IEEE Conference Proceeding 0-7803-3704-2/97. pp. 135-141.

Tang, Y. 1997. Analysis of Steep-fronted Voltage Distribution and Turn Insulation Failure in Inverter Fed AC Motor. IEEE Industry Application meeting, Vol. 1, pp. 509-516.

Tavner, P. J., Jackson, R. J. 1988. Coupling of discharge currents between conductors of electrical machines owing to laminated steel core. IEE Proceedings, Vol. 135, Pt. B, No. 6, pp. 295 –307.

Thorsen, O. V., Dalva, M. 1995. A survey of faults on induction motors in offshore oil industry, petrochemical industry, gas terminal and oil refineries. IEEE Trans, on Industry Applications, Vol. 31, No. 5, pp. 1274-1279.

Von Jouanne, A., Enjetti, P., Gray, W. 1995. The Effect of Long Motor Leads on PWM Inverter Fed ac Motor Drive Systems. IEEE Conference Proceedings, pp. 592-597.

Weed, J. M. 1922. Prevention of transient voltage in windings. AIEE Journal, Vol. 41, p. 14.

Weeks W. T. 1972. Multi-conductor transmission line theory in the TEM approximation. IBM Journal of Research and Development, Vol. 16, No. 6, pp. 604-611.

Wright, M. T., Yang, S. J., Mcleay, K. 1983a. General Theory of Fast-Fronted Inter-turn Voltage Distribution in Electrical Machine Windings. IEE Proc. Vol. l30, Pt. B, No. 4, pp. 245-256.

Wright, M. T., Yang, S. J., Mcleay, K. 1983b. The Influence of Coil and Surge Parameters on the Transient Inter-turn Voltage Distribution in Stator Windings. IEE Proc. Vol. 130, Pt. B, No. 4, pp. 257-264.